Evaluation of uncertainty associated with projections of climate change-driven coastline variations in Japan

Master thesis

S.A.W. De Roover s1363840

Colloquium on 29-11-2018

UNESCO IHE DELFT

UNIVERSITY OF TWENTE.

Evaluation of uncertainty associated with projections of climate change-driven coastline variations in Japan

Master Thesis project by
S.A.W. de Roover
University of Twente, Enschede, the Netherlands
s.a.w.deroover@student.utwente.nl

Head of the graduation committee
Prof. Dr. R.W.M.R.J. Ranasinghe
IHE, Delft, the Netherlands
r.ranasinghe@un-ihe.org

Daily advisors
Dr. J. J. Warmink
University of Twente, Enschede, the Netherlands
j.j.warmink@utwente.n

Dr. K. Udo
Tohoku University, Sendai, Japan
udo@irides.tohoku.ac.jp

Dr. A. Dastgheib
IHE, Delft, the Netherlands
a.dastgheib@un-ihe.org

Picture on front page: The beach near Onahama port, Japan.

Abstract

Global population and wealth are increasingly concentrated in coastal zones. On the other hand, climate change-driven sea level rise (SLR) will result in increased coastal erosion and thus, land loss. To avoid socio-economic losses, projections of coastal retreat have to be made. These projections ideally should fit in contemporary coastal management, in which hazard risk assessment is a key tool; knowledge of exceedance probabilities of coastal recession is therefore important.

In Japan, projections of future beach erosion (up to 2100) have already been estimated using the Bruun rule (Udo & Takeda, 2017). However, Bruun rule-derived coastline projections (Bruun, 1962) are difficult to use in coastal hazard risk assessment, because they are deterministic and uncertainty from storms is not included (Cooper & Pilkey, 2004; Ranasinghe & Stive, 2009).

The research goal was to quantify uncertainty related to sea level rise and storm definition in the Bruun rule-derived future shoreline positions in Japan, by comparing these projections with the results of the PCR models (Ranasinghe, Callaghan, & Stive, 2012). The comparison was carried out for three sites in Japan with sandy beaches and (almost) no hard structures. Beach evolution time series were unavailable and only a few (dated) profile cross-sections were acquired from literature. Visits to the sites did not resolve these issues. The erosion (Mendoza & Jiménez, 2006) and recession models were adopted from the PCR model for Hazaki beach, Japan (Da Cruz, 2018). Site 1 was considered similar in structure and wave climate and the Hazaki model was applied to site 1 without large differences. Sites 2 and 3 were not similar to Hazaki beach, but the erosion and recession models were still applied. Recalibrating the erosion and recession models was not possible due to insufficient data. For sites 1 and 2, two different storm definitions or detection methods were used. For site 3, one method was used. This resulted in five PCR models. With each model setup, shoreline positions were simulated between 2018 and 2100 over four SLR scenarios. This resulted in twenty data sets of simulated shoreline positions.

Empirical cumulative distribution functions (ECDFs) describing coastal recession exceedance probabilities were produced with the PCR model results. Two ECDFs were made per data set based on annual maximum landward shoreline positions (R_{max}) and shoreline positions derived from 5-year trend lines (R_{trend}). Exceedance probabilities for Bruun estimates were derived with these ECDFs. For 2100 and the most severe SLR scenario, the exceedance probabilities derived with the ECDFs for R_{max} for Bruun rule estimates were: 49% and 44% with the two PCR models for site 1; 18% and 77% with the two PCR models for site 2; and 43% with the single PCR model for site 3.

The uncertainty due to SLR and storm definition could thus be quantified with the use of PCR produced shoreline ECDFs. The models were significantly more sensitive to the choice of storm detection method than to the choice of SLR scenario. However, no general quantified relation could be evaluated between Bruun rule estimates and their exceedance probabilities derived with the PCR model results. The shape of the curve that describes the temporal change of these exceedance probabilities is closest to an observable general relation. Besides these main conclusions, also other findings were reported:

- PCR exceedance probabilities of Bruun rule estimates changed over time due to 1) the temporal increase of the SLR and Bruun rule recession projections and 2) the increase of exceedance probabilities of the same shoreline positions in the PCR model results;
- The Hazaki PCR modelling methodology could be generalised to other sites with relative ease. The predictive successfulness of the models was unknown due to the lack of beach evolution data for validation;
- Validated dates of erosion at one site could be used to sample storm wave characteristics from wave time series of a nearby beach, given that the nearby beach has a similar wave climate and beach structure.

Acknowledgements

This document features my Master thesis project, marking the end of my Master studies of Civil Engineering. This project was carried out partially at the IHE Delft and partially at the University of Twente. Additionally, also a three-week trip was undertaken to Japan. Having been in so many places during my research, I want to take the opportunity to thank multiple people.

Firstly, I want to thank Ali Dastgheib as my daily supervisor, who was always available for questions or answered them as soon as possible. Besides him, I also want to thank my supervisors Rosh Ranasinghe and Jord Warmink for ensuring that I documented my research in such a way that it was comprehensible for people who were unfamiliar with the research topic. Additionally, I express my gratitude for Keiko Udo and the students and PHDs of the Environmental Change Risk research group, as the study areas were half a world away and I would not have been able to acquire the needed data or to visit the sites without their help. Lastly, I would like to thank my friends and family for giving helpful comments for my report or otherwise supported me during my research.

And then there is you, the reader, whom I hope to interest with my findings.

Sam de Roover

[This page is left intentionally blank for layout purposes.]

Table of Contents

List of abbreviations 7
List of symbols 7
1 Introduction 8
1.1 Background 8
1.2 Research objective 10
1.3 Research questions 10
1.4 Methodology 10
1.5 Outline 14
2 Theoretical framework 15
2.1 Climate change, and its impact on sea level and wave climate 15
2.2 The Bruun Rule method 19
2.3 Description of the PCR model 22
3 Study area selection and data collection 31
3.1 Requirements 31
3.2 Site 1 – Near Onahama port 33
3.3 Site 2 – Tottori sand dunes 36
3.4 Site 3 – Yumigahama 39
3.5 Site 4 – Yaizu and Shizunami beaches 42
3.6 Conclusions 45
4 Applicability of the Hazaki model 46
4.1 Influence of water levels 47
4.2 Wave climate comparison 48
4.3 Beach structure comparison 51
5 Implementation of the PCR 53
5.1 Overview of PCR model setups 53
5.2 Site 1 – Near Onahama port 54
5.3 Site 2 – Tottori sand dunes 55
5.4 Site 3 - Yumigahama peninsula 56
6 PCR-Bruun rule comparison 57
6.1 PCR results into ECDFs 57
6.2 Comparison of the Bruun rule with the PCR 62
6.3 Alternative PCR-Bruun Rule comparison 67
7 Discussion 70
7.1 Inclusion of water levels in the wave height-eroded volume relation 70

7.2 Similarities between the HORS and the study areas 70
7.3 PCR model application 71
7.4 Comparison between Bruun rule estimates and PCR results 73
7.5 Summary of issues 75
8 Conclusion 76
9 Recommendations 78
10 References 79

Appendices

Appendix I: PCR model inputs 82
I.1 Site 1 – Near Onahama port, Hazaki storm dates 82
I.2 Site 1 – Near Onahama port, 97th wave thresholding 85
I.3 Site 2 – Tottori sand dunes, 99th wave thresholding 88
I.4 Site 2 – Tottori sand dunes, 97th wave thresholding 91
I.5 Site 3 – Yumigahama peninsula, 97th wave thresholding 94
Appendix II: Equilibrium profile fitting 97
II.1 Site 1 – Near Onahama port 97
II.2 Site 2 – Tottori sand dunes 98
II.3 Site 3 – Yumigahama peninsula 98
Appendix III: ECDFs with averaged shoreline positions 99
III.1 Site 1 – Near Onahama port, Hazaki storm dates 99
III.2 Site 1 – Near Onahama port, 97th wave thresholding 99
III.3 Site 2 – Tottori sand dunes, 99th wave thresholding 100
III.4 Site 2 – Tottori sand dunes, 97th wave thresholding 100
III.5 Site 3 – Yumigahama peninsula 101

List of abbreviations

AOGCM – atmosphere-ocean general circulation model
CDF – cumulative distribution function
CMIP5 – climate model Intercomparison project phase 5
COWCLIP – coordinated ocean wave climate projection
ECDF – empirical cumulative distribution function
GMSL – global mean sea level
GP – generalised pareto (distribution function)
HORS – Hazaki Oceanic Research Station
IPCC – Intergovernmental Panel on Climate Change
JMA – Japan Meteorological Agency
MSWL – mean sea water level
NOWPHAS – Japanese Nationwide Ocean Wave information network for Ports and Harbours
PCR – probabilistic coastal recession
RCP – Representative Concentration Pathway
SLR – sea level rise

List of symbols

α – profile slope angle
A – beach profile coefficient (Bruun rule)
B – berm or dune height
d^* – transition depth (Mendoza-Jiménez erosion model)
D50 – mean sediment size
dt – storm durations
ΔV – beach volume change
h – water depth
h_{DoC} – DoC or Depth of Closure (Bruun rule)
$H_{e,t}$ – significant wave height that is exceeded only 12 hours per t years
H_s – offshore significant wave height
L – length equilibrium profile till DoC (Bruun rule)
R – recession or landward shoreline movement
R_{max} – maximum landward shoreline positions produced by PCR models
R_{trend} – shoreline positions derived from 5-year trend lines produced by PCR models
S – sea level rise (SLR)
$T_{e,t}$ – period associated to $H_{e,t}$
T_s – offshore significant wave period
w_S – fall velocity of the sediment

1 Introduction

This chapter discusses the background of the study, the goal of this study, and the outline of the report. Section 1.1 discusses coastal erosion, its link with sea level rise and coastal communities, the methods for predicting the resulting shoreline movement, and the necessity of this research. Section 1.2 and 1.3 present the associated research goal and questions. Section 1.4 presents the methodology. Section 1.5 presents the further outline of the report.

1.1 Background

Areas of population and wealth growth are primarily located in coastal zones. In 2003, more than half the world's population was living within 200 kilometres of a coastline (Creel, 2003). Japan is one of the countries that have high population concentration living at the coast. In 1997, already 77% of the total Japanese population lived in urban areas near or along the coast (Hinrichsen, 1998). Coastlines are susceptible to erosion. Erosion could happen over time due a deficiency in the sand budget of the beach, or suddenly during storms. If the erosion is not avoided or compensated for by natural processes or artificial nourishment, then the shoreline would move landward. Urban areas and infrastructure are hard to move, but the landward movement of the coast would result in damages or even loss of life if nothing is done.

The concept of storm erosion of coastal areas with 'soft' materials (e.g. sandy beaches) is well-explained Zhang, Douglas, and Leatherman (2004, p.42): "It is most commonly realised during coastal storms. These storms are accompanied by a temporary increase of local sea level (the storm generated surge above the normal astronomical tide) so that energetic storm waves are able to attack higher elevations of the beach and dune. Sediment there is extracted and put into suspension by the wave and carried off-shore." Additionally, sediment could also be carried over dunes and deposited behind them (overwash), thus also removing sediment from the system.

Coastal erosion as a challenge is not new to coastal engineers, but a relatively new aspect has made the challenge more complex. Climate change results in sea level change and, in most cases, this means sea level rise (SLR). A direct result of increased sea level is inundation. Depending on the slope of an area, the loss of area will be severe if it is a flat area, and less severe if the area has a steeper inclination. This is illustrated by Figure 1-1.

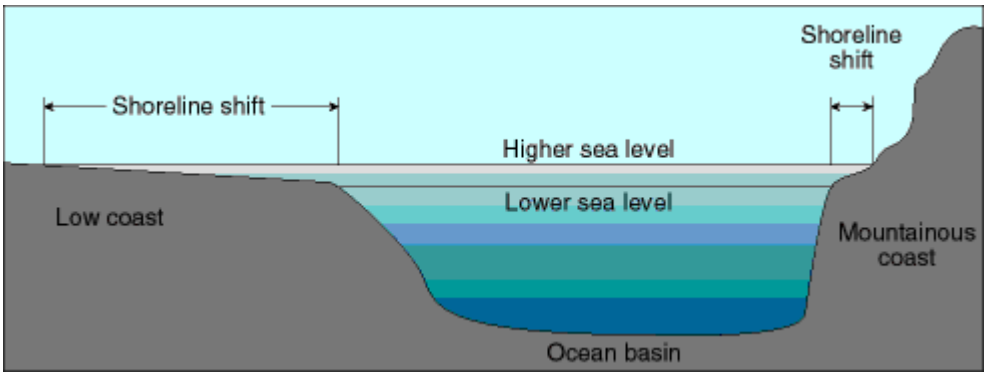

Figure 1-1. Inundation due to sea level rise. Adopted from (Watson, 2018)

Coastal erosion is worsened by SLR. A higher sea level acts as a permanent surge that increases over time. Beach sections that were first untouched by storm erosion could in the future be eroded by coastal storms. This results in landward shoreline movement.

The Bruun rule method (Bruun, 1962) is widely used for predicting landward coastline movement caused by coastal erosion and SLR. It describes the upward and landward movement of a

beach profile using a given SLR, and local extreme wave and beach profile characteristics. The model is easy to apply, but often the requirements for application are not met. Critics have provided multiple reasons against the use of the model (Cooper & Pilkey, 2004). The inability to include the uncertainty of storm characteristics is another issue of the method. It only uses one extreme wave height and period and does not consider e.g. the occurrence of other waves. No interpretation could be given on the probability of the coastal recession projection, because the Bruun rule only produces a recession estimate for a certain year and not the probability of occurrence. This deterministic nature of the Bruun rule makes it difficult to fit the model in contemporary coastal risk management. For risk assessment of coastal hazards, probabilistic recession estimates are needed (Ranasinghe & Stive, 2009).

Callaghan et al. (2008) and Ranasinghe et al. (2012) proposed a method for setting up a probabilistic framework to account for uncertainty in storm characteristics. This is the Probabilistic Coastal Recession (PCR) framework. In the framework, full temporal simulations of beach profile simulations are made. Analytical, semi-empirical, and process-based models could be used in the framework to describe the evolution. The simulations are done in a Monte Carlo setup. This ensures that a sufficient amount of possible coastal recessions is generated to create a cumulative distribution of future coastal recession.

Creating estimates with a PCR model for a beach requires significantly more effort than with the Bruun Rule method. When a probability of exceedance is assigned to the Bruun rule estimate, the severity of future recession could be evaluated with both the recession projection and the associated exceedance probability. In PCR results, both the recession estimates and their probabilities are known. The Bruun rule recession estimate could be compared with the PCR results to derive the associated probability of the Bruun rule estimate. If Bruun Rule estimates at several locations would have comparative exceedance probabilities according to cumulative distributions from the PCR results for the same locations, then the derived 'level' of conservativeness of Bruun rule estimates could be used to make indicative projections at similar beaches. Subsequently, it could be judged whether the situation is severe enough for a certain site to create a PCR model to have more detailed predictions for recession.

Da Cruz (2018) made a PCR model for the Hazaki beach near the Hazaki Oceanic Research Station (HORS) in Japan and evaluated the Bruun rule estimates locally with the method of Udo and Takeda (2017). Da Cruz subsequently compared the results of both methods. The modelling methodology of Da Cruz (2018) could be applied to other beaches in Japan to compare the Bruun rule estimates with PCR results. If the results from the comparisons are the same, Bruun rule estimates could be used as indicators of coastal retreat severity. Uncertainty related to storm characteristics is then accounted for, because this is quantified with the given probabilities.

1.2 Research objective

The research goal was to quantify uncertainty related to sea level rise and storm definition in the Bruun rule-derived future shoreline positions in Japan. The storm definition uncertainty in this research was defined as the uncertainty caused by choice for different storm characteristics. The goal was carried out by comparing the Bruun rule estimates with coastal recession exceedance probabilities as produced by the PCR framework for several sites in Japan. The modelling methodology applied at the Hazaki Oceanic Research Station (HORS) (Da Cruz, 2018) was modified and applied at several Japanese sites to inspect the behaviour of the PCR framework. Shoreline position simulations are produced from 2018 till 2100 with the PCR model and Bruun rule method over four SLR scenarios.

1.3 Research questions

To achieve the research goal, the following research question was answered:
"To which extent can storm and sea level rise uncertainty in the Bruun rule-derived climate change-driven future coastline recession in Japan (Udo & Takeda, 2017) be quantified with the PCR model?"
To solve this question, sub questions are answered:

1. To what extent could the correlation between Hazaki wave heights and eroded volumes on which the Hazaki erosion model is based be improved with the inclusion of water levels in wave heights?
2. To what extent are study areas and the HORS similar, concerning beach profile and wave climate?
3. How to setup the PCR models for the study areas with the HORS PCR model methodology?
4. What are the exceedance probabilities of the Bruun rule-derived recession estimates according to the PCR results?

1.4 Methodology

The following five sub sections discuss the methods used for selecting areas for PCR model application and for answering the four research questions. General explanations of the methods are given in this chapter. Elaborate explanations and equations are provided in the associated chapters.

1.4.1 Selection of study areas and data collection

To successfully apply the PCR framework, sites were chosen that were suitable for the application of PCR models according to the methodology of Hazaki. The sites had to meet five requirements. These requirements were checked with different data sources. Sources of data were:

- Papers describing the study area with beach cross-sections and sediment sizes;
- Google Earth satellite imagery;
- The Japanese Nationwide Ocean Wave information network for Ports and Harbours (NOWPHAS) providing bihourly measured wave heights, periods and directions;
- The Japan Meteorological Agency (JMA) providing hourly measured water levels;
- The expert opinion of professor Keiko Udo of Tohoku University, Sendai, Japan;
- Site visits that provided photos, verification of beach descriptions from literature, and sediment samples.

Three sites were chosen to apply the PCR framework to, being the beach near Onahama port, the Tottori sand dunes, and the beach along the Yumigahama peninsula. Descriptions of the sites are given in chapter 3.

1.4.2 Analysis of the Hazaki data

In chapter 4, Pearson correlation coefficients were derived to answer research question 1. Da Cruz (2018) determined correlation coefficients between wave heights and beach volume changes, and

between wave heights and shoreline movement. Only weak correlations were found when using wave heights (Da Cruz, 2018), both for the complete time series and time series divided into months for a seasonality check. The methodology used for the HORS model, though, was based on the assumption that a strong correlation existed between the mentioned variables. In this research, the correlation analysis was redone with the Hazaki data. Instead of using solely wave heights, water levels were added to wave heights. These were known as water surface heights. It was expected that significant correlations would be found between water surface heights and beach volume changes, and between water surface heights and shoreline movement. A significant correlation would justify the assumption on which the methodology for the HORS model was based, and would justify the use of the same methodology for the study areas. Water levels had then to be included in the PCR models as input variables in the model, besides the other input variables.

Scripts were used that were already written by Da Cruz in MATLAB. Correlation coefficients were calculated with the complete time series. Correlation coefficients were also calculated with wave heights, beach volume changes, and shoreline movements during particular months to check for differences due to seasonality.

1.4.3 Data comparison study areas and Hazaki

In chapter 4, a twofold data comparison was made to answer research question 2. Wave climates and beach profiles of the study areas were compared with those of the HORS. If wave climates and beach profiles were similar, then it was decided that the recession model of the HORS model could be used in the PCR model of the certain site.

Firstly, the comparison was done between wave climates. Wave heights were plotted to observe whether the same extremes were present. Wave roses were made to observe from which angle waves approached the beach. Also, wave heights at the Hazaki beach were plotted against the wave heights at a study area. If wave heights were aligned, it meant that at the same dates the same wave pattern was present. It was then assumed that erosion would occur at the study area if pn the same date erosion occurred at the HORS.

Secondly, the comparison was done between beach profiles. Profile cross-sections at the HORS (Da Cruz, 2018) and the study areas were plotted while joined at the waterline. It was visually observed whether a beach profile of a study area was sufficiently similar to the average beach profile of the HORS.

1.4.4 PCR model application to sites

Research question 3 was answered in chapter 5 with the application of the PCR model per site following the methodology used for the HORS model. The PCR models were made in MATLAB. In the PCR models, storms were generated with cumulative distribution functions (CDFs) of storm variables (wave height, period and storm duration). These CDFs were constructed with storm variables observed during storms. These storms were detected based on certain requirements that were defined by the used storm detection method. Different storm detection methods could be used per site. A PCR model was made per storm detection method. One site could thus have multiple PCR models. For all sites, at least 97^{th} percentile wave height thresholding was used for detecting storms from wave height time series. In each PCR model, the time in between storms and the recovery rate in between storms were calibrated. Based on the findings of research question 2, the decision was made whether to use the recession model in the Hazaki model, or another recession model. The erosion model (Mendoza & Jiménez, 2006) and the implementation of the effect of SLR were taken from the HORS model.

In total five PCR models were made for the three sites. Two of the three sites had two PCR models, because for these sites two different storm detection methods were used. The additional storm detection methods were derived from the comparison with Hazaki data or from literature. No additional storm detection method was used for the third site, because no evidence was found to base

an additional storm detection method on. Each PCR model used four different scenarios for including SLR. Twenty PCR model simulations were carried out in total for the three sites. Figure 1-1 explains with an overview of the differences between the PCR model simulations.

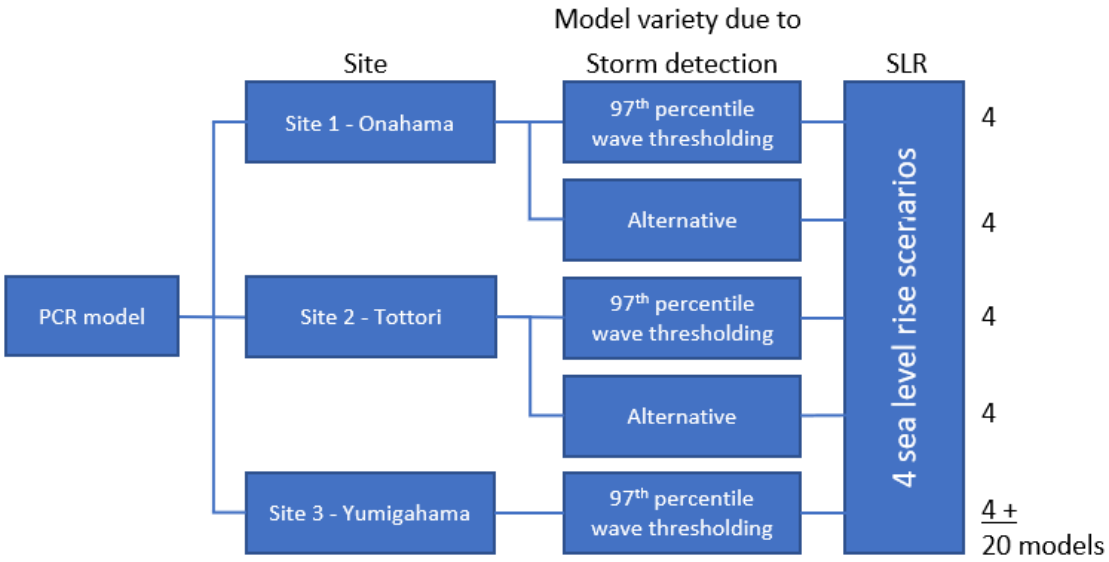

Figure 1-2. Setup of the different PCR models.

1.4.5 Comparison between the PCR and Bruun rule results

Research question 4 was answered in chapter 6 by determining probabilities for the Bruun rule estimates with the distribution functions for shoreline position. These distribution functions were made with the shoreline positions generated by the PCR models. The PCR models simulated shoreline positions from 2018 till 2100 for 50,000 times.

From the generated shoreline position time series, empirical cumulative distribution functions (ECDFs) were constructed that described the exceedance probabilities of: 1) annual maximum landward shoreline positions R_{max}, and 2) shoreline positions from a trend over 2095-2100 R_{trend}. R_{trend} was derived by fitting a trend through shoreline positions before and after storms between 2095 and 2100. A shoreline position was derived from this trend in the middle of the 5-year period. Shoreline positions were extracted from the 50,000 temporal simulations and ECDFs were made per model. For each year between 2018 till 2100, an ECDF for R_{max} was made. For R_{trend}, this was only done for the 5-year period of 2095-2100. R_{trend} could also be evaluated for other periods, but only the period 2095-2100 was used due a lack of time. Per model setup, 332 ECDFs (for 83 years times 4 SLR scenarios) were made with R_{max}, and 4 ECDFs (for 1 period times 4 SLR scenarios) were made with R_{trend}.

Bruun rule estimates were generated per site from 2018 till 2100 for four SLR scenarios. Per site, 332 recession estimates (for 83 years times 4 SLR scenarios) were calculated with the Bruun rule. These were generated according to the method that Udo and Takeda (2017) described in their research (see section 2.2 in this report). The method required standardised beach profiles. These were created by fitting an equation to the beach profiles.

A comparison is hard to make between the results of the Bruun rule and the PCR models, since PCR models produce probabilistic results and the Bruun rule produces deterministic results. Besides, it is important to understand what the results of both methods represent. Ranashinghe, Watson, Lord, Hanslow, & Cowell (2007) reported that in countries where the Bruun rule estimates are used in coastal hazard assessment, the likelihood of occurrence of predicted recessions is associated with the likelihood of SLR scenarios. Predicted recessions associated with the lower bound of SLR (lower boundary of the grey shaded areas in Figure 2-1) are assumed to be exceeded for certain. Predicted recessions associated with the higher bound of SLR (higher boundary of the grey shaded areas in Figure

2-1) are assumed very unlikely to be exceeded. The likelihood of Bruun rule estimates made with the 'average' SLR, as done in this study, is then considered to be in between the two extremes (Ranasinghe et al., 2007). In this study, it was therefore assumed that the Bruun rule estimates represented the average recession due to SLR in a certain year. In the opinion of the author, not average but extreme recessions are relevant for policy makers in coastal risk management, because assets are more endangered by extreme recessions than by average recession. This is the reason for the use of the maximum landward positions R_{max} as produced by the PCR models in the comparison with the Bruun rule estimates. This setup for the comparison is also the approach that was used by Ranasinghe et al. (2012), Li et al. (2014), Dastgheib et al. (2017), and Da Cruz (2018).

The R_{trend} between 2095 and 2100 represent, in the opinion of the author, more or less average recessions, because the maximum seaward shoreline position after a period of recovery and the maximum landward shoreline position after a storm are taken into account. The averaged 'nature' of R_{trend} corresponds then better with the Bruun rule estimates than is the case with R_{max}. Therefore, also a comparison between these PCR results and the Bruun rule was made.

The comparison between Bruun rule estimates and the different PCR results (R_{max} or R_{trend}) was done following the same method. For a particular site, year and SLR scenario, the Bruun rule estimate and the PCR results were compared. As mentioned above, an ECDF was made with the PCR-simulated shoreline positions. In the ECDF, a Bruun rule estimate would correspond to a PCR shoreline position and, since the exceedance probability of the PCR shoreline position was known, the exceedance probability of the Bruun rule estimate according to the PCR results could be derived. Figure 1-3 illustrates this method. Because multiple storm detection methods were used in a PCR model, multiple exceedance probabilities were associated with the same Bruun rule estimate that was calculated for one site for one year for one SLR scenario.

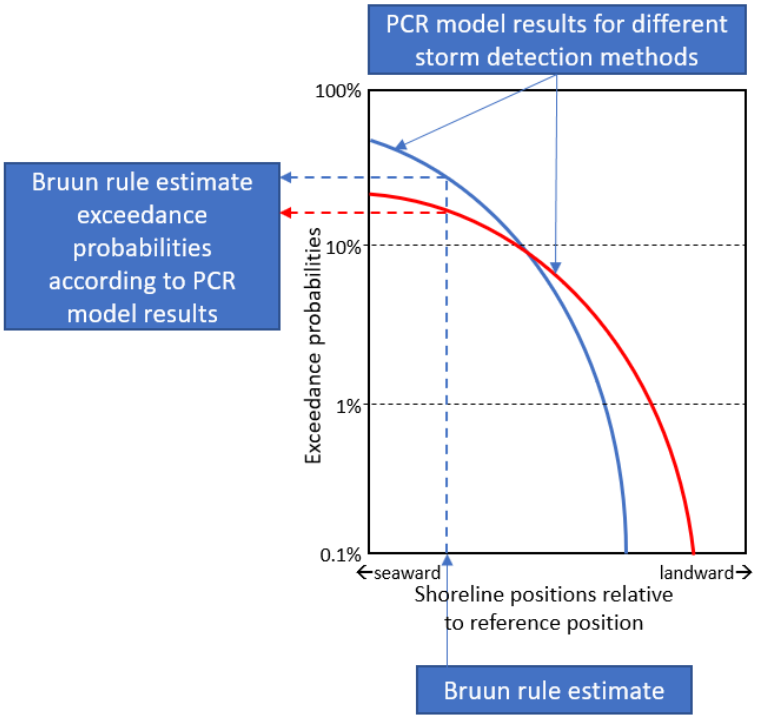

Figure 1-3. Explanation of the comparison of Bruun rule estimates with PCR model results. The example shown are hypothetical results of a PCR model and Bruun rule calculation for one site for one SLR scenario for one particular year.

1.5 Outline

Figure 1-4 illustrates the research structure. Prior to the answers to the research questions, a theoretical framework was given in chapter 2 that elaborated on the four different climate change and SLR scenarios, the Bruun rule method and the coastal retreat projections made by Udo and Takeda (2017), and the PCR framework and the methodology applied at the HORS.

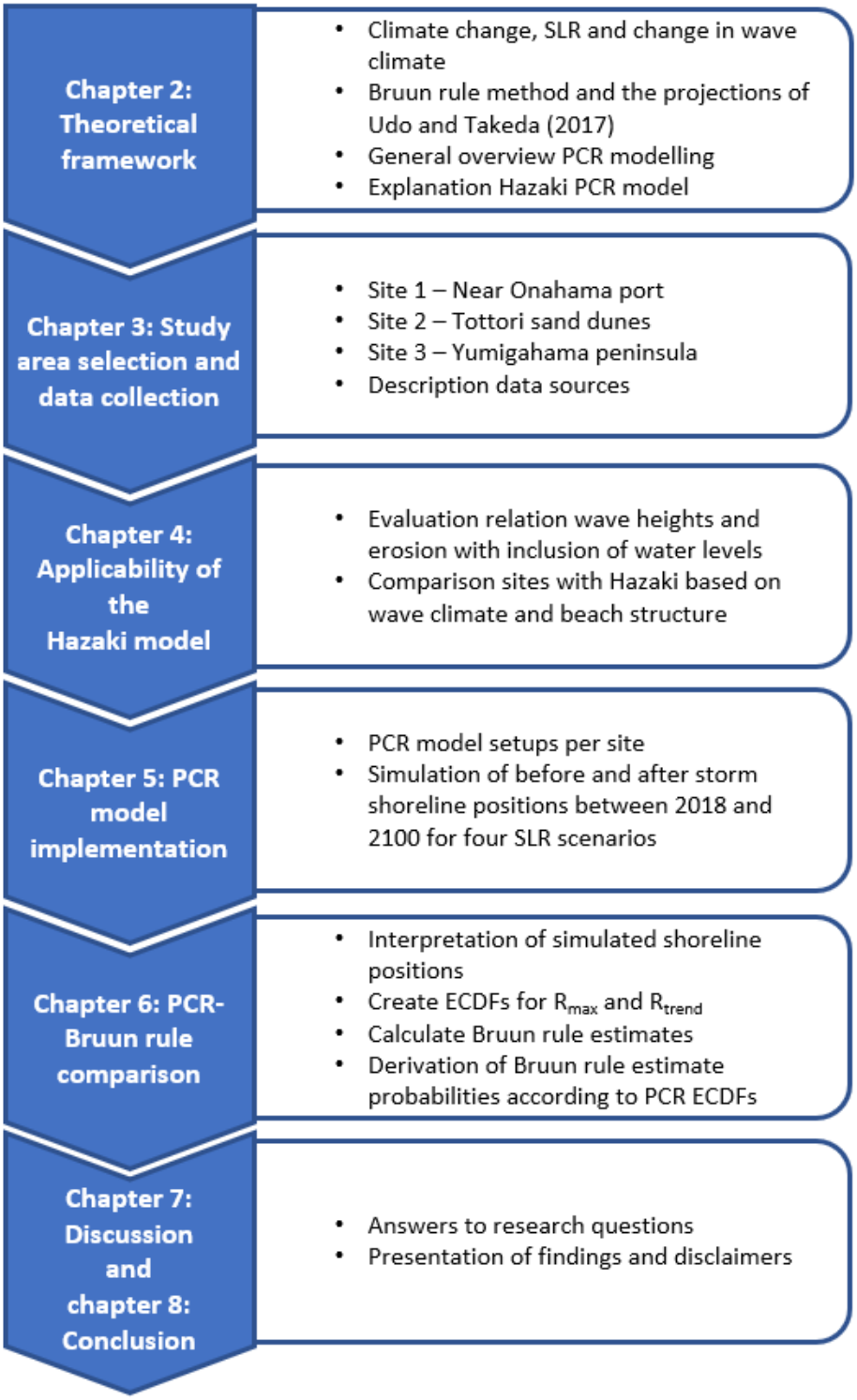

Figure 1-4. Flowchart illustrating the structure of the report.

2 Theoretical framework

In this theoretical framework, findings in literature were presented on which this study was built. Section 2.1 describes the four different climate change scenarios from which the four SLR scenarios are derived. The influence of climate change on wave climate in Japan is also discussed. In section 2.2, an elaborate explanation of the Bruun rule method is given. Furthermore, the Bruun rule implementation and the results of Udo and Takeda (2014) are discussed. These are important for deriving the Bruun rule estimates locally. Section 2.3 discusses the general PCR framework and application of the framework to the beach at the HORS by Da Cruz (2018). Their methodology was used for PCR modelling at the study areas.

2.1 Climate change, and its impact on sea level and wave climate

SLR is driven by climate change. Climate change also (in)directly influences local wave climates and storm characteristics. The Intergovernmental Panel on Climate Change (IPCC) is a global organisation focusing on climate change and its impacts. The IPCC produces reports which are based on scientific literature. In its most recent report, attention was given to the different greenhouse gas emission scenarios as a starting point to describe the climate change scenarios. To the emission scenarios was referred as the Representative Concentration Pathways (RCPs) (Church et al., 2013). Different greenhouse gas emissions translate to different projections for SLR. Four scenarios were considered:

- RCP2.6 – a drop in emissions in 2020, becoming equal to zero or negative after 2100;
- RCP4.5 – emissions peaking in 2040, stabilising in 2080 at 1960 concentration levels (4 GtonC/yr), and dropping further after 2100;
- RCP6.0 – emissions peaking in 2080 at 17 GtonC/yr, and dropping thereafter;
- RCP8.5 – emissions growing till stabilisation in 2100 at 29 GtonC/yr.

The RCPs were named after the radiative forcing, or the net energy input into the global system (in W/m2), compared to the radiative forcing predating the industrial revolution. This approach was different from the previous assessment reports, in which SRES scenarios were used. SRES scenarios explained a certain narrative in which economic focus and population growth were key factors. Possible greenhouse gas emission scenarios were linked to these narratives. With the RCPs, the narrative was made after predictions on emissions had been made.

This radiative forcing influences certain processes that contribute to changes in ocean water volume and thus to changes in sea level (Church et al., 2013):

- Thermal expansion of ocean water; and
- Melting of glaciers and the Greenland and Antarctic ice sheets. Church et al. (2013) also considered rapid dynamical change of ice sheet contribution due to e.g. breaking, but ruled these effects to be relatively small.

Together with these climate sensitive processes, also other factors contribute to changes in (relative) sea level, such as change in water storage on land.

It was unknown exactly how these contributors exactly influenced the global and regional sea level. The Climate Model Intercomparison Project Phase 5 (CMIP5) was started with the goal to give relevant input for the 5th IPCC assessment report (IPCC, 2013). In the approach, 21 Atmosphere-Ocean General Circulation Models (AOGCMs) were applied. With these AOGCMs were, among others, the global mean sea level (GMSL) rise projected for the four different RCPs, which are shown in Figure 2-1.

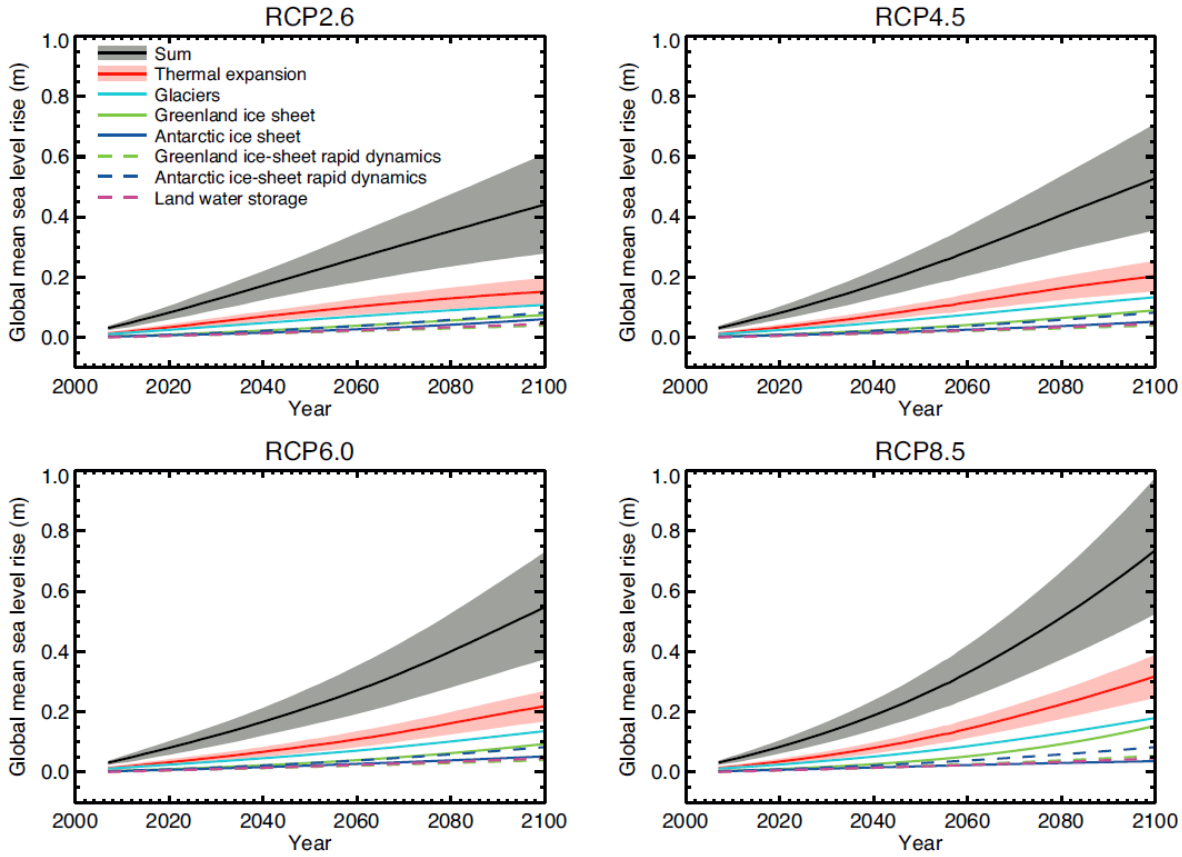

Figure 2-1. Projections from process-based models of global mean sea level (GMSL) rise relative to 1986-2005. The lines show the median projections. For GMSL rise and the thermal expansion contribution, the likely range is shown as a shaded band. The contribution from ice sheets include the contributions from ice-sheet rapid dynamical change, which are also shown separately. Adopted from Church et al. (2013).

Church et al. (2013) said that in some areas sea level changes were similar to the global average. According to them some coastlines on the other hand had sea level changes significantly different from the GMSL change. The discrepancy between global and regional (relative) sea level changes was due to several factors:

- ocean dynamical processes, being changes in surface winds, ocean currents, temperature and salinity;
- movements of the sea floor. Tectonics were not included in the 5th assessment report of the IPCC (IPCC, 2013);
- changes in gravity due to water mass redistribution with the melting of ice masses;
- vertical land movement due to, among others, glacial isostatic adjustment and subsidence.

The AOGCMs of the CMIP5 primarily included the heat uptake by the ocean and changes in the wind forcing as drivers for dynamical sea level changes.

These AOGCMs were applied on a global grid, and also regional sea level changes relative to 1986-2005 could be evaluated. Udo and Takeda (2017) analysed the IPCC results for Japan. The long-term SLR relative to 1986-2005 is presented in Table 2-1. It is seen that the Japanese ensemble mean SLR and the global mean SLR were almost equal, which was also concluded by Udo and Takeda (2017).

Table 2-1. Estimated Sea Level Rise in meters for 2081-2100, relative to 1986-2005. Adapted from IPCC (2013) in: (Udo & Takeda, 2017).

Greenhouse gas development models	Smallest SLR (Towards northern coast of Japan)	Largest SLR (Towards southern coast of Japan)	Japanese mean SLR	Global mean SLR
RCP2.6	0.34	0.45	0.38	0.40
RCP4.5	0.41	0.54	0.46	0.47
RCP6.0	0.42	0.55	0.48	0.48
RCP8.5	0.56	0.71	0.63	0.63

The IPCC (2013) included in its report projections on sea level extremes and the climate change-driven change in storm and wave climate. It was said that the probability of extreme sea levels occurring more frequently is high, and that "there is a *low confidence* [or high uncertainty] in region-specific projections of storminess and associated storm surges (Church et al., 2013, p. 1140)."

Regarding wave climate, the IPCC referred to the Coordinated Ocean Wave Climate Projection (COWCLIP) project (Hemer, Fan, Mori, Semedo, & Wang, 2013), in which a multi-model ensemble was built with dynamical (Fan, Held, Lin, & Wang, 2013; Hemer, Katzfey, & Trenham, 2013; Mori, Yasuda, Mase, Tom, & Oku, 2010; Semedo et al., 2013) and statistical models (Wang & Swail, 2006). The projected changes in wind-wave conditions are given in Figure 2-2. It is seen that wave heights would only increase notably in the ocean surrounding Antarctica, and the mid-south region of the Pacific Ocean. Church et al. (2013) remarked on these results that the overall uncertainty in wave projections was high, because of:

- uncertainties regarding future wind states (particularly storm geography);
- the limited number of model simulations used in the ensemble averages;
- the different methodologies used to downscale climate model results to the regional scale (Hemer, Katzfey, et al., 2013).

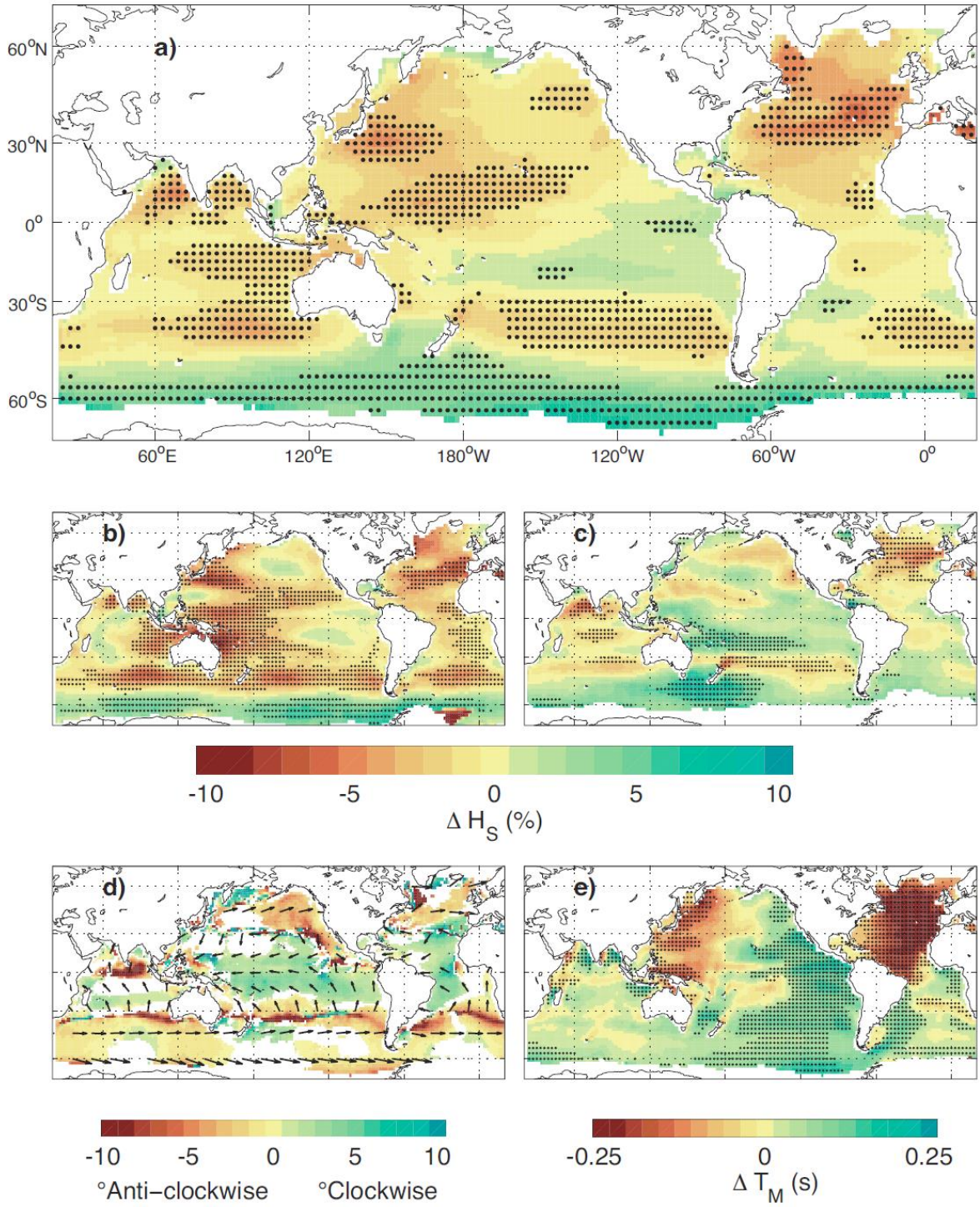

Figure 2-2. Projected changes in wind-wave conditions (~2075-2100 compared with ~1980-2009) derived from the Coordinated Ocean Wave Climate Projection (COWCLIP) project (Hemer, Fan, et al., 2013). (a) Percentage difference in annual mean significant wave height. (b) Percentage difference in means of January to March significant wave height. (c) Percentage difference in means of July to September significant wave height. Hashed regions indicate projected change is greater than the 5-member ensemble standard deviation. (d) As for (a), but displaying absolute changes in mean wave direction, with positive values representing projected clockwise rotation relative to displayed vectors, and colours shown only where ensemble members agree on sign of change. (e) As for (a), but displaying the absolute changes in mean wave period. The symbol ~ is used to indicate that the reference periods differ slightly for the various model studies considered. Adopted from Church et al. (2013)

2.2 The Bruun Rule method

The Bruun rule is a two dimensional mass conservation method, that explains the upward and landward shift of the equilibrium beach profile in response to sea level rise (Bruun, 1962). The equilibrium beach profile was described as the beach profile that would form under constant wave conditions; the cross-shore sediment transport would be in equilibrium as the forcing remains constant. An equilibrium profile would never be reached, because the wave conditions constantly change. Evolution towards this equilibrium profile though does occur in the form of erosion and accretion. An equilibrium profile could be described with the length of the profile *L*, the profile slope angle α, the berm or dune height *B*, and the depth of closure (DoC) h_{DoC}. The DoC is the depth at the base of the profile beyond which significant sediment exchange with the offshore does not occur. With sea level rise, the equilibrium profile would shift upward with the sea level rise *S*, and landward with the horizontal recession distance *R*, which could be expressed with the Bruun rule equation:

$$R = \frac{SL}{B + h_{DoC}} = S/\tan\alpha \quad (1)$$

The beach profile could then be described with

$$h = Ay^{\frac{2}{3}}, \quad (2)$$

where *h* is the water depth, y is the distance in the offshore direction, and *A* is the coefficient of the beach profile, which is strongly correlated with sediment size (Dean, Walton, & Kriebel, 1994).

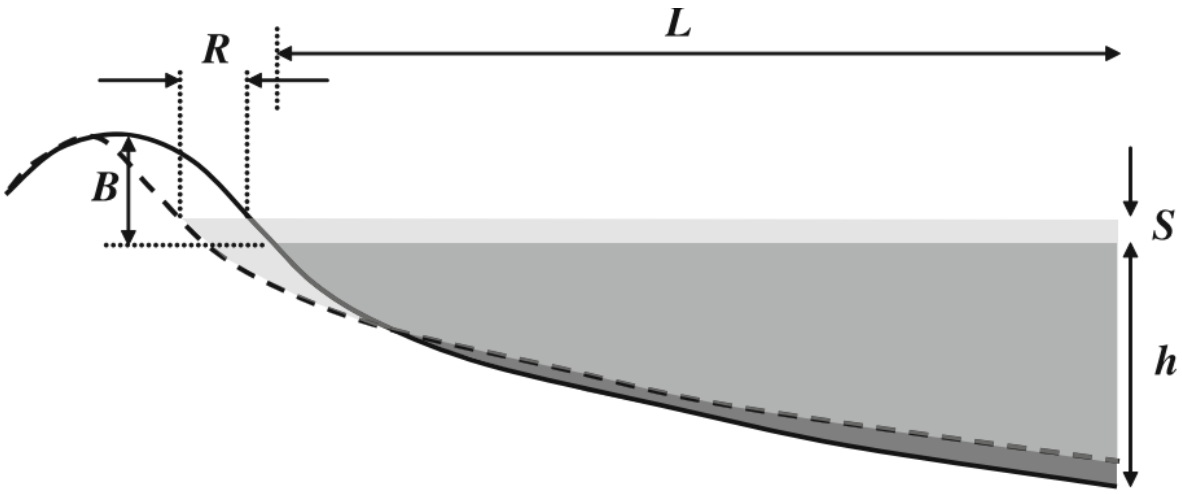

Figure 2-3. The evolution of the equilibrium beach profile according to the Bruun rule. The solid line is the initial equilibrium profile and the dashed line is the equilibrium profile after SLR. The dark grey shaded area represents accretion and the light grey shaded area represents areas where water is present after SLR. Adopted from (Ranasinghe et al., 2012)

The method is easy to use, but several assumptions have to be made:

- a uniform shape of the shoreline is present, that is described by the equilibrium profile;
- the cross-shore sediment balance budget is closed;
- all cross-shore sand movement is caused by waves;
- no hard structures are present in the beach profile;
- there is no net long-shore sand transport.

These assumptions limit the application of this method severely, as among others it does not accommodate any 3-dimensional variations along the coastline (Ranasinghe & Stive, 2009). Examples of these spatially complex coastlines are urban coastlines with hard structures, estuaries, and river outlets (or a combination). Cooper and Pilkey (2004) argued that the model should not be used

anymore for making projections of coastline retreat. The method however is still actively used, and Cooper and Pilkey (2004) have indicated factors attributing to this fact:

1. Appeal of a simple, easy to use analytical model that is in widespread use;
2. Difficulty of determining the relative validity of studies proving and disproving the method;
3. Ease of application;
4. Positive advocacy by some scientists;
5. Application by other scientists without critical appraisal;
6. The simple numerical expression of the model;
7. Lack of easy alternatives.

Another weakness is the current role it plays in coastal management. Society increasingly relies on risk based assessment, and the deterministic outcomes of the Bruun rule are hard to fit in, because probabilistic coastal projections are needed (Ranasinghe & Stive, 2009). Besides, a major source of uncertainty is the DoC and subsequently the active slope, as there are different estimation methods with significant different outcomes. Application of the different DoC derivation methods resulted in recession estimates that could vary by approximately 500% (Ranasinghe & Stive, 2009). Wave characteristics and local water level setup and their stochastic nature are not included, although storm events are thought to be the driving forces of coastal erosion in combination with SLR.

Udo and Takeda (2017) made a study on general beach loss projections in Japan. They used the Bruun rule method and explored the effects of the uncertainties on the projections. For the coastal retreat per point in the profile, the following equation was used (Udo & Takeda, 2014):

$$\Delta y/y_* = -S/(h+B)\,, \tag{3}$$

where Δy indicates the distance of shoreline retreat, y_* is the horizontal distance to the critical depth for sediment movement, B is the berm height, and DoC h is calculated according to the relation that Nicholls, Birkemeier, and Hallermeier (1996) proposed:

$$h = 2.28H_{e,t} - 68.5(H_{e,t}^2/gT_{e,t}^2), \tag{4}$$

where $H_{e,t}$ is the significant wave height that is exceeded only 12 hours per t years, $T_{e,t}$ is the associated wave period, and g is the gravitational acceleration.

B in Equation 3 is obtained by the equation proposed by Takeda and Sunamura (1983):

$$B = 0.125H_b^{5/8}(gT_s^2)^{3/8}\,, \tag{5}$$

where H_b is the breaking wave height, and T_s is the mean significant wave period. H_b is then calculated by the equation proposed by Sunamura (1983) using the mean significant wave height H_s, beach slope tan α, and the mean significant wave length L_s:

$$H_b/H_s = (\tan\alpha)^{0.2}(H_s/L_s)^{-0.25} \tag{6}$$

Udo and Takeda (2017) excluded uncertainty from DoC determination method, because they only used the Nicholls method (Nicholls et al., 1997). They quantified uncertainty related to other sources. They did this by analysing the difference in results caused by the different CMIP5 models and sediment sizes (for which they used 0.3 mm (Udo & Takeda, 2014), and 0.2 and 0.6 mm as lower and upper boundaries). These differences in coastal retreat estimates may be best described by Figure 2-4. The largest difference in beach loss percentages for the same SLR with variating sediment sizes was reported to be 38%.

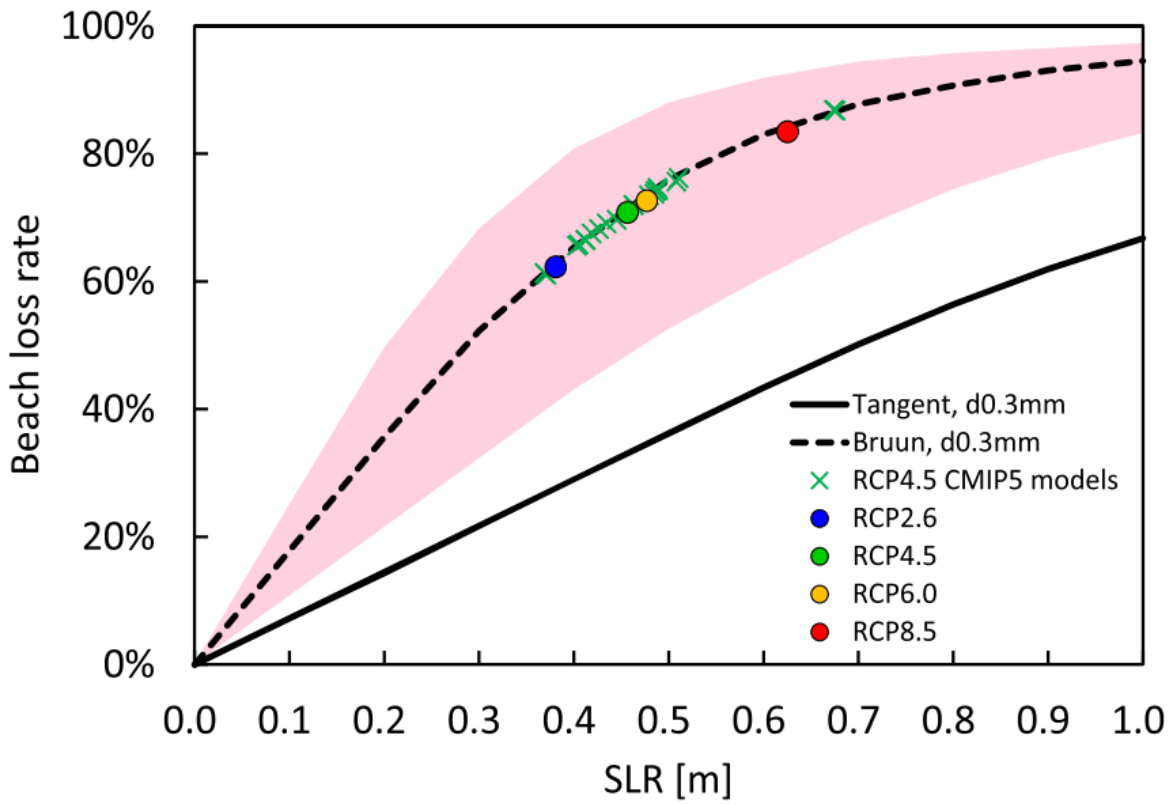

Figure 2-4. Projections of beach-loss rate of the 0.3 mm sediment size and for average SLR along the entire coastline of Japan. The points show the rates projected using the BR for SLR in 2081-2100 for the RCP scenarios. The solid and the dashed lines show the rates projected using the tangent and Bruun rules for the same SLR along the entire Japanese coastline, respectively (Udo & Takeda, 2014). The tangent line is the line indicating what the beach loss would be if only inundation of the coastline due to SLR would be considered (Udo & Takeda, 2017). The uncertainty caused by the 0.2-0.6 mm sediment size is also shown by the pink shading in the figure. Adopted from Udo and Takeda (2017).

Uncertainties and problems aside, the Bruun rule results could be useful as a first estimation for erosion. It was reported that when results were compared to probabilistic coastal recession estimates, they corresponded to exceedance probabilities of either less than 8% (Ranasinghe et al., 2012) or in between 1% and 35% (Toimil, Losada, Camus, & Díaz-Simal, 2017). This indicated that Bruun rule estimates had a conservative nature in these studies and were applicable as initial coastal erosion projections. It was, however, noted by Toimil et al. (2017) that this assumed conservativeness depends on what erosion models are employed in the probabilistic modelling frameworks with which the Bruun rule estimations were compared. Da Cruz (2018) made a PCR model for a site in Japan and compared her results with Bruun rule estimations generated with the approach of Udo and Takeda (2017). Da Cruz found that the Bruun rule estimations had exceedance probabilities between 39% and 45% in 2100. These exceedance probabilities were considerably less conservative than the earlier reported exceedance probabilities.

2.3 Description of the PCR model

Da Cruz (2018) made a PCR model for the beach at the HORS. The model was built based on the PCR descriptions presented by Callaghan, Nielsen, Short, and Ranasinghe (2008) and Ranasinghe, Callaghan, and Stive (2012). The HORS was chosen to build a PCR model for, because beach volume change time series were available. The erosion and recession models could be calibrated and validated with these time series. In section 2.3.1, the general setup for a PCR model is explained, and the PCR model setup for Hazaki (Da Cruz, 2018) is discussed in section 2.3.2.

2.3.1 Explanation of the PCR model

Callaghan et al. (2008) and Ranasinghe et al. (2012) developed a method for setting up a probabilistic framework. In the framework, full temporal simulations of beach profile simulations are made. Analytical, semi-empirical, and process-based models could be used in the framework to describe beach evolution. The simulations are done in a Monte Carlo setup. This ensures that a sufficient amount of possible coastal recessions is generated to create cumulative distribution of future coastal recession. Their setup first focuses on generating a synthetic storm series (Callaghan et al., 2008):

1. Identify meteorologically independent storm events from measured data;
2. Fit extreme value distributions to offshore wave heights and storm durations;
3. Fit the dependency distributions between offshore wave height and storm duration, and between offshore wave height and storm surge;
4. Fit the conditional distribution between offshore wave height and wave period;
5. Determine the empirical distribution for offshore wave direction;
6. Fit a non-homogeneous Poisson distribution to the temporal spacing between storms;
7. Generate a database of storms for the desired simulation period using data derived joint probability distributions of storm characteristics within a Monte Carlo simulation;

The next steps are then involved with translating the synthetic storm time series to shoreline position time series. Ranasinghe et al. (2012) presented the following steps:

8. Using IPCC projections (IPCC, 2013), estimate the SLR at the time each storm occurs;
9. For each storm, estimate dune recession using an erosion model, which also allows coastal recovery between storms;
10. Estimate the final dune toe or berm position by temporally averaging the position in the last 2 years from this simulation;
11. Subtract the initial dune toe or berm position from the final position to estimate coastal recession between 1990 and 2100;
12. Repeat 7-11 until exceedance probabilities greater than 0.01% converge (i.e. bootstrapping).

Da Cruz (2018) followed this approach. A difference was that the Hazaki model simulated shoreline positions from 2018 till 2100 instead of from 1990 till 2100. In Figure 2-7, a diagram is shown of Da Cruz's PCR implementation for the HORS. The model consisted of three parts. Part 1 (green) was the generation of storm events. The total amount of generated storm events was 50,000 times the expected number of storms between 2018 and 2100. Part 2 (yellow) was the translation of storms into a shoreline movement database (step 9). Part 3 (blue) were the model runs themselves, in which 50,000 times the shoreline locations over the period 2018-2100 were simulated (step 8). Storm characteristics were generated before and not during the actual simulation. This resulted in reduced computation time.

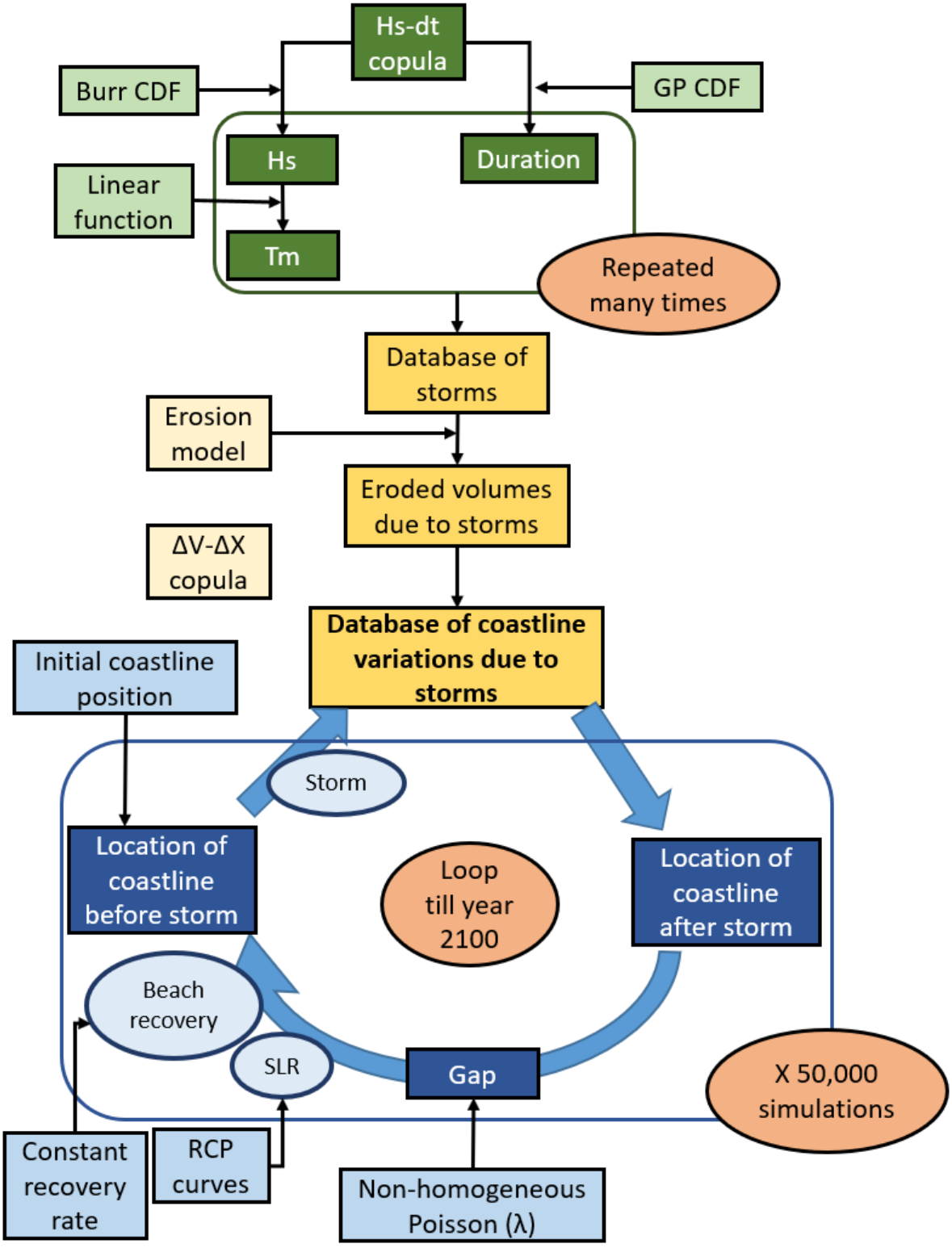

Figure 2-5. Diagram of Da Cruz's PCR implementation. Adopted from Da Cruz (2018).

2.3.2 Step by step explanation of the Hazaki model

The HORS PCR model is discussed in this section. The PCR framework structure as mentioned in the previous section is used to explain the modelling choices of Da Cruz (2018).

Step 1 – Storm event detection

Wave heights, wave periods and storm durations were needed as storm characteristics for the Hazaki model. No literature was available on storm characteristics at Hazaki. Da Cruz tried to find storm characteristics by correlating wave characteristics and volume changes of the beach, but no significant correlation was found. Small waves were occasionally observed together with erosion, and large waves were occasionally observed with accretion or without beach response. It was chosen to record the wave heights during the observed negative beach volume or erosion events. If it was observed that an eroded volume exceeded a chosen erosion threshold, a storm was detected. The largest wave height and appurtenant period during the period of erosion was recorded. Da Cruz referred to storm wave characteristics detected in such a manner as 'erosion events'. For determining the erosion events, Da Cruz used beach profiles that were measured on a daily basis. They could not determine the storm durations, because the temporal spacing of the observations was too large. Storm durations were instead recorded from thresholding wave heights. If a certain threshold was exceeded, it was marked as a storm event. Storm events that were detected within 24 h were marked as one storm event. The duration from the start till the end of a storm event was recorded as the storm duration. Da Cruz referred to wave characteristics detected in this manner as 'wave events'

Da Cruz thus used two kinds of thresholds for detecting storms: the 95th percentile of negative beach volume change for determining wave heights and periods during these events, and the 97th percentile of wave heights to determine storm durations.

Step 2 – Extreme value distribution fitting

In the HORS model, a Generalised Pareto (GP) distribution was fitted to the wave heights found with wave thresholding (wave events). A Burr distribution was fitted to wave heights found with erosion thresholding (erosion events). A GP distribution was fitted to the storm durations Da Cruz found with the wave events.

Step 3 – Dependency distribution wave heights, storm durations and storm surges

Da Cruz used a copula to model the dependency between wave heights and storm durations. Modelling the dependency between wave heights and storm durations was done in a similar fashion in other implementations of the PCR framework (Dastgheib et al., 2017; Li et al., 2014). Copulas are joint probability CDFs and could be divided into two families: Clayton and Gaussian. A Clayton copula proved to have the best fit to the Hazaki data. In this copula, the CDFs for the wave heights (erosion events) and storm durations (wave events) were joined. Da Cruz gave a justification for using storm durations found with wave events. It was assumed that certain wave heights were linked to certain storm durations. This relation was independent of the complex relation between wave heights and beach volume change that was mentioned in step 1.

Da Cruz did not analyse the effect of storm surges nor were storm surges input variables for the used erosion model. These were the reasons for not including storm surges in the HORS model.

Step 4 – Relation between wave height and period

Wave heights and periods from erosion events were plotted together, and a linear relation was fitted through the data points. When the wave height was generated, the period could be derived with this relation.

Step 5 – Empirical distribution wave direction

In the analysis of Hazaki wave data, Da Cruz found that wave directions were independent from wave heights. Wave directions were also not a variable in the erosion model used in the Hazaki model. Therefore, wave direction data was not used in the PCR model.

Step 6 – Distribution of storm gaps

The time between storms, or storm gaps, proved to be sensitive to seasonality. Callaghan et al. (2008) proposed a non-homogeneous Poisson distribution from which the time gaps in between storms could be generated in the PCR model simulation. They found that this method solved the issue of seasonal effects of storms. Da Cruz (2018) came to the same conclusion. A trial-and-error method was used to estimate the event rate parameters of the monthly distributions. The goal was to generate an average number of events per month that resembled the observed average number of events per month. The number of events per month was influenced by the storm gaps. After each iteration, the event rate parameters for the distributions of the storm gaps were adjusted. This continued until a satisfactory resemblance of monthly events was found.

Step 7 – Generating storm events

Synthetic storm time series were generated with the extreme value distributions made in step 2 and 3. Two random numbers were generated from the wave height-storm duration copula, one corresponding to a non-exceedance probability for wave heights, and one corresponding to a non-exceedance probability for storm durations. A wave height was found with the generated non-exceedance probability via the Burr distribution for wave heights. A storm duration was found with the generated non-exceedance probability via the GP distribution for storm durations. Wave periods were calculated with the derived linear relation between wave heights and periods. Figure 2-6 shows the process of storm generation.

Step 8 – Sea level rise

The SLR was determined at the start of each storm. With the SLR, the upward and landward displacement of the beach profile due to SLR could be determined. Da Cruz only considered the 2.6, 6.0 and 8.5 RCP scenarios. Da Cruz concluded that the SLR projections at the HORS were very similar to the global projections and decided to use the global projections. The effects of subsidence and uplift were excluded, because no data was available to check those effects. The rate of SLR and its acceleration were modelled with an equation described by Nicholls et al. (2011):

$$\Delta SLR = a_1 \times t + a_2 \times t^2 \,, \tag{7}$$

where ΔSLR is the sea level rise since 1990, t the number of years since 2018, a_1 the trend in sea level change, and a_2 the change in the rate of sea level change. Da Cruz changed the origin to 2018.

Da Cruz fitted Equation 7 to the SLR projections. The fitted equation was used to determine what the SLR was relative to 2018. Da Cruz assumed the beach to be stable, thus near equilibrium. Based on this, it was assumed that the beach profile would move upward with SLR, and landward with a distance dependent on the beach slope. The slope was derived from the interval between the water line and water line plus the maximum expected SLR in one year. The maximum SLR was derived from the year with the highest rate, being 2099-2100. The landward displacement of the shoreline could then be calculated with:

$$R_{SLR} = \frac{\Delta SLR(current\ storm) - \Delta SLR(previous\ storm)}{beach\ slope}, \tag{8}$$

where R_{SLR} is the recession due to SLR.

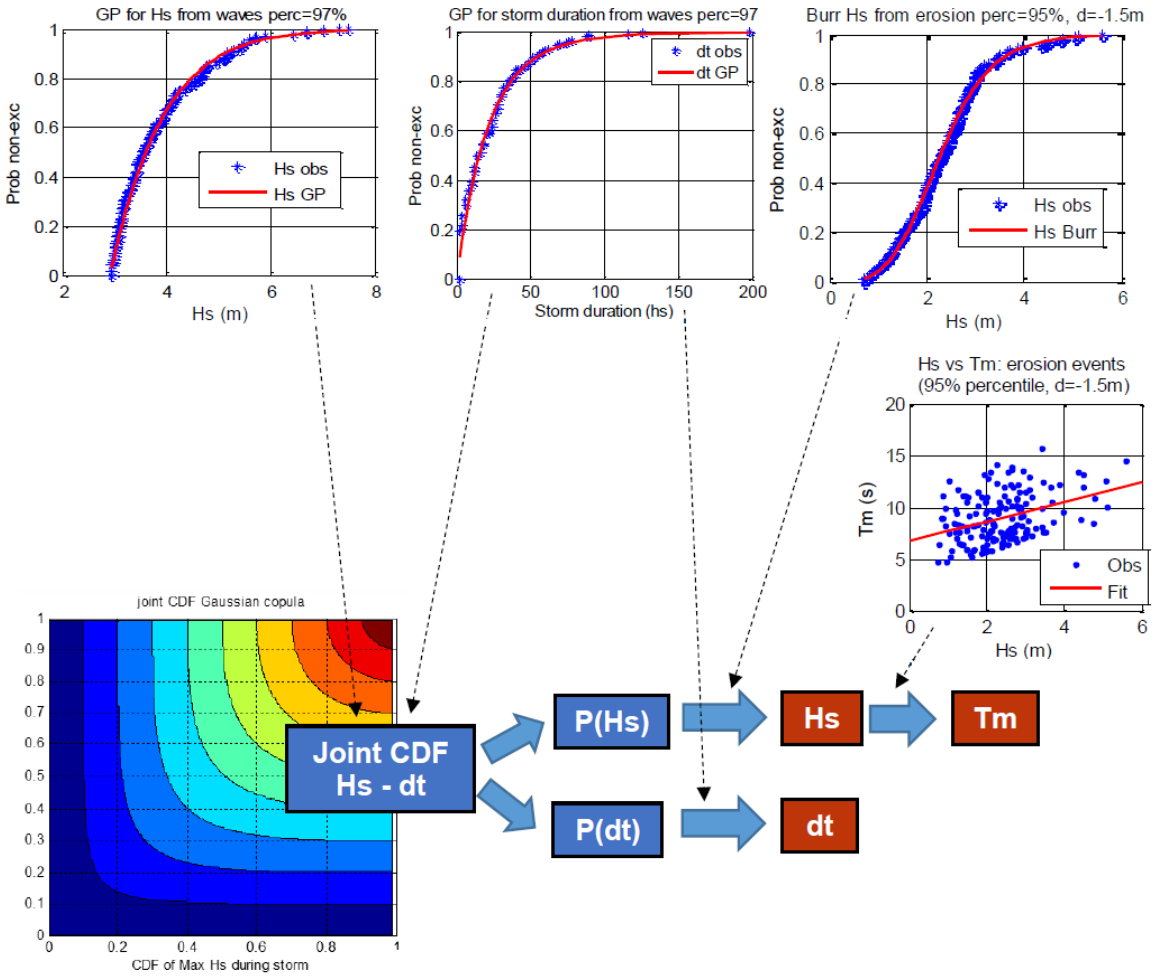

Figure 2-6. Setup for storm generation. Adopted from Da Cruz (2018).

Step 9 – Erosion and recession models with recovery

Erosion model

Da Cruz used the Mendoza-Jiménez model (Mendoza & Jiménez, 2006) for modelling erosion. The assumption central to this model is that an empirical relation exists between significant offshore wave heights and storm durations on the one hand, and erosion volumes on the other hand. This relationship is thought to be linear, with a predictor acting as a parameter summarising the driving forces. Mendoza and Jiménez (2006) analysed three existing predictors (Jiménez, Sánchez-Arcilla, & Stive, 1993; Jiménez, Sánchez-Arcilla, & Valdemoro, 1997) that 'summarise' wave characteristics and beach sediments. These predictors act as coefficient in the linear relation:

$$\Delta V = a \times predictor \times dt + b\,, \qquad (9)$$

with a and b being calibrated parameters, ΔV the beach volume change in m^3, and dt the storm duration. Storm durations were added as Mendoza and Jiménez (2006) found that this addition caused the model to yield better correlation coefficients between wave characteristics and eroded volumes.

This coastal erosion model was successfully used for simulating erosion of dissipative and reflective beaches in the study of Mendoza and Jiménez (2014), and was used in PCR modelling by Dastgheib et al. (2017). The limitations of the model are that it does not include overwash processes, which is crucial if dunes are present, and that the inclusion of hard structures on the beach is not possible. Beach profile change is also excluded from the model. Da Cruz chose to use this model due

to its simplicity. The exclusion of overwash did not have implications for the HORS model, because the dunes at the HORS are too far away from the water line.

Mendoza & Jiménez (2006) used for their model a certain schematisation of the beach. This is shown in Figure 2-7. The cross-section of the beach is divided into two sections: an upper section that erodes during storms, and a lower section that accretes during storms. The transition point between these two sections is the depth d^*.

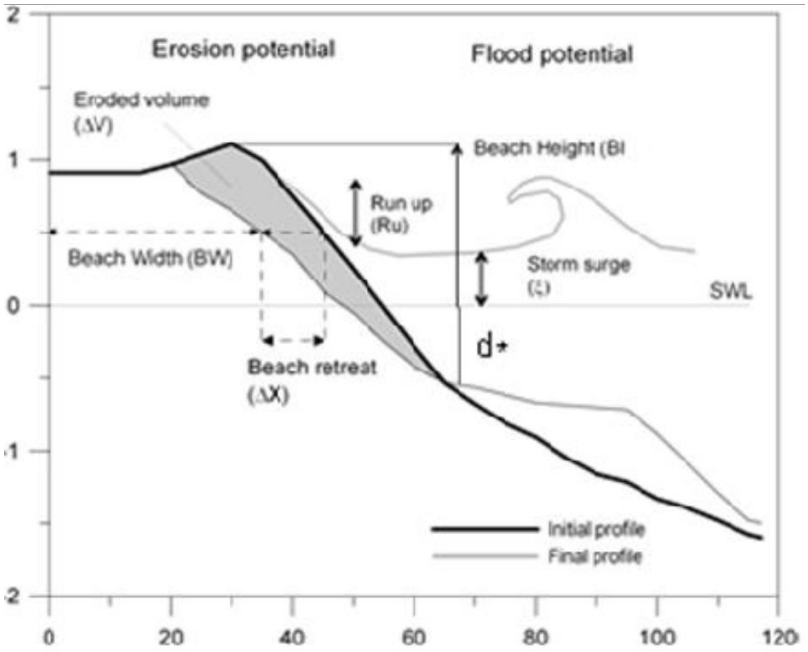

Figure 2-7. A schematisation of the storm-induced beach profile changes, according to the Mendoza-Jiménez model. Adopted from Jiménez et al. (1993) in: (Dastgheib et al., 2017).

Da Cruz (2018) did not find a clear transition depth in her beach profiles. The parameters *a* and *b* were calibrated with multiple setups. This not only involved varying d^*, but also varying the predictor types. Besides, Da Cruz varied the distributions of storm durations and wave heights, by changing the thresholds with which the values were determined. An overview of the final choices is shown in Table 2-2.

Table 2-2. Erosion model setup by Da Cruz (2018).

Erosion event threshold	95th percentile
Wave event threshold	97th percentile
Transition depth d^*	1.5 m
Predictor	P
Parameter *a*	1.482e-6
Parameter *b*	26.95

The P predictor is calculated as follows:

$$P = \frac{H_s^2}{w_s^3 \times T_s}, \quad (10)$$

where H_s and T_s are the offshore significant wave height and period, and w_s is the fall velocity of the sediment. The P predictor was proposed by Kraus, Larson, and Kriebel (1991). w_s of a particle size could be determined from Figure 2-8

An erosion time series was calculated with the generated storm time series.

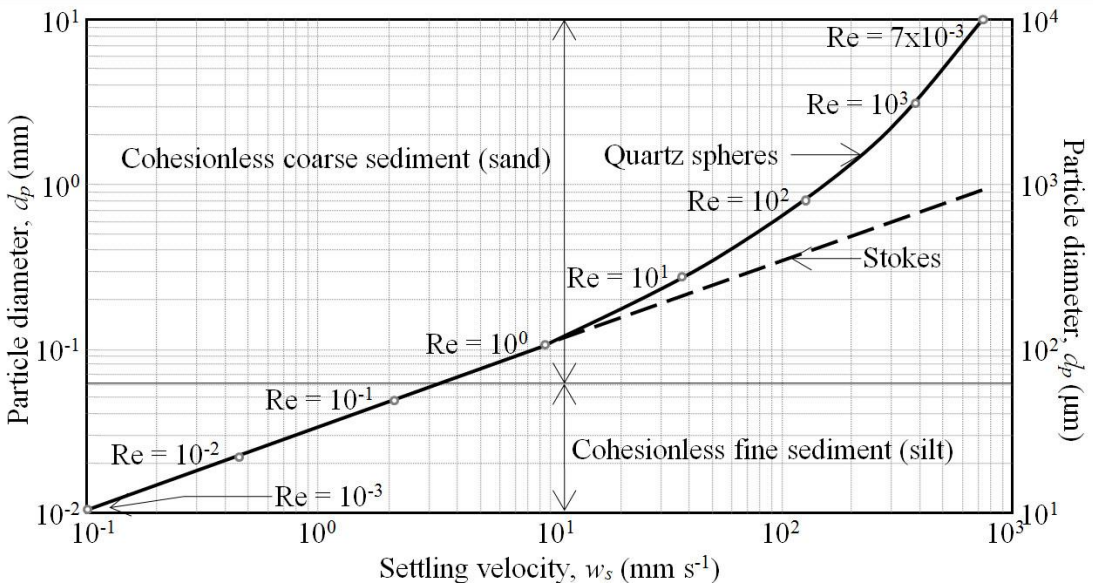

Figure 2-8. Particle diameter as a function of settling velocity for quartz spheres and Stokes law. Adopted from (Mehta, Khare, & Andrew, 2016)

Recession

Beach retreat due to storm erosion could be calculated from eroded volumes via the following expression (Mendoza & Jiménez, 2006):

$$R_{erosion} = \frac{\Delta V}{B + d^*}, \tag{11}$$

where $R_{erosion}$ is the shoreline retreat due to storm erosion, and B the berm height.

Da Cruz found that only a weak correlation was present between shoreline position and beach volume changes in the Hazaki data; when net erosion was observed, occasionally a seaward shift of the coastline was observed. Rather than using Equation 11, Da Cruz proposed to handle these variables as stochastics. A GP distribution was fitted to the observed eroded volumes and a Burr distribution was fitted to the associated observed shoreline movements. The CDFs were joined in a copula of the Gumbel family. The non-exceedance probability of a generated eroded volume was extracted from the fitted GP CDF. With this probability and using the joint CDF, a coupled probability of non-exceedance for shoreline movement was generated. This probability was created with a copula random value generator. The associated value of shoreline movement was then extracted from the Burr CDF for shoreline movement. This recession model also allowed seaward shoreline movement to occur. Non-exceedance probabilities and values for eroded volumes and shoreline movements that were used in the Hazaki copula are shown in Figure 2-9.

Storm gaps

Storm gaps were not pre-generated in the HORS model like the shoreline movements, but generated during the shoreline simulation. Storm gaps described the number of days in between storms. The start date of the storm gap determined the month from which the Poisson distribution was used. The length of the storm gap was determined from the distribution with a random number generator. Each storm gap was indirectly dependent on the previous storm gap. This dependency made it impossible to generate storm gaps outside of a loop. A while loop was used to simulate the storms gaps. This while loop continued with the generation of storm gaps, until the end date of the simulation was reached.

The mentioned monthly Poisson distributions were based on the event rate parameters. The event rate parameter represents the number of events happening in a given amount of time, or the rate of events happening. The monthly observed number of events could not be used as values for the

rate parameters. Some months had a low event rates, which produced large storm gaps that could span over months with high event rates. Observed high event rates during these 'over shadowed' months could then not be expressed. To overcome this problem, monthly rate parameters were calibrated until the number of monthly generated events matched the observed number of events. In the calibration, the monthly rate values were increased or decreased. After each adjustment, storm gaps were simulated and generated monthly rates were compared to observed monthly event rates. Calibration continued until both event rates were considered sufficiently similar.

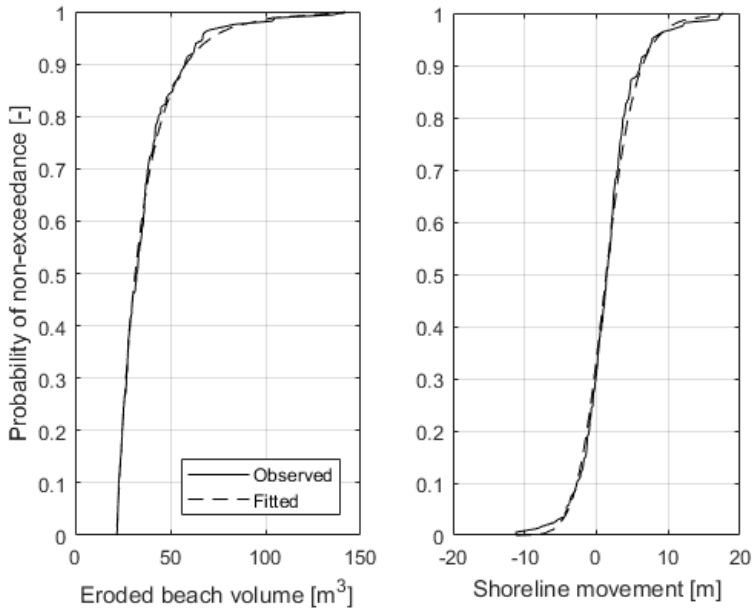

Figure 2-9. Non-exceedance probabilities and values for eroded volumes and shoreline movements that were used in the Hazaki copula (Da Cruz, 2018).

Recovery

Beach recovery was described as the seaward movement of the shoreline in metres per day. Since the recovery rate and the number of days in a storm gap were known, the recovery of the beach or the seaward shoreline movement could be determined. This allowed a beach to accrete further seaward than the profile had been before the last storm. Da Cruz determined the rate of recovery by trial-and-error. Hazaki beach was assumed to be stable. This meant that the location of the shoreline should remain roughly in the same place without SLR. If an ECDF for shoreline movement was made, the exceedance probability of zero movement should be around 50%. Da Cruz found that the beach recovery rate for Hazaki was approximately 4.78 centimetres per day or 17.4 metres per year.

Step 10 and 11 – Determining the shoreline position and total recession

After shoreline movements had been simulated till 2100, the final shoreline position was evaluated. The shoreline before each storm was determined with:

$$Shoreline_{new,before\ storm} = shoreline_{old,after\ storm} - R_{SLR} + recovery\ rate \times storm\ gap \quad (12)$$

The shoreline position after each storm was determined by adding $R_{erosion}$ to (12):

$$Shoreline_{new,after\ storm} = shoreline_{old,after\ storm} - R_{erosion} - R_{SLR} + recovery\ rate \times storm\ gap \quad (13)$$

The final position was then subtracted with the initial coastline position to determine the total recession or displacement of the shoreline. This is illustrated by Figure 2-10.

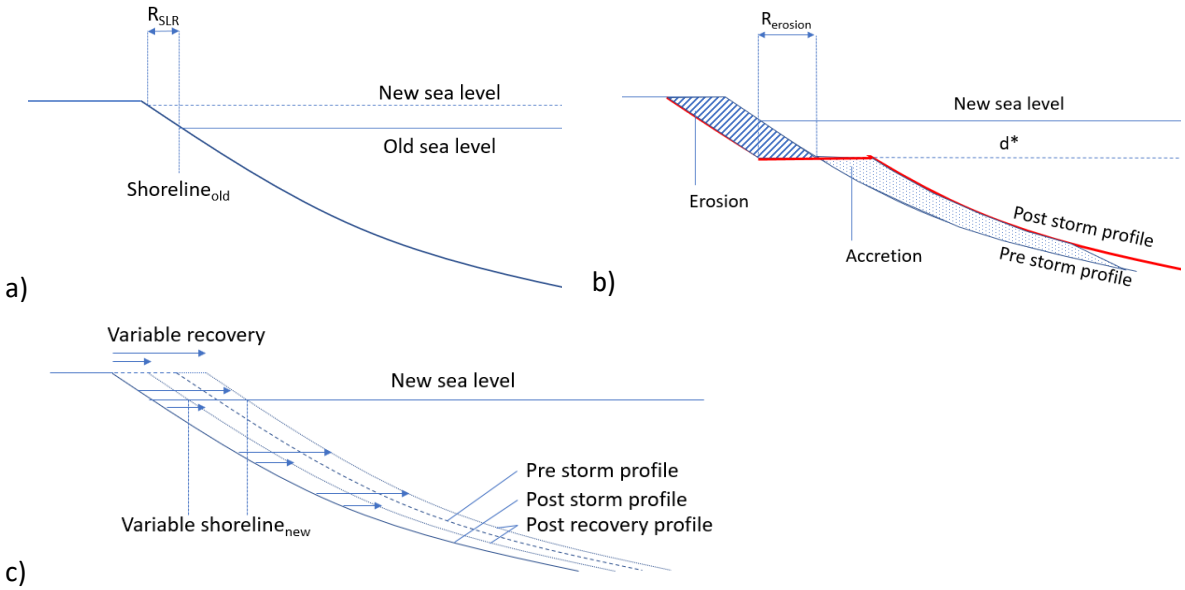

Figure 2-10. Determining the new shoreline position from the old shoreline position. Movement is influenced by (a) SLR, (b) storm erosion, and (c) recovery in between storms.

A downside of the beach evolution modelling approach in the HORS model (Da Cruz, 2018) is that beach profile change is not included. It was assumed that the beach profile will always be the same profile before a storm. If a storm happened only a few days after a previous storm, the beach profile would probably not have recovered. In the model, the beach profile would have regained the equilibrium profile at the shoreline to which the beach had recovered. Storm waves that would have broken on the accreted submerged profile, cause erosion on the superficially recovered beach profile.

Step 12 – Creating exceedance probabilities for recession

In the HORS model, coastline displacement was simulated for three RCP scenarios between 2018 and 2100 simulation for 50,000 times. In these 50,000 runs, storm gaps were generated and shoreline positions were evaluated per storm. The recessions for these simulations had already been calculated before the loop. Instead of repeating steps 7 to 11 as Ranasinghe et al. (2012) proposed, only steps 8, 10 and 11 had to be repeated in the loop. This reduced the computation time significantly, according to Da Cruz (2018).

Da Cruz created ECDFs based on the annual maximum landward position. For every year, the maximum landward shoreline position was determined. This was done for all 50,000 temporal simulations. Thus, for each year an empirical distribution could be made, which showed the maximum landward shoreline positions and the associated exceedance probabilities per year per RCP scenario.

3 Study area selection and data collection

This chapter presents the selection of locations where the PCR model was applied and the data collection needed for PCR application. In section 3.1, the requirements are given that a site had to meet for implementation of the PCR model. Besides, an overview is given of the sites to which field trips were undertaken. Sections 3.2 to 3.5 describe these sites and the conclusions from the fieldtrips. In section 3.6, the final selection of sites is given that were used in this study.

3.1 Requirements

Da Cruz (2018) created a PCR model for the Hazaki beach near the Hazaki Oceanic Research Station (HORS). This site was chosen for several reasons:

1. The abundance of data on wave characteristics, water levels, and daily profile change;
2. The width of the beach;
3. The sandy sediment (D50 < 1 mm);
4. The absence of hard structures on or in front of the beach;
5. The stability of the beach.

These requirements were used for selecting sites to implement the Hazaki PCR model for. Professor Keiko Udo of Tohoku University, Sendai, Japan, recommended a multitude of sites based on data availability. It was checked whether the sites on the list met the requirements. Different checks were done, which are described in the following. Figure 3-1 shows the flowchart for the selection of sites.

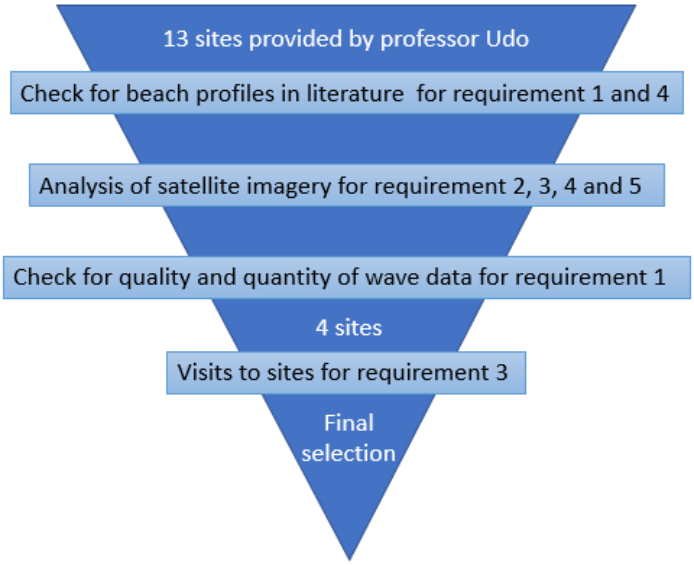

Figure 3-1. Flowchart of the selection of sites based on the requirements.

Beach profiles were provided for some sites in journal papers. The 13 sites were checked for requirements 1 and 4 with this information.

The next step was to analyse the beaches with satellite imagery from Google Earth. These imageries were taken at multiple points in time, thus the evolution of a beach over the years could be observed. The sites were checked for requirements 2, 4 and 5 with this information, and to some extent also requirement 3 was checked.

The final step for the initial selection of the sites was checking for the availability of local wave characteristics and water level data (requirement 1). At most sites, bihourly wave characteristics data (wave height, period, and direction) were available. These data were recorded by the Japanese Nationwide Ocean Wave information network for Ports and Harbours (NOWPHAS) from 1970 on. The

recorded significant wave heights and periods were the most important wave characteristics for this research. These are denoted respectively by H_s and T_s. The Japan Meteorological Agency (JMA) provided hourly water level data, measured since the 1950s. They also provided the measurement datums relative to Tokyo Peil.

The four sites that met requirements 1, 2, 4 and 5 were:

1. The beach near Onahama port;
2. The Tottori sand dunes;
3. The coast along the Yumigahama peninsula;
4. The Yaizu and Shizunami beaches.

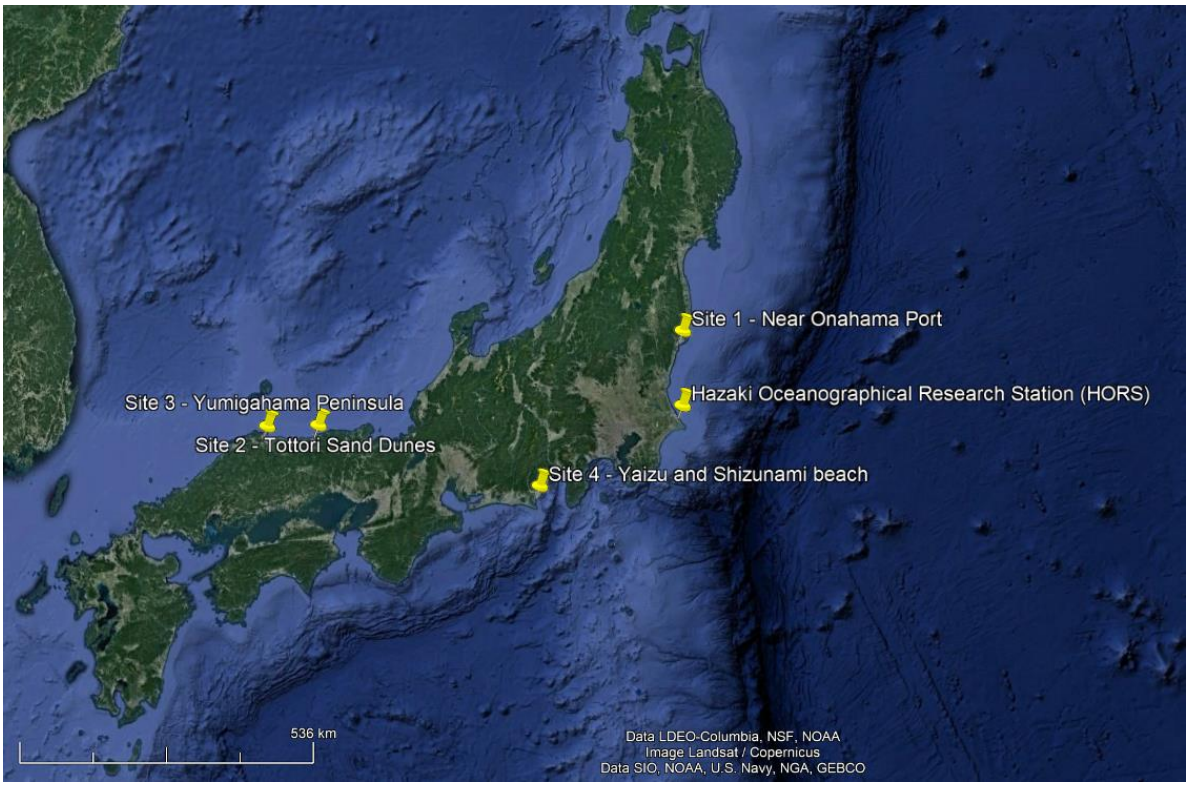

Figure 3-2. Map of Japan with the initial selection of sites, and the HORS. Acquired from Google Earth

To make a final selection for PCR model application, requirement 3 had to be checked. For sites 1, 2 and 4, information was found on the median grain size, but the papers providing this information were dated (site 1) or the location of the sample did not match the target location (site 2 and 4). Fieldtrips were undertaken to sample sediments at the study areas. Every 100 to 200 m one sample was taken at the waterline, and one on the berm or dune foot. Samples usually weighed around 0.4 kg, including water content. After the samples were dried, sieving tests were done with the sieve sizes of 2 mm, 1 mm, .5 mm, .25 mm, .125 mm and .0625 mm.

Besides taking sediment samples during the fieldtrips, it was tried to make a cross-section of the beach above the mean sea water level (MSWL), but this failed for all beaches. Beach width measurements succeeded with the use of a small hiking GPS tracker. Furthermore, visual observations and evaluations of the profiles were made. Beach angle measurements were recorded with a phone application at the water line. Observations were done every 100 to 200 metres along the beach. People on the beaches were also interviewed about local storm characteristics and beach change, but this failed due to a lack of knowledge of the Japanese language.

3.2 Site 1 – Near Onahama port

3.2.1 Description

The beach is located at the mouth of the river Sama. This river supplies sediment to this beach (Abe, Fukuyama, Sato, Isobe, & Kumagai, 2002). The beach has undergone numerous changes, which could be seen in Figure 3-3. The river Sama used to turn north-east at the back of the beach, and after flowing in between the beach and the sea wall at the back of the beach, the river would turn south-east after several hundred metres. There, the river flowed out to sea (Figure 3-3 a and b). Because dams were built upstream in the river Sama, the river flow was under heavy control, resulting in a stable beach. The river layout on the beach changed in 1984. A power station bordering the river and the sea required another flow route of the river. A groyne was placed were the river previously had turned east along the sea wall, and it forced the river to flow out directly into the sea (Figure 3-3 c and d). The previous river mouth persisted, because it was fed with cooling water from the power plant. Three sections of beach existed after the placement of the groyne: a western, a middle and an eastern section. The western section is characterised as a sand bank, partly barring the mouth of the river Sama. The middle section is protected on its south-western end by the mentioned groyne, and on its north-eastern end by an outlet structure of the power plant. The eastern section is situated next to the outlet structure till the cliffs at the northern end.

On March 11th 2011, the Great East Japan earthquake happened. Ensuing the earthquake with its epi-centre of the coast of the Sendai prefecture, a major tsunami crashed against the coast. At site 1, the western part of the beach was completely eroded, and the other sections were heavily eroded (Figure 3-3 d). In the following years, it seemed that the beach had recovered itself to the pre-tsunami lay-out. The beach was less wide than before (Figure 3-3 f, g and h). Information of the beach profile was acquired from Abe et al. (2002). They measured the cross-section at the red line shown in Figure 3-3 c. It seemed that the contemporary beach was similar to the pre-tsunami beach. It was then assumed that the cross-sections of the pre-tsunami beach could be used for the contemporary beach.

3.2.2 Fieldtrip results

The fieldtrip produced the following observations of the beach. A continuous slope of 3° was present towards a height of 2 m. Behind this point the beach was almost flat. After the 'highest' point on the beach, the beach sloped down with a very small gradient toward the ponds and the sea wall at the back of the beach. Grass and other vegetation were only seen within 50 m of the sea wall. Scarps were seen along the beach 200 to 250 m before the water outlet. This was at 600 m from the point where the historical cross-section was taken. This difference along the coast could have been created by the partial sheltering of cliffs and breakwaters of Onahama port from waves from the east to north-east. On the southern side of the outlet, it seemed that the beach was higher, even featuring some taller vegetation than grass. The river did not seem to have a high discharge and was thought to be highly influenced by the tides. The photos in Figure 3-4 give an impression of the beach.

The D50 found at site 1 was 0.22 mm, which meant that the beach was sandy. This satisfied requirement 3. The sieving curves are given in Figure 3-5. It was observed that from the north-eastern end of the beach towards the water outlet the sediment became coarser. In Figure 3-6 and Figure 3-7, an overview is given of the direct surroundings of the beach and the locations on the beach where the samples were taken. The red line along the waterline was the waterline as recorded on the 26th and 27th of May 2018. The red lines perpendicular to the waterline are the dry sections of the beach as recorded on those dates.

a) March 1966

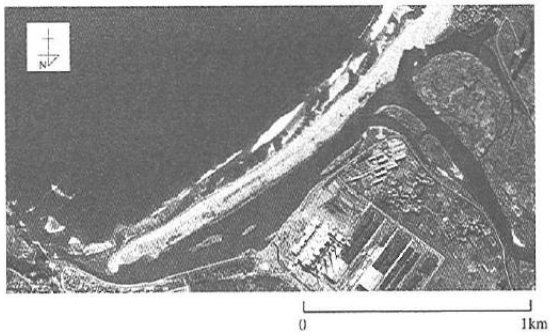

b) March 1976

c) February 1998

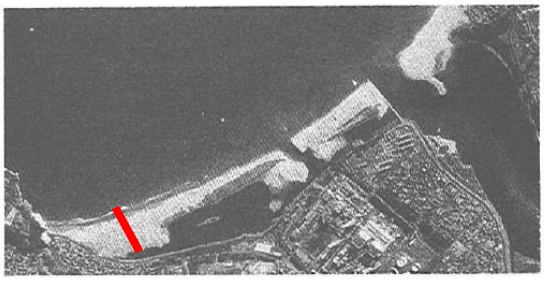

d) April 2005

e) March 12th 2011

f) February 2012

g) March 2014

h) January 2015

Figure 3-3. Aerial overviews (with dates) of site 1. a) to c) are adopted from Abe et al. (2002), and d) to h) are acquired from Google Earth. In c) is marked with the red line where the cross-section of the beach profile was taken.

Figure 3-4. Photos of the beach at site 1. The left-hand photo shows the flatness of the beach. The red line gives an impression of the profile. The right-hand photo is taken at the back of the beach, showing water and the seawall.

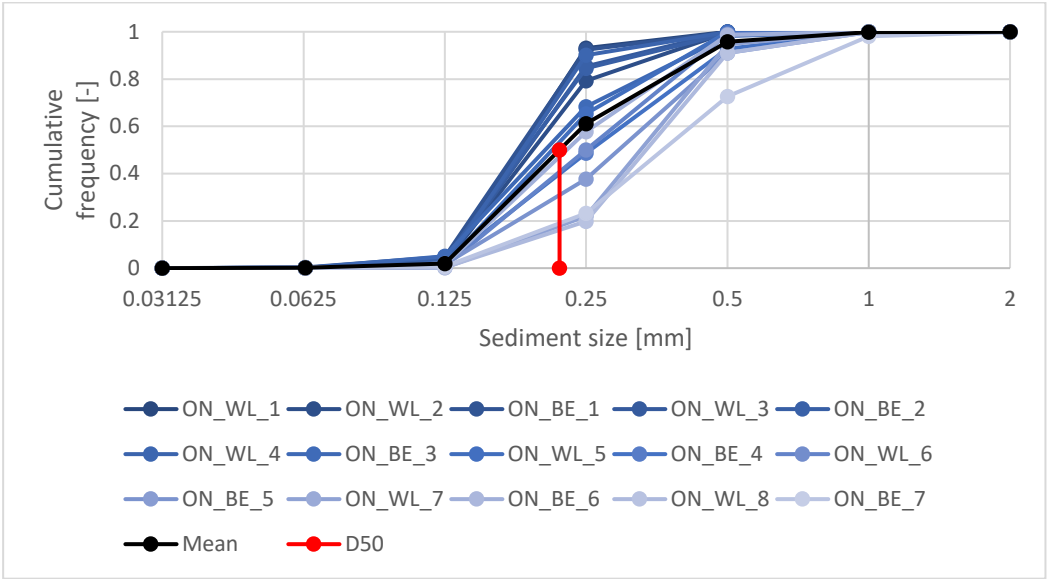

Figure 3-5. Sieving curves site 1. Samples are coloured with different shades, going from the south-westernmost sample (darkest) to the north-easternmost (lightest). In black is the average sieving curve given.

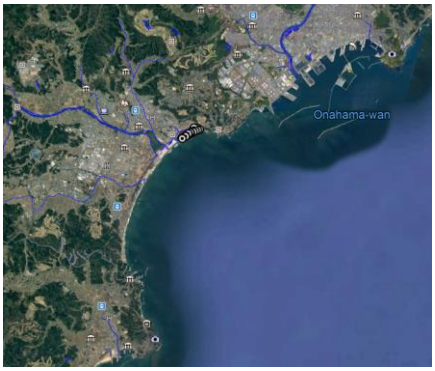

Figure 3-6. Overview direct surroundings of site 1. Acquired from Google Earth

Figure 3-7. Sampling locations and walking paths along the beach. This satellite image was taken in March 2014 and was provided by Google Earth.

3.3 Site 2 – Tottori sand dunes

3.3.1 Description

The Tottori sand dunes formed over multiple millennia to the east of the mouth of the river Sendai, near the city of Tottori. This beach faces the Sea of Japan. Toshima (1970), Yasumoto, Uda, Matsubara, and Hirano (2007) and Shibutani, Kuroiwa, and Matsubara (2016) reported changes of the local coastline. Before 1970, the coastline was relatively uninterrupted by hard structures. In the 1960s, Tottori port was developed and larger breakwaters were constructed around the port and river mouth. The supply of sand to the Tottori sand dunes was severely hindered by this development. It was concluded that beach sections in front of the dunes were eroding (Yasumoto et al., 2007). This conclusion was made based on the comparison between bathymetries from 1947 and 2005, and based on the comparison of aerial photos. Toshima (1970) also concluded that the dunes were eroding. In 2005, a nourishment project was started. Sand was dredged from Tottori port and a fishing port to the east of Tottori, and deposited near the erosion sites at offshore and backshore locations (Shibutani et al., 2016). Two major injections happened in 2010 and 2011. Slight recovery of the beach was observed (Shibutani et al., 2016).

It was concluded that the beach was not stable without nourishments. This undermined the assumption for using the PCR model that the beach should be stable (requirement 5). Nevertheless, from Shibutani et al. (2016) it was seen that the beach was stable with the nourishments. If it was assumed that these nourishments would continue in the future, this beach could be considered to remain stable. In the cross-sections of the beach profiles (Toshima, 1970), newer measurements showed a retracted coastline when compared to the older observations. Only four cross-sections were provided between 1968 and 1969. These profile measurements predated the nourishment programme.

Another problem was the fact that Toshima (1970) provided for cross-sections of both the above and under water sections, except at the actual dunes (point 1 and 2 in Figure 3-8). This was resolved by comparing the sieving curves.

Figure 3-8. Overview of the Tottori sand dunes coastline. A satellite image from May 2017 of Google Earth is overlain with the study area map of Toshima (1970). The numbers indicate where in the research the profiles were taken. The red line indicates the most prominent dune ridge.

3.3.2 Fieldtrip results

The beach width along the Tottori beach varied by a few metres. Also the extent of vegetation varied in longshore direction, with the dune toe of the tallest dune being completely free of vegetation. The beach profile along the shore was relatively constant, but differed at the back of the beach due to different dune built-up behind the beach. Dune shapes were present where historical profiles were taken (points 3 to 10 in Figure 3-8), and had steep sides due to erosion. The dunes were almost mistaken for a large scarp. The dune crests at these points were completely overgrown.

The slope along the beach differed only slightly. Angles between 7° and 14° were measured, and as maximum an angle of 27° was observed. Along this beach, beach cusps were observed. This feature explained the variation in angle, since at the horns the angle would be steeper than at the embayments. The beach along the actual dunes and the beach where the historical profiles were taken (points 4 to 10 Figure 3-8) was similar, except for the built-up behind the beach. At the bottom of the swash zone, a small threshold was observed, where the waves collapsed upon coming into the swash zone. The swash zone was sloped with the mentioned angles until the berm crest, where the beach profile transitioned via a concave curve to a near flat profile towards the dune foot. Sometimes, the transition was a small sharp upstanding edge. The photos seen in Figure 3-9 give an impression of the beach.

Figure 3-9. Photos of the beach at site 2. The photo on the left is taken closer to the location of the historical profiles when compared to the photo to the right. This photo was taken in front of the dune ridge. The red lines give an impression of the profile.

Twice a boat was seen unloading sand just in front of the coast. This was probably part of the offshore nourishment project for the beach reported by Shibutani et al. (2016). No instruments were available to measure the distance between the boat and the beach .

The locations of the samples are shown in Figure 3-10. The red line along the waterline represents the waterline on the 29th of May 2018. The lines perpendicular to the waterline are the beach widths until the dune feet.

The D50 was 0.44 mm. This satisfied requirement 3 (sandy beach) for site 2. It was seen that the sieving curves for samples taken in front of the dunes resembled the samples taken near the historical profiles (Figure 3-11). It was thus assumed that the submerged part of the beach profile at point 4 (Figure 3-8) could be used as the submerged beach profile in front of the actual dunes. The submerged beach profile was combined with the above MSWL beach profiles of the actual dunes. This resulted in a complete beach cross-section at the actual dunes.

Figure 3-10. The locations of the samples projected on a May 2017 satellite image from Google Earth. The red lines indicate the path walked while acquring the samples. Sample locations 1 to 6 were in front of the dunes, and in between locations 6 to 9 some of the historical profiles were taken presented by Toshima (1970).

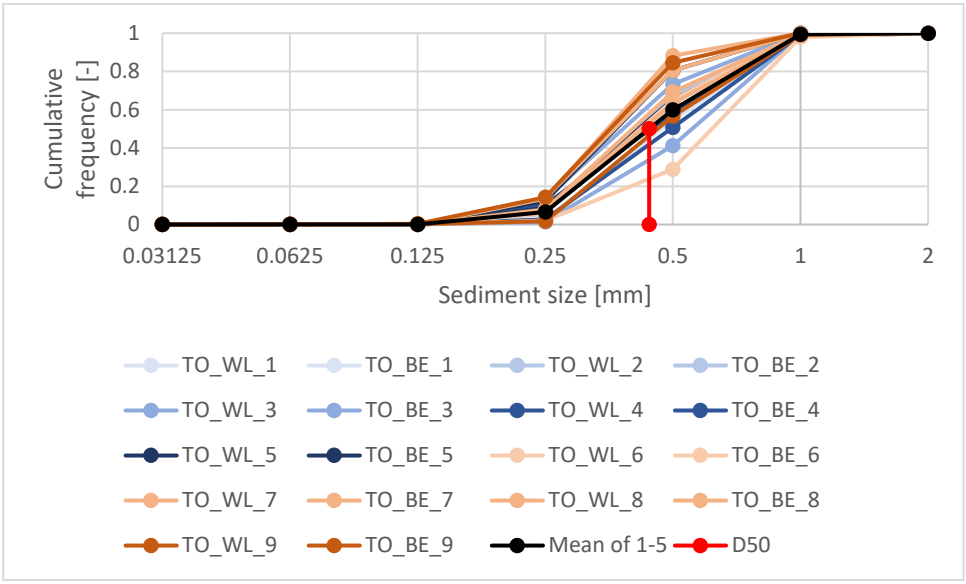

Figure 3-11. Sieving curves site 2. The blue lines indicate samples taken in front of the dunes. Orange lines indicate samples taken at the historical beach profiles, to the east of the dunes. The shading describes the relative position between west and east. The lighter a colour, the farther west the sample is taken; the darker a colour, the farther east. The black line is the average sieving curve for the samples taken in front of the dunes (samples 1 to 5).

3.4 Site 3 – Yumigahama

3.4.1 Description

The Yumigahama peninsula grew over multiple millennia as a sandspit from the mouth of the river Hino (Kakani & Sadakata, 2006). This river is located to the south of the peninsula. The peninsula is a flat plain with a maximum height of 5 m above mean sea level that provided space for buildings and agriculture. A beach is present along the whole peninsula, except for the parts where ports had been developed. The peninsula is sheltered from waves of the Sea of Japan by another peninsula and islands off the coast. The result is that waves from the Sea of Japan could only approach the beach directly when coming from the North-North-East to North-East.

Beach profiles were acquired from a paper discussing the coastline change along the peninsula (Kuroiwa, Matsubara, Fujimoto, & Ichimura, 2013). Only three cross-sections were provided. These were the average profiles from annual measurements (1986-2011). The goal of the paper was to give estimates for coastal retreat with the Bruun Rule. It was observed that over the years accretion took place at the northern end, whereas erosion took place at the southern end (Kuroiwa et al., 2013). Kakani and Sadakata (2006) also observed this coastline evolution in their work. They mainly discussed the erosion at the southern end of the peninsula, near the mouth of the river Hino. Due to human activities, sediment supply from the river to the peninsula had reduced. Since the net longshore transport happened from south to north, the southern end of the peninsula suffered from erosion. Breakwaters were built in response. Some were quickly undermined by scour. Subsequently, sections of the peninsular beach north of the breakwaters are eroding. Sections further north are still accreting. One of the three cross-sections provided by Kuroiwa et al. (2013) is located in the transition zone from erosion to accretion and is assumed to be stable. The beach section linked to this cross-section is then also assumed stable.

Figure 3-12. Overview of the Yumigahama peninsula. The section of interest is indicated with the black and white markers. Acquired from Google Earth.

3.4.2 Fieldtrip results

The hinterland of this site is a flat plain. That is the only similarity it shares with site 1. The plain is more elevated at site 3 and there is no seawall separating the beach from the hinterland, only a small strip of coastal forest. In front of this forest, a flat back beach is present with low vegetation. The beach is cut by multiple small water flows flowing out to the sea.

Along the coastline, a relatively constant beach profile was observed. At the seaward end of the swash zone a threshold could be observed, similar to Tottori beach. Approximately at this point the waves collapsed. Gravel was occasionally seen atop the sand at this location in the profile. Landward of this point was a sandy slope observed with an angle of approximately 15° toward the top of the swash zone. In some cases a flat terrace was observed at the top of the swash zone of several metres wide. This was followed by a steep angled slope, and subsequently a less steep slope towards the back beach. At one section along the coast a rather abrupt transition from flat to steep was observed. Based on visual observation, it could be said that along the analysed extent of beach the sediment got coarser from north to south. The photos in Figure 3-13 give an impression of the beach.

Figure 3-13. Photos of the beach at site 3. The photo on the left showcases a scarp-like structure, whereas the photo on the right shows a much smoother transition. The red lines give an impression of the profile.

The weather was calm on the day that the beach measurements were taken (April 30th 2018), with only little waves hitting the coast. In the afternoon, a thunderstorm was drifting across the bay, causing a strong landward wind. This generated larger waves. These waves did not change the beach profile significantly. The only effect was that the swash zone became slightly less steep.

The D50 of this site was 0.44 mm. This meant that the beach was sandy and satisfied requirement 3 for site 3. The sieving curves are shown in Figure 3-14. Figure 3-15 shows the locations of the samples. It was observed that on top of the berm the sediment distribution was different from the sediment distribution at the waterline. The sediment on top of the berm was finer than the sediment at the waterline. The difference in sediment size increased towards the south of the section.

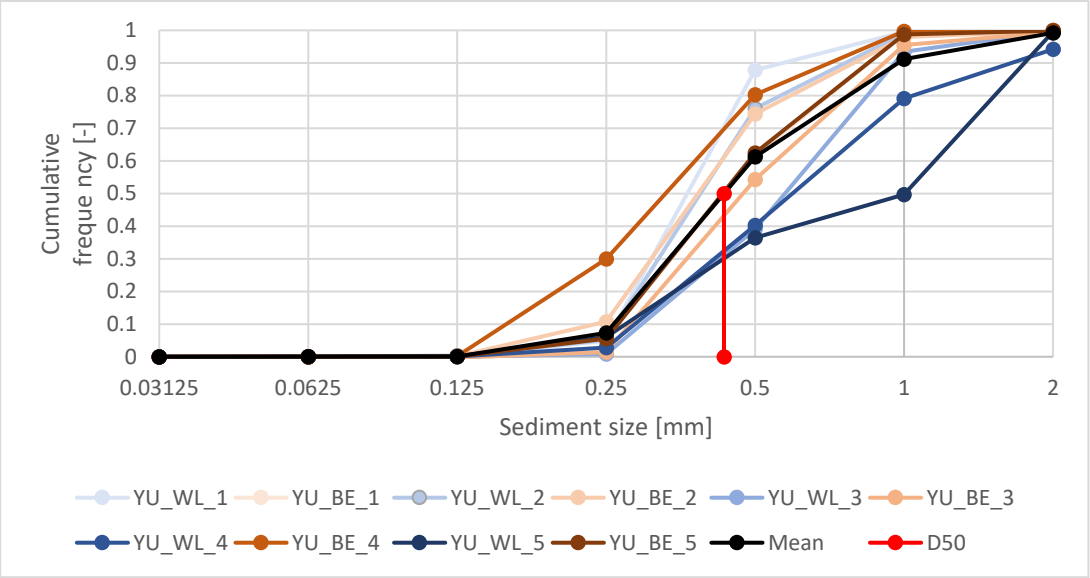

Figure 3-14. Sieving curves site 3. The blue lines represent samples taken at the waterline. The orange samples represent samples taken on the berm. The shading of the colour depends on where the sample was taken; the lightest shades are the northernmost sampling locations, and the darkest the southernmost. The mean of all samples is represented by the black line.

Figure 3-15. The locations of the samples projected on a June 2017 satellite image acquired from Google Earth. The red lines are the paths walked during the sampling.

3.5 Site 4 – Yaizu and Shizunami beaches

3.5.1 Description

The beaches near Yaizu and Shizunami are beaches located near the river Ooi on the west side of Suruga Bay. These beaches are sections of a continuous strip of beaches, that is cut up by minor river outlets and hard structures. Saito and Kosuge (1988) reported on the sediment distribution along the coast in the bay, as well as on the bathymetry of the bay. They reported that the floor of the bay is deep enough for oceanic waves to enter the bay unperturbed. These waves distribute sediment coming from the river Ooi and other minor rivers over adjacent beaches. The coastline section supplied by the river Ooi is divided by the same river in a distinct northern and southern area. Close to the mouth of the river Ooi, different coastal protection structures are present. At the northern (Shizunami) and southern (Yaizu) ends of the beach no structures are present, except for a seawall at the back of the beach. These sections were of interest for this research, as they satisfied requirement 4.

The profiles for the beach were provided by Mamoru, Takami, Kaoka, Oishi, and Yamamoto (1991). They measured the profiles at many sections along the coast and published in their paper profiles for only two sections, located close to the mouth of the river Ooi, which were also dated. Besides, from the paper it was seen that the sediments along the coast were quite coarse, as towards the mouth of the river Ooi a sediment size increase towards 20 mm was reported (Saito & Kosuge, 1988).

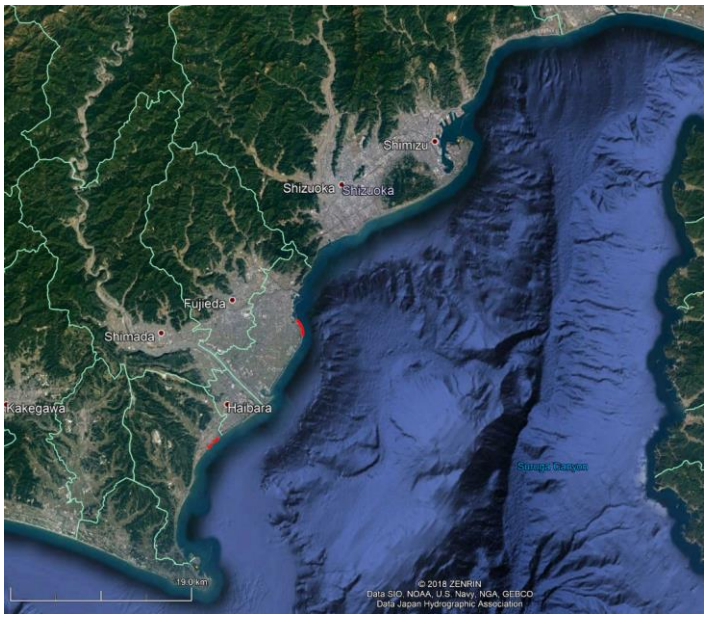

Figure 3-16. The Suruga bay, with the location of the Shizunami beach (northern red line) and the Yaizu beach (southern red line). Acquired from Google Earth.

3.5.2 Fieldtrip results

3.5.2.1 Shizunami beach

Shizunami beach is a beach south of Yaizu on the Suruga bay. It is directly supplied with sediment from the rivers Katsumata and Sakuchiya. A groyne separates the beach from the river Katsumata. Furthermore, the beach is bisected by a groyne approximately halfway the beach. It was observed that the two subsections of beach had different sediment sizes. The profiles of the beaches shared some features: 1) the presence of a submerged bar in front of the beach; 2) the presence of a continuous slope from the swash zone to the berm crest; and 3) the presence of beach cusps, both in the swash zone and along the berm crest.

The section analysed first was the section south of the groyne. The top layer was sandy, but when one dug one or two centimetres, sublayers containing a mix of gravel and sand were reached. Gravel was also seen on the surface in some places on the beach. It was sometimes seen at horns of small beach cusps in the swash zone. Gravel was mostly observed higher up the beach, on the berm. These large heaps of gravel were probably the result of storms or large waves, that probably also created the large beach cusps along the berm crest.

The second section had a sandy top layer between the swash zone and the berm and behind the berm. Occasionally stones were also seen. The swash zone had a mix of sand and mostly gravel. On the berm crest, only gravel and stones were observed. Figure 3-17 shows photos adding to the descriptions of the beach.

Figure 3-18 and Figure 3-19 show respectively the sieving curves and locations per sample. It is seen in Figure 3-18 that indeed the sediment is too coarse to be used in the research, because the D50 of most samples represented very coarse sand or gravel (>1mm) instead of fine sand.

Figure 3-17. Photos of Shizunami beach. The left-hand photo shows the beach to the south of the groyne on the beach, and the right-hand photo shows the beach to the north of the groyne. The red lines give an impression of the beach profile.

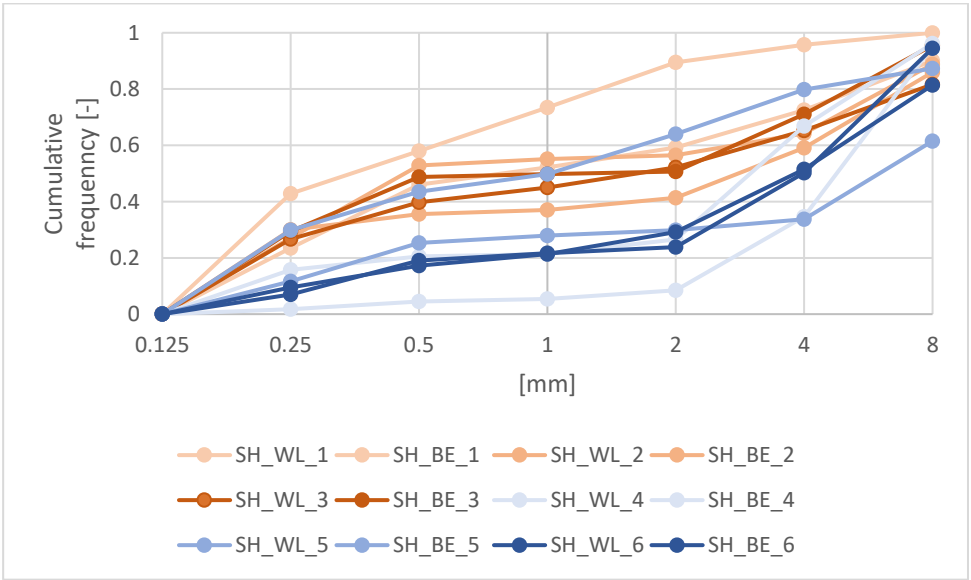

Figure 3-18. Sieving curves Shizunami. The lines describe samples taken to the south of the groyne, blue lines describe samples taken to the north of the groyne. The darker a shade, the more to the north a sample is taken.

Figure 3-19. Locations of the samples for Shizunami beach, projected on a January 2018 satellite image acquired from Google Earth. The red lines indicate the paths walked while sampling.

3.5.2.2 Yaizu beach

The coastal town of Yaizu has an extensive coastline that is mostly protected by breakwaters or other hard structures on and/or in front of the beach. The section of beach that only has a sea wall at the back of the beach is bordered by the Yaizu port in the north and by the section of the beach with hard structures in the south.

Sediment became less well sorted from north to south, because gradually more sand was seen in the swash zone. Gravel and stones dominated along the whole beach. Results from previous storms were well observed along the beach, because the beach sloped rather steeply to one or multiple berms. From the top berm, a downward slope towards the back beach was present. From the back beach till the sea wall fine gravel and sand was present with some stones. Figure 3-20 adds to the description of the beach.

Figure 3-20. Photo of Yaizu beach. The red line gives an impression of the beach profile.

Sediment samples were not taken. It would have been unrealistic to take samples of 400 grams, because the stones would have individually already weighed several hundred grams. However, pictures were taken that showed the sediment with a tapeline.

3.6 Conclusions

The final selection with the available data is presented in Table 3-1, together with the sources of the data used in the research. The Yaizu and Shizunami beaches were not selected, since the sediment on those beaches was too coarse for them to qualify as sandy beaches.

Table 3-1. The final beach selection with data sources.

Site	**Wave data (NOWPHAS)**	**Water level data (JMA)**	**Beach profiles**		**Median grain size D50 [mm]**
			Authors	Most recent observation	
1 – Near Onahama port	1980-2015	From the 1950s till 2018	Abe, Fukuyama, Sato, Isobe, and Kumagai (2002)	November 1998	0.22
2 – Tottori sand dunes	1979-2015		Toshima (1970)	January 1970	0.44
3 – Yumigahama peninsula	1996-2015		Kuroiwa, Matsubara, Fujimoto, and Ichimura (2013)	2011	0.44

[This page is left intentionally blank for layout purposes.]

4 Applicability of the Hazaki model

To know which parts of the PCR methodology at Hazaki could be used for PCR modelling at the study areas, a data analysis was done to compare Hazaki data and study area data. The analysis was done on two topics: 1) the influence of water levels on the relation between waves and beach change (section 4.1), 2) the (dis)similarity of the wave climates and beach structures at the HORS and the target locations (sections 4.2 and 4.3).

4.1 Influence of water levels

Da Cruz took only wave characteristics into account during storms, and excluded the influence of water levels. This section features the results shown of a short analysis of the relation between wave height plus water level and beach changes. The conclusion was that water levels had no influence and consequently, that they were not used in the rest of the research.

Hourly water level data and bihourly wave data were available for the HORS. A time series of bihourly water levels was created by determining the maximum of every even and following odd hour and recording this maximum for the even hours. These water levels were added to the wave heights that were observed at the same time. This time series is referred to as the water surface height time series. Da Cruz's MATLAB script could be used by replacing the wave heights with surface heights.

In Table 4-1, the Pearson correlation coefficients of relations are shown that Da Cruz had analysed. The negative values were expected, because higher waves were assumed to cause negative beach volume change and landward shoreline movement. Positive correlation coefficients were expected between recession width and wave heights. It is seen that the correlation coefficients with surface heights were similar or closer to zero when compared to their wave height counterparts. The coefficient was even positive when the surface heights were correlated with the volume changes thresholded with the 95th percentile. Correlation coefficients were slightly higher when surface heights were compared with the recession widths than was the case for wave heights.

Table 4-1. Pearson correlation coefficient values. Key: Hs = wave/surface heights; ΔV = volume change; R = Recession; /date = period of recorded values; extreme # = 95th percentile threshold.

	Wave heights	**Surface heights**
Hs – ΔV /year	-0.11	-0.10
Hs – ΔV /Jan-Apr	-0.03	-0.01
Hs – ΔV /May-Aug	-0.01	0.01
Hs – ΔV /Sep-Dec	-0.11	-0.09
Hs – extreme ΔV	-0.24	-0.24
Extreme Hs – ΔV	-0.02	0.06
Hs – R	-0.13	-0.13
Hs – extreme R	0.16	0.18
Extreme Hs - R	0.05	0.06

The beach volume changes in this analysis were measured between two points, being a point 60 m landward of the waterline and a point 155 m seaward of the waterline. Da Cruz did not vary this distance. In this research, the distance was varied. The correlation coefficient between wave/surface heights and volume changes (thresholded with the 95th percentile) was taken as the objective variable in the optimisation.

For both relations, it was found that correlation was best if the beach volumes were taken between the points 20 metres landward of the waterline and 100 metres seaward of the waterline. The found correlation coefficients between beach volume change and wave height, and beach volume change and surface height were both -0.36. This was better than -0.24 (see Table 4-1), but still described only a weak correlation.

4.2 Wave climate comparison

No similarities in wave climate were assumed to exist between the study areas on the Sea of Japan (sites 2 and 3) and the HORS, as the latter faces the Pacific Ocean. Site 1 (near Onahama port) borders the Pacific ocean and is located in relative proximity to the HORS (beeline 120 km). It was decided to check the wave similarity. This was done by comparing the wave characteristics (height, period and direction) of both beaches for the same dates.

Wave climate at site 1 shared similar features with the wave climate at Hazaki beach, because both data sets had extremes of 7 m wave heights and extremes happened at approximately the same time (see Figure 4-1a). Both data sets though included gaps of varying width. It was found that the wave heights and directions for the same dates had a correlation coefficient of respectively 0.74 (Figure 4-1b) and 0.64 (Figure 4-1c). Subsequently, dates were determined at which wave heights at Hazaki exceeded the 97th percentile threshold. Waves corresponding to these dates were extracted from both the Hazaki and the Onahama wave time series. When wave heights of these new time series were correlated, the correlation coefficient reduced to 0.51.

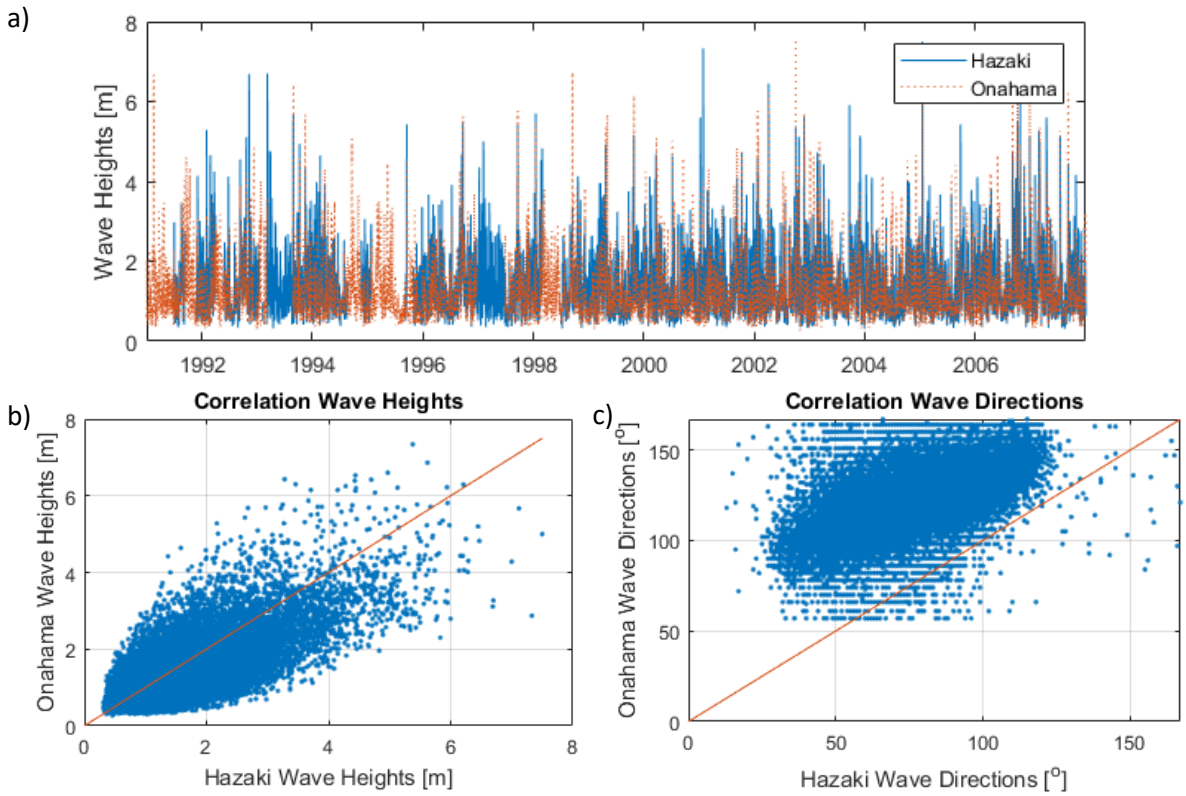

Figure 4-1. Comparison between Hazaki and Onahama. The time series were plotted a) in time (wave heights), and against each other with b) wave heights wave directions and c) wave directions (with north being 0°). The red lines in b) and c) represent the line on which the points should be if the values of both locations would be exactly equal at the same time.

In Figure 4-2, the comparison is shown based on wave direction. It is seen that angle of wave approach for the two locations was quite different (approximately 45^{O}). The waves approached Hazaki beach perpendicularly, whereas the waves approached Onahama beach under an angle. This may be explained by the fact that Hazaki beach is oriented towards the Pacific Ocean, whereas the perpendicular of site 1 was oriented south-east along the coast of Japan. Da Cruz (2018) reported that a distinction could be made between the waves based on direction. Waves from the north-east were mainly generated from extratropical cyclones. Waves from east-south-east to north-east were associated with typhoons. Erosion events were mainly observed during typhoons. Although site 1 was

sheltered from extratropical storms according to these findings, it was not sheltered from typhoons. This meant that when erosion-causing, typhoon-related waves reached the HORS, similar erosion-causing, typhoon-related waves reached site 1.

The wave climates at the HORS and site 1 showed similarities, but were not the same. The correlation coefficients did not show a strong correlation (Figure 4-1), and wave directions were quite different (Figure 4-2). The wave climate at the HORS was not copied to site 1. Instead, the dates at which the erosion events happened at the HORS were used for extracting storm events at site 1. In conclusion, it was assumed that the storm dates were the same, and that the storm wave characteristics were not the same.

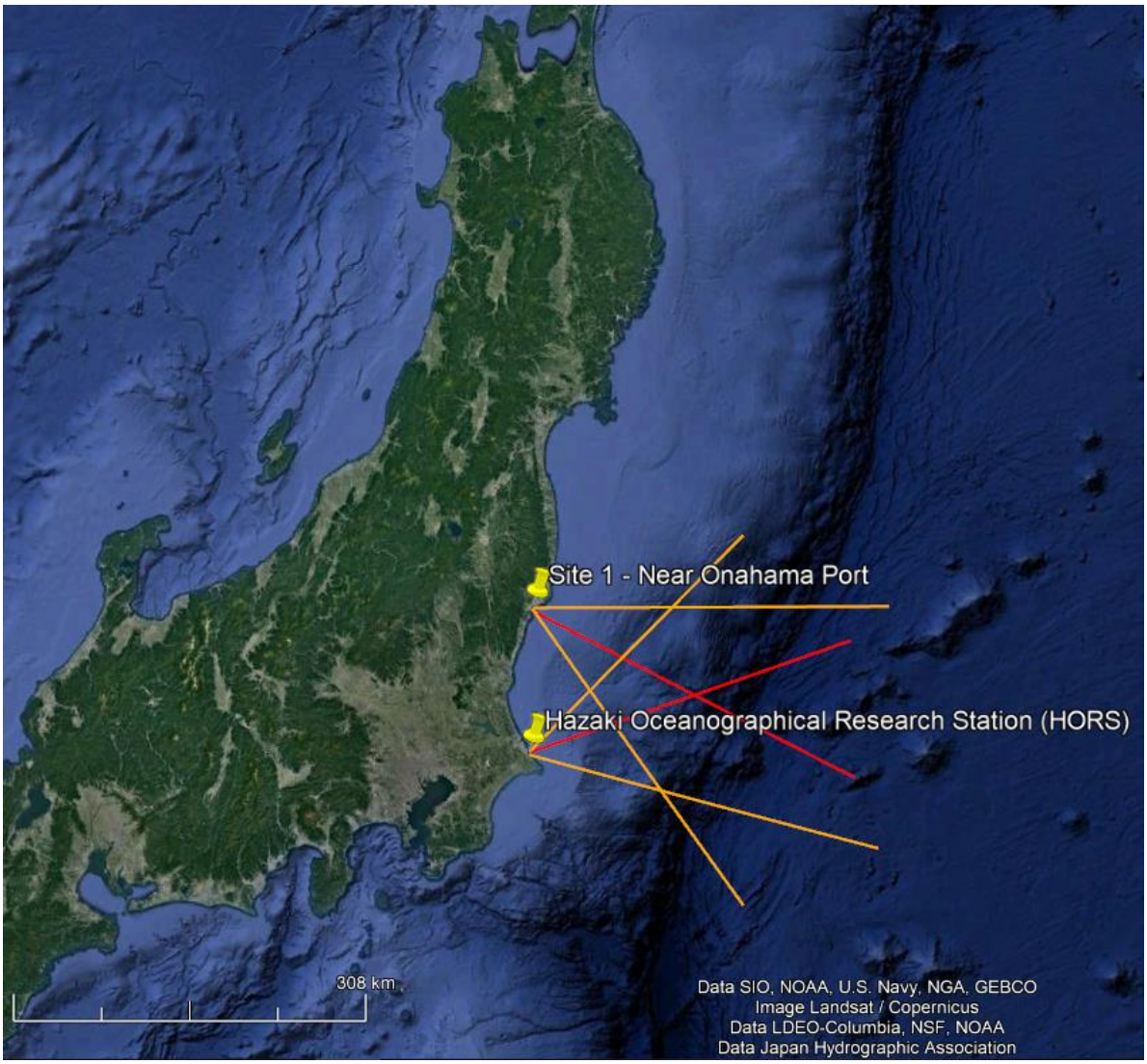

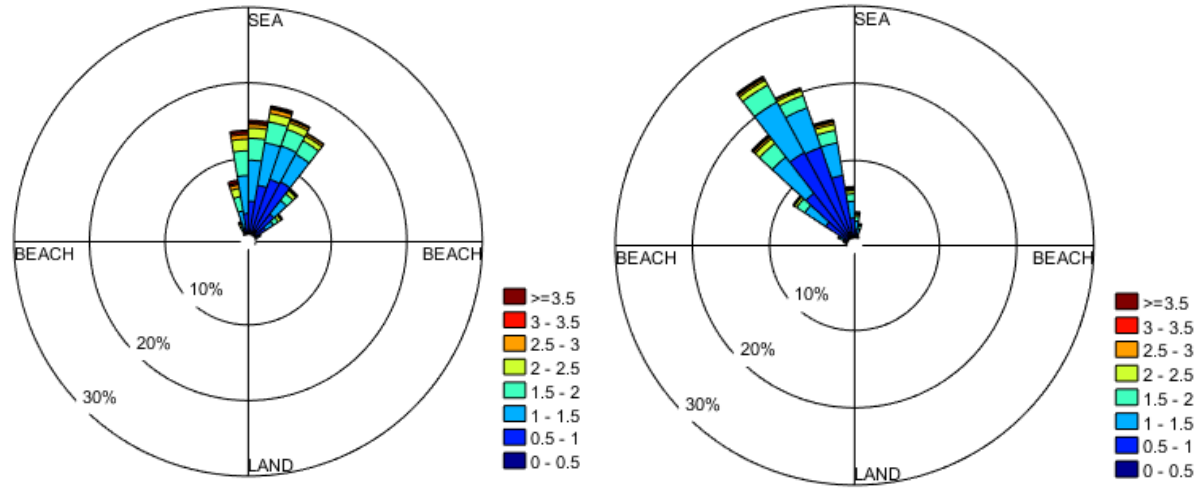

a) b)

Figure 4-2. Wave roses for a) Hazaki and b) Onahama. The percentage shares of the total amount of values are shown per wave height bin per wave direction bin. Values shown are values at dates for which both locations had wave data. If one of the stations had a gap, then the date was excluded for both data sets. The perpendiculars of the Hazaki and Onahama beaches are respectively 57° and 145°, the North being 0°. In the satellite image are the ranges shown of the wave directions. The orange lines are the outer limits, and the red lines represent the directions that have the largest share.

4.3 Beach structure comparison

The erosion and recession models in the PCR model for the HORS were calibrated for Hazaki beach. Similarity in beach structure between the HORS and a study area meant that there was justification to use the erosion and recession models of the Hazaki model in the PCR model of the study area. The beach profiles and sediment sizes at the study areas were compared with those of Hazaki beach. The beach at site 1 was similar to Hazaki beach in some aspects, which was not true for sites 2 and 3. The conclusions of the wave comparison were similar. Based on the conclusions of the wave and beach comparisons, justification was given for using the erosion and recession models of the Hazaki model at site 1, but not at sites 2 and 3.

The beach profiles for the study areas were only provided as graphs in papers. These had to be digitised for use in the model and for the comparison with Hazaki beach. This was done by overlaying them with scatterplots in Excel and adjusting the points till they were fitted to the graph. In Figure 4-3, the beach profiles are shown of Hazaki beach (Da Cruz, 2018), of the beach near Onahama port (Abe et al., 2002), of the Tottori sand dunes (Toshima, 1970) and of the Yumigahama peninsula (Kuroiwa et al., 2013).

A major side note in the comparison of beach profiles is the validity of the beach profiles. The beach profile used for Hazaki beach was a mean over 17 years of daily profiles, whereas the profiles of sites 1 and 2 were averages over a few biannual profiles or adjacent beach profiles. The beach profile of site 3 was a mean taken over 22 years of annual measurements. Concluding, the used profile of the HORS was a temporal average, whereas the profiles of the study areas were mostly snapshots in time. Observing the evolution of the beach profile in between or after the measurements was thus excluded. Consequently, it was unknown how well the beach profiles from literature resembled the actual beach profiles. The only verification was acquired from the visual observations during site visits. Furthermore, this could only be done for the above water extent of the profiles.

Photographs shown in Figure 3-4, Figure 3-9, Figure 3-13 and other photos were used for the verification of the beach profiles. People standing near the waterline (like fishermen or surfers) were used as measurement reference. The height of these people was estimated during the interviews mentioned in section 3.1, based on the height of the author. The beach profiles in Figure 4-3 were roughly validated with the photos and measurement references. From the waterline, the author also estimated the height of the back of the beach. This only served to validate the highest points in the profiles.

For sites 1 and 3, the beach profiles resembled the actual beaches. At site 2, the profile resembled the actual beach, except for the section between the end of the swash zone and the dune toe. It was thought that this section had an angle of 10^{o} rather than 14^{o}. In Figure 4-3, the extent between approximately x = -30 m and x = -10 m should have a reduced angle. However, this had no consequence for the use of the profile in the model, because only the slope at the waterline was used for determining the effects of SLR (see section 2.3.2).

The validated beach profiles were used for a comparison with the beach profile at the HORS. The submerged profile of site 1 was the most similar to the submerged profile at the HORS. The profile at site 2 was steeper at the waterline than the profiles of the HORS and site 1, but a similar slope was present at larger depths. The submerged profile at site 3 was in no aspect similar to the other sites.

The profile of site 1 was less steep above MSWL than the profile of the HORS. Beach profiles of sites 2 and 3 above MSWL were both steeper than at Hazaki. Sites 2 and 3 had a similar slope near MSWL.

The back beach of site 1 was not as high as at Hazaki. At the HORS, dunes were reported (Da Cruz, 2018), whereas a flat beach was observed at site 1. At site 3, a relatively flat beach was observed

after the beach had ascended till 3.5 m. The back beach of site 2 was in no aspect similar to other sites, since large dunes were present close behind the waterline. The D50 that was used at Hazaki was 0.2 mm, which was very similar to the D50 of 0.22 mm found at site 1 (see section 3.2.2). The D50 at sites 2 and 3 was 0.44 mm (sections 3.3.2 and 3.4.2), which was twice as large as at Hazaki.

Since the slope at the waterline was the most important part of the profile in the Hazaki model (for determining the effects of SLR, see section 2.3.2), and since the D50 at Hazaki and site 1 was nearly the same, it was concluded that the beaches were similar in structure. Considering the differences in profile and D50 when compared to Hazaki, it was concluded that sites 2 and 3 were dissimilar in structure to Hazaki beach.

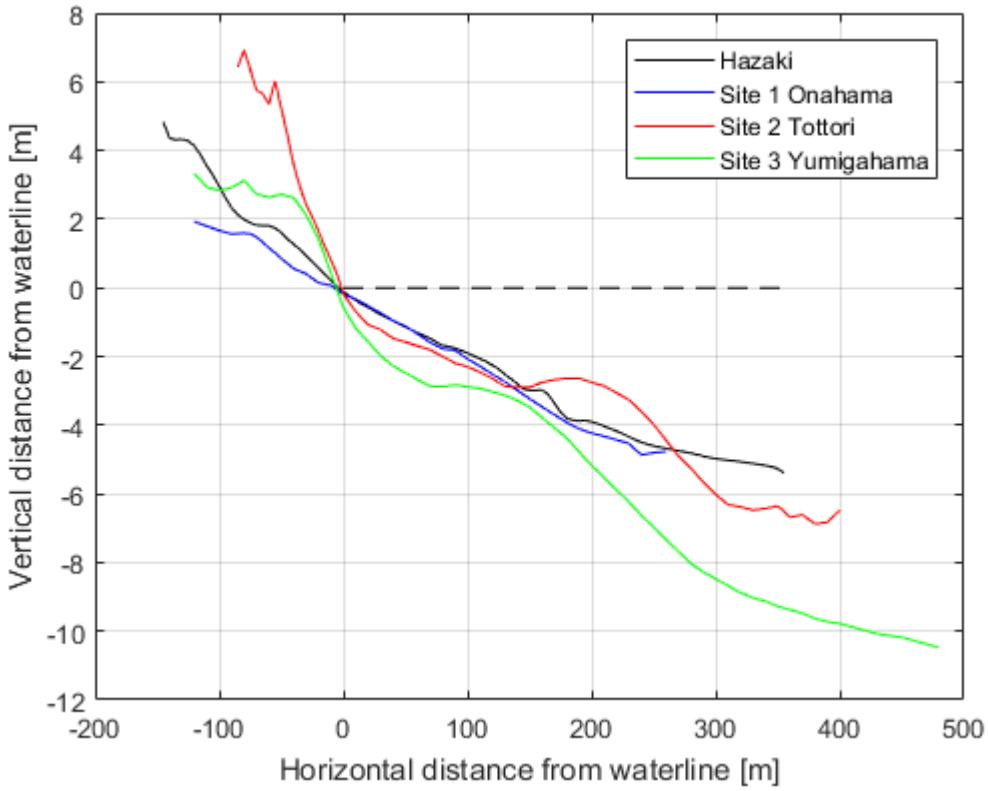

Figure 4-3. Mean beach profiles at the HORS and sites 1, 2 and 3. The profiles were joint at the waterline. The dashed line represents the mean sea level.

5 Implementation of the PCR

This chapter shows the implementation of the PCR framework to the study areas. A short overview is given in the first section. Elaborate explanations and analysis of input data are shown per site in following sections, with overviews of the input variable values shown in Appendix 1. The shoreline positions were simulated with the PCR models between 2018 and 2100 for 50,000 (sites 2 and 3) or 100,000 times (site 1).

5.1 Overview of PCR model setups

In Table 5-1, the setups are shown of the PCR models for the HORS and the study areas. It could be seen what choices were made for the PCR implementation at Hazaki beach, and what was used in the PCR implementations of the study areas.

Table 5-1. PCR implementations at the different sites.

Site	Model name	Storm detection method	Storm gaps	Eroded volumes	Erosion to recession	Recovery rate
HORS (Hazaki)		Erosion 95	All months	Mendoza-Jiménez model (Mendoza & Jiménez, 2006), calibrated for the Beach at the HORS	Copula	Calibration based on assumption of stable beach, thus if no SLR: P(R = 0 m) = 50%
1 (Near Onahama port)[1]	$PCR1_{Haz}$	Hazaki erosion dates	Hazaki storm gaps		Hazaki copula	
	$PCR1_{97}$	Waves 97[3]	All months			
2 (Tottori sand dunes)[1]	$PCR2_{99}$	Waves 99[3]	Exclusion summer months		Hazaki copula	
	$PCR2_{97}$	Waves 97[3]				
3 (Yumigahama peninsula)	PCR3	Waves 97[3]	All months		Hazaki copula	

[1]) At sites 1 and 2, other approaches for storm detection were also used. For these sites, two PCR models were constructed.

[2]) Da Cruz (2018) detected storms at the HORS with erosion thresholding (see section 2.3.2). The number indicates the percentile for which is thresholded.

[2]) Storms were detected with wave height thresholding. The number indicates the percentile for which is thresholded.

Storm events in the PCR models for the study areas were detected by 97th percentile wave thresholding ($PCR1_{97}$, $PCR2_{97}$ and PCR3). Besides this approach, also other approaches were used for sites 1 and 2. The alternative approach at site 1 is based on the similarity between the wave climate and beach profile (sections 4.2 and 4.3). In the alternative approach for site 1 ($PCR1_{Haz}$), wave heights during Hazaki storm dates were used as storm wave heights, and the storm gap distribution and the erosion to recession model of the Hazaki model were adopted in site 1. This was done because of the similarity of site 1 with the HORS in wave climate and beach structure. At site 2, the alternative approach features a different choice for a wave threshold for storm detection ($PCR2_{99}$). A wave threshold was used that is based on literature, which corresponded to the 99th percentile of the wave height data at site 2. Because of the alternative approaches in storm detection, two PCR models were made for sites 1 and 2. Thus, five PCR models were made in total for three sites.

5.2 Site 1 – Near Onahama port

Storm events

Two different storm detection methods were used: Hazaki erosion dates ($PCR1_{Haz}$) and 97th percentile wave thresholding ($PCR1_{97}$). The former is explained first. As described in section 2.3.2, Da Cruz (2018) detected storms with eroded volumes rather than with waves. If an eroded volume at Hazaki exceeded the 95th percentile erosion volume (or remained below the 5th percentile net beach volume change), the maximum wave height and period at that date were recorded from the Hazaki wave time series. The dates at which the erosion threshold was exceeded were used for site 1. At these storm dates, the maximum significant wave heights (and appurtenant wave periods) were recorded from the wave time series of site 1. To this wave data set for site 1 was thus referred as the Hazaki storm dates wave time series. Wave heights were fitted with a Burr distribution and are shown in Figure I-1 (Appendix I section 1).

Another wave characteristics time series was created solely with the recorded wave climate for $PCR1_{97}$. It was created with wave thresholding (section 2.3.2). Waves exceeding the 97th percentile of wave heights were recorded. An additional requirement was that wave heights exceeding this threshold should be spaced at least 24 h from each other to count as separate storm events. Wave heights were fitted with a GP distribution and are shown in Figure I-6 (Appendix I section 2).

The storm durations were the same for both PCR1 models. The erosion events detected by Da Cruz (2018) for Hazaki were based on daily observations rather than on bihourly observations and thus too 'coarse' for determining storm durations in hours. This was also the case with the Hazaki storm dates wave data set ($PCR1_{Haz}$). Therefore, storm durations were derived from the 97th percentile thresholded wave data set. A GP distribution was fitted to the storm durations (Figure I-3 in Appendix I section 1 and Figure I-8 in Appendix I section 2).

Storm gaps

The observed number of storm events was the number of detected storms per month over multiple years. A vector with monthly event rates, or rate parameters for the non-homogeneous Poisson distribution, was fitted to these observed events. This was done by adjusting the rate parameters on a trial-and-error basis, like in Da Cruz's (2018) methodology (step 9 in section 2.3.2). After an adjustment, the storm gaps were generated from 2018 till 2100 for 2000 times. Dates of storm occurrence were determined from this data set. The number of observed and generated events per month were compared visually, and the decision was made whether more adjustment was needed or that the results were satisfactory. The final result for the $PCR1_{97}$ is shown in Figure I-10 (Appendix I section 2). For $PCR1_{Haz}$, the same rate parameters were used as were used in the Hazaki model. The subsequent storm event distribution is shown in Figure I-5 (Appendix I section 1).

Erosion to recession

The same erosion to recession model was used for both PCR1 models. This was the erosion to recession copula that Da Cruz (2018) had created (step 9 in section 2.3.2). It was assumed that the beaches at the HORS and at site 1 had enough similarity in beach profile and sediment to do so (see section 4.3).

Recovery rate

The recovery rate was determined following the method of Da Cruz (2018) (section 2.3.2). For $PCR1_{97}$, a recovery rate was found of 40.2 m/year, and for $PCR1_{Haz}$ 5.8 m/year. This difference is explained by event rates for both models. It is observed in Figure I-5 ($PCR1_{Haz}$) and Figure I-10 ($PCR1_{97}$) that event rates per month were twice as high for $PCR1_{97}$ as they were for $PCR1_{Haz}$. More events meant more erosion. A higher recovery rate was needed to still satisfy the stable beach requirement for null SLR (section 2.3.2).

5.3 Site 2 – Tottori sand dunes

Storm events

Two different storm detection methods were used: 99th percentile ($PCR2_{99}$) and 97th percentile wave thresholding ($PCR2_{97}$). The former is explained first. Literature reported the occurrence of abnormal waves in the Sea of Japan (Lee, 2013; Lee, Kim, Yamashita, Komaguchi, & Mishima, 2010). These waves caused severe damages along the coast of the Toyama prefecture and prefectures further north along the west coast of Japan, as well as damages on the Korean coast. Dates that the researchers reported were December 20th 2003, October 23rd 2005, 12 October 2006, February 23rd 2008 (Lee et al., 2010), and April 4th 2012 (Lee, 2013). Peaks in the wave data set of site 2 contained peaks at these dates. It was assumed that the abnormal storm waves also hit the beach at site 2 and caused significant erosion. The lowest wave height occurring at these events corresponded to approximately the 99th percentile wave height. Storms were then detected by thresholding with this value. An additional requirement was that wave heights exceeding this threshold should be spaced at least 24 h from each other to count as separate storm events. Wave heights were fitted with a GP distribution and are shown in Figure I-11 (Appendix I section 3).

Similarly, waves were recorded that exceeded the 97th percentile wave height (given that also the spacing requirement was met) ($PCR2_{97}$). Wave heights were also fitted with a GP distribution and are shown in Figure I-16 (Appendix I section 4).

The storm durations were recorded from the Tottori wave time series with the 97th percentile wave height threshold ($PCR2_{97}$) and with the 99th wave height threshold ($PCR2_{99}$). The acquired storm duration data sets were different. For $PCR2_{97}$, longer wave height exceedances were recorded within 24 h (longer storm durations) than for $PCR2_{99}$. A Gamma distribution was fitted to the storm durations found with 99th wave thresholding (Figure I-13 in Appendix I section 3) and an Exponential distribution to those found with 97th wave thresholding (Figure I-18 in Appendix I section 4).

Storm gaps

The observed number of storm events was the number of detected storms per month over multiple years. A vector with monthly event rates, or rate parameters for the non-homogeneous Poisson distribution, was fitted to these observed events. This was done by adjusting the rate parameters on a trial-and-error basis, like in Da Cruz's (2018) methodology (step 9 in section 2.3.2). After an adjustment, the storm gaps were generated from 2018 till 2100 for 2000 times. Dates of storm occurrence were determined from this data set. The number of observed and generated events per month were compared visually, and the decision was made whether more adjustment was needed or that the results were satisfactory. The final result is shown in Figure I-15 (Appendix I section 3) for the $PCR2_{99}$ and in Figure I-20 (Appendix I section 4) for $PCR2_{97}$.

It was observed that for $PCR2_{99}$ (almost) no storm events occurred in the months of May, June, July and August. For $PCR2_{97}$, (almost) no storm events occurred in the months of June, July and August. To cope with this, it was programmed that no storms would occur during these months. If after one of the storm months the next storm event would occur in one of the stormless months, the event would be postponed till after the non-storm period. The delay was determined by evaluating how many days into the calm period the storm would have happened. This delay was then added to the end date of the stormless period to know when the next storm occurred. Figure 5-1 illustrates this approach.

Erosion to recession

For both PCR2 models, the erosion to recession copula was adopted that Da Cruz (2018) created. The beach at site 2 shared no similarities with the beach at the HORS (section 4.3), so there was no justification to use the copula. However, the copula of Da Cruz (2018) was still used, because the

Mendoza-Jiménez recession model (Mendoza & Jiménez, 2006) (Equation 11 in section 2.3.2) proved not to be applicable.

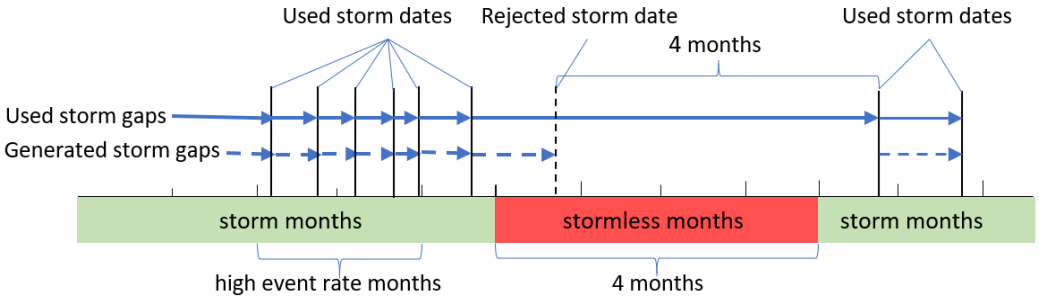

Figure 5-1. Explanation of storm gap generation at site 2.

Recovery rate

This was done with the same method as Da Cruz (2018) used (section 2.3.2). For $PCR2_{97}$, a recovery rate was found of 9.2 m/year, and for $PCR2_{99}$ 1.6 m/year.

5.4 Site 3 - Yumigahama peninsula

Storm events

For site 3, one setup for the PCR model was used. This setup was based on storm detection with 97th percentile wave height thresholding. A second setup was not used because there was no evidence for using other methods for storm detection. The wave heights were fitted to a GP distribution and are shown in Figure I-21 (Appendix I section 5). Storm durations were also fitted to a GP distribution and are shown in Figure I-23 (Appendix I section 5).

Storm gaps

The observed number of storm events was the number of detected storms per month over multiple years. A vector with monthly event rates, or rate parameters for the non-homogeneous Poisson distribution, was fitted to these observed events. This was done by adjusting the rate parameters on a trial-and-error basis, like in Da Cruz's (2018) methodology (step 9 in section 2.3.2). After an adjustment, the storm gaps were generated from 2018 till 2100 for 2000 times. Dates of storm occurrence were determined from this data set. The number of observed and generated events per month were compared visually, and the decision was made whether more adjustment was needed or that the results were satisfactory. The final result is shown in Figure I-25 (Appendix I section 5).

Erosion to recession

For the PCR3 model, the erosion to recession copula was adopted that Da Cruz (2018) created. The beach at site 3 shared no similarities with the beach at the HORS (section 4.3), so there was no justification to use the copula. However, the copula of Da Cruz (2018) was still used, because the Mendoza-Jiménez recession model (Mendoza & Jiménez, 2006) (Equation 11 in section 2.3.2) proved not to be applicable.

Recovery rate

This was done with the same method as Da Cruz (2018) used (section 2.3.2). For PCR3, a recovery rate was found of 4.5 m/year.

6 PCR-Bruun rule comparison

Probabilistic coastal recession projections were made with the five PCR models for the three study areas (section 6.1). The storm and SLR uncertainties in the Bruun rule estimates were quantified by linking the recession estimate with the associated probability in PCR results (section 6.2). Bruun rule estimate probabilities were derived with PCR results that were prepared according to two different methods. The main method was determining the annual maximum landward shoreline position R_{max} (section 6.1), and the additional method was determining shoreline positions from a trend over five years R_{trend} (section 6.3).

6.1 PCR results into ECDFs

The PCR models generated 100,000 (site 1) or 50,000 (site 2 and 3) time series of shoreline positions from 2018 till 2100 relative to the MSWL location in 2018. Positive values indicated a shoreline position landward of the reference point (recession) and negative values indicated shoreline positions seaward of the reference point (accretion). The recorded shoreline positions were measured directly after storms, meaning that these positions were the maximum landward positions before a period of recovery occurred until the next storm. It was decided to focus on these maximum landward shoreline positions (R_{max}), because for coastal hazard risk management these extreme shoreline positions would be the most interesting.

ECDFs for R_{max} were made for 83 years. For a certain year, the R_{max} was determined in all simulated time series. An ECDF was made for that particular year with these maximum landward coastline positions. This was done for all years from 2018 to 2100. Per model setup, 332 ECDFs (for 83 years times 4 SLR scenarios) were made with R_{max}. The ECDF the probabilities of exceedance of a shoreline position, i.e. if a shoreline position has a 10% exceedance probability it means that only 10% of the other R_{max} were more landward.

If one understands this concept, it could be extended to exceedance probabilities with negative shoreline positions, or accretions. These probabilities should not be read as the probabilities for accretions, but rather only as the probability for this negative landward shoreline position to be exceeded. This reasoning could be turned upside-down, if a probability of non-exceedance is used (1 – probability of exceedance). This was illustrated with an example given by Da Cruz (2018); a negative shoreline position of -50 m could have a probability of exceedance of 70%, meaning that 70% of R_{max} will be more landward than this shoreline position. This point has then a probability of non-exceedance of (1-0.7=) 30%, meaning that 30% of R_{max} are less landward than -50 m, or that 30% of R_{max} are more seaward than this point. Thus, probabilities of exceedance of these negative landward shoreline positions, or accretions, should be interpreted as probabilities of non-exceedance.

In Figure 6-1 a) and b), the exceedance probability curves are shown for $PCR1_{97}$ and $PCR1_{Haz}$. The exceedance probability that the whole beach was eroded in 2100 was 30% with $PCR1_{97}$, and 12% with $PCR1_{Haz}$.

In Figure 6-2 a) and b), the exceedance probability curves are shown for respectively $PCR2_{97}$ and $PCR2_{99}$. The exceedance probability of total beach erosion in 2100 was smaller than 0.1% for both models.

In Figure 6-3, the exceedance probability curves are shown for PCR3. It was observed that the exceedance probability for total beach erosion was 20% in 2100.

In all graphs, it was observed that RCPs had little influence on the PCR results. In Figure 6-1 a) and b) (site 1), it is observed in 2100 that the RCP8.5 recessions were 10 metres larger than the recessions for the other RCPs, and in Figure 6-3 (site 3) it is seen that small differences are present between the RCP curves in 2100.

Besides, it is observed in all graphs that the exceedance probability for the same recession increased over time, except for the recessions up to 100 m in Figure 6-2 b). This is explained by the fact that with longer temporal simulations, more unique maximum landward shoreline positions were simulated. A simulation period of 80 years allows more possible shoreline positions to exist than a simulation period of 20 years. This means that extremes of maximum landward shorelines were larger in the 80 years period than they were for the 20 years period. The exceedance probability of a maximum landward shoreline position after 80 years is then larger than it was after 20 years due to the existence of larger extremes after 80 years.

For site 1, it was seen that the recessions for the model with the 97th wave height thresholding ($PCR1_{97}$) (Figure 6-1.b) were considerably larger when compared to the results from the model with the Hazaki storm dates ($PCR1_{Haz}$) (Figure 6-1.a). This was observed with the exceedance probabilities of total beach erosion. The exceedance probability that the whole beach was eroded in 2100 was 30% with the 97th wave thresholding ($PCR1_{97}$), whereas in the other setup ($PCR1_{Haz}$) this was 12%. A large difference between results of the PCR1 models was also seen when comparing the R_{max} in 2100 with an exceedance probability of 0.1%. For this exceedance probability, the maximum landward position for $PCR1_{Haz}$ with RCP8.5 was 418 m. This was 672 m for $PCR1_{97}$. This difference in results between the two PCR2 models was significantly smaller for site 2. The R_{max} with an exceedance probability of 0.1% for $PCR2_{99}$ with RCP8.5 was 359 m, and this was 377 m for $PCR2_{97}$. The large difference in results for site 1 could be caused by two factors. The first factor is the difference in the number of generated storms between $PCR1_{97}$ and $PCR1_{Haz}$ (see Figure 6-4). The second factor is the fact that only large wave heights were taken into account in $PCR1_{97}$, whereas in $PCR1_{Haz}$ also small wave heights were considered. Considering the wave height CDFs for $PCR1_{Haz}$ and $PCR1_{97}$ (respectively Figure I-1 and Figure I-6 in Appendix I), the non-exceedance probability for 3 m waves is 90% for $PCR1_{Haz}$ and 30% for $PCR1_{97}$. The small differences in extreme recessions at site 2 were probably not caused by a small difference in the number of events, because the relative difference in generated events between $PCR2_{99}$ and $PCR2_{97}$ is for several months larger than between $PCR1_{Haz}$ and $PCR1_{97}$ (see Figure 6-4). The small differences in extreme recessions at site 2 are then probably caused by the similarity in wave height CDFs used as input for the PCR models (see Figure I-11 and Figure I-16 in Appendix I). The two PCR setups for site 2 had more similar storm detection methods than for site 1, and subsequently generated similar storms and erosion.

It was observed for sites 1 and 3 that the null recession had a probability of 60% for all years and RCPs. It seems thus that the beach would remain stable over the years, which is interesting considering that SLR was expected to destabilise the beach.

This was different for site 2, because it was seen that the null shoreline position had either a considerably larger exceedance probability (Figure 6-2.a) (between 77% in 2030 for RCP8.5 and 92% in 2100 for RCP8.5 for $PCR2_{99}$), or a considerably smaller exceedance probability (Figure 6-2.b) (between 50% in 2030 for RCP8.5 and 28% in 2100 for RCP8.5 for $PCR2_{97}$). This indicated that the beach was not stable with SLR in both PCR setups. It was suspected that this was a reaction of the model to the stormless months, or to the way these were incorporated into the model.

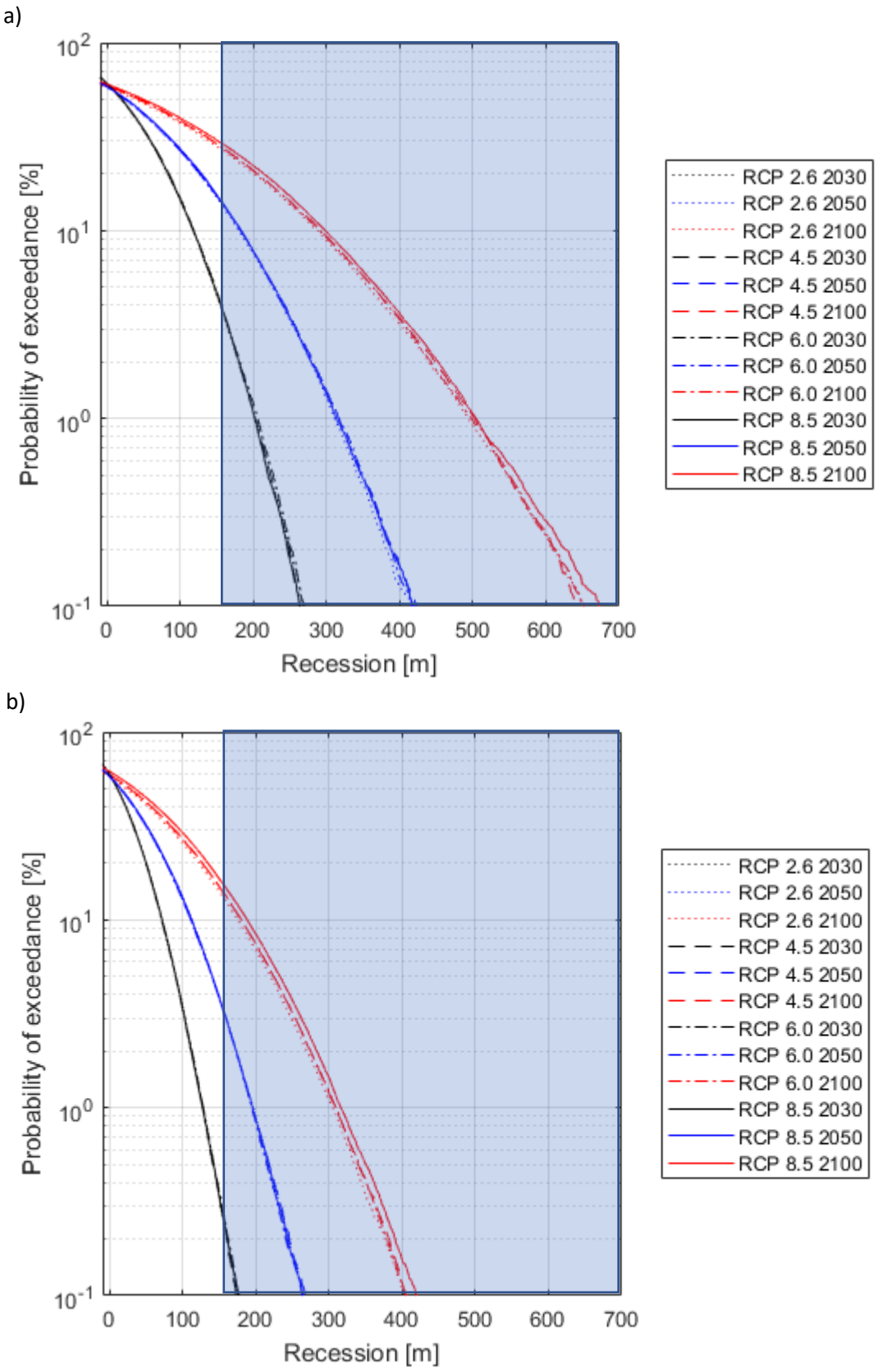

Figure 6-1. Exceedance probabilities for site 1 for the years 2030, 2050 and 2100. In a) were recessions generated with the $PCR1_{97}$ model. In b) were recessions generated with the $PCR1_{Haz}$ model. The blue rectangle indicates impossible shoreline positions, as the beach at site 1 is only 160 metres wide. The years for which the ECDFs are shown were arbitrarily chosen.

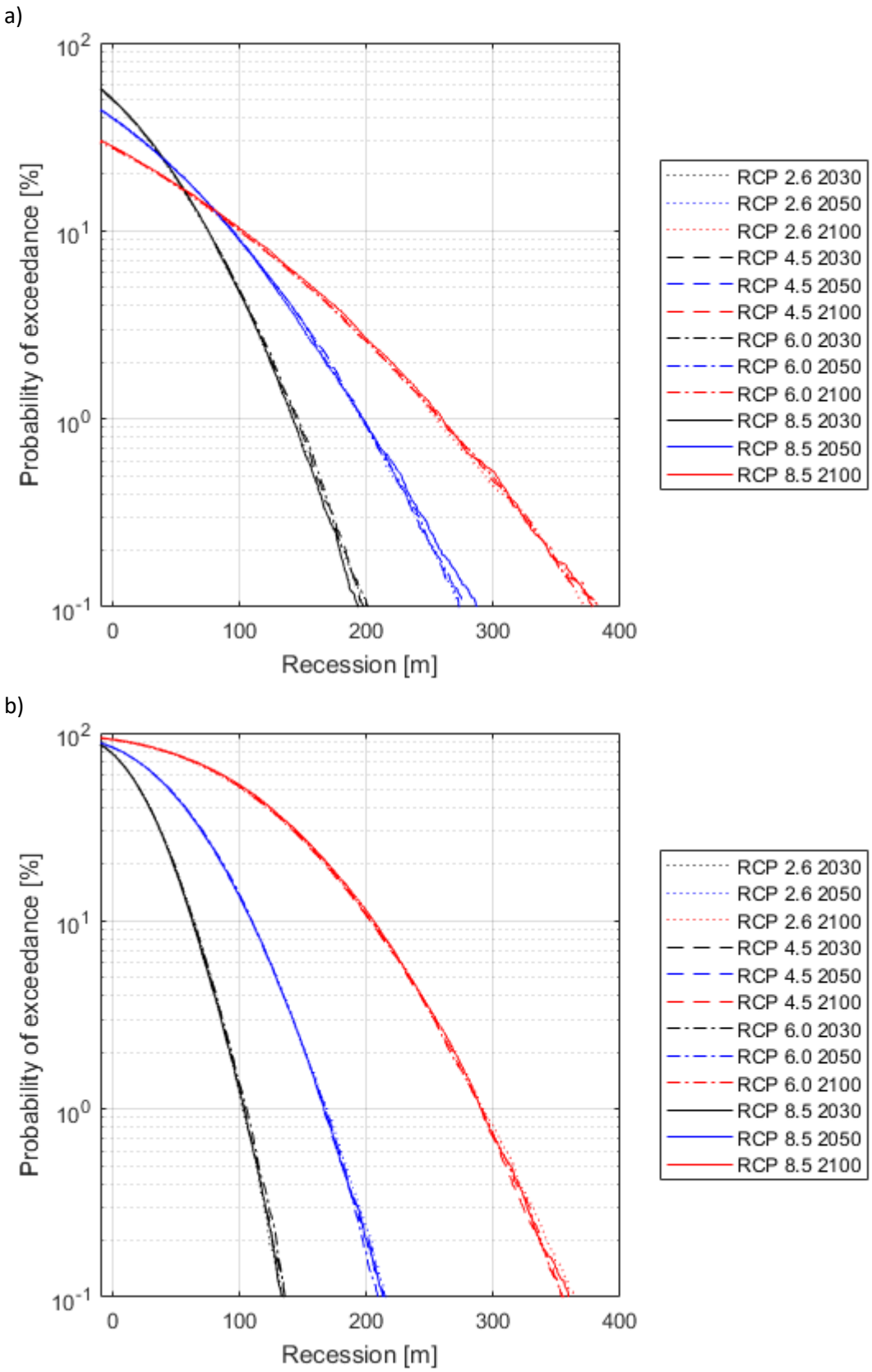

Figure 6-2. Exceedance probabilities for site 2 for the years 2030, 2050 and 2100. In a) were recessions generated with the $PCR2_{97}$ model. In b) were recessions generated with the $PCR2_{99}$ model. The years for which the ECDFs are shown were arbitrarily chosen.

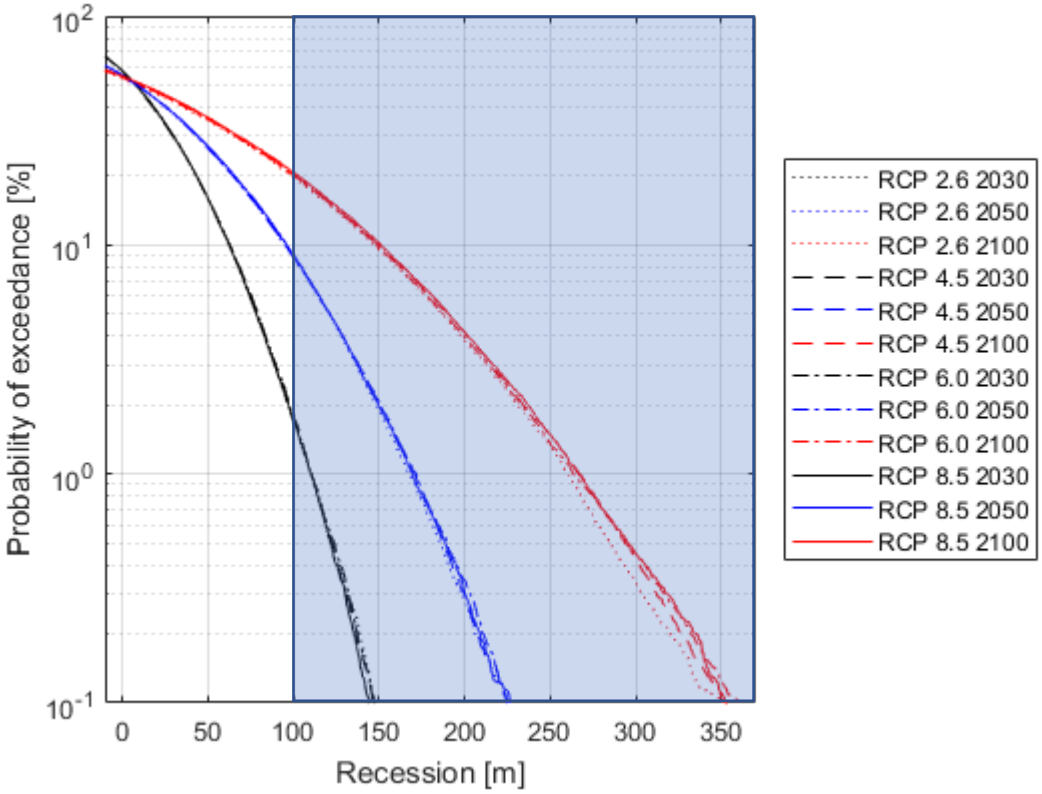

Figure 6-3. Exceedance probabilities for site 3 for the years 2030, 2050 and 2100. Recessions were generated with the PCR3 model. The blue rectangle indicates impossible shoreline positions, as the beach at site 1 is only 100 metres wide. The years for which the ECDFs are shown were arbitrarily chosen.

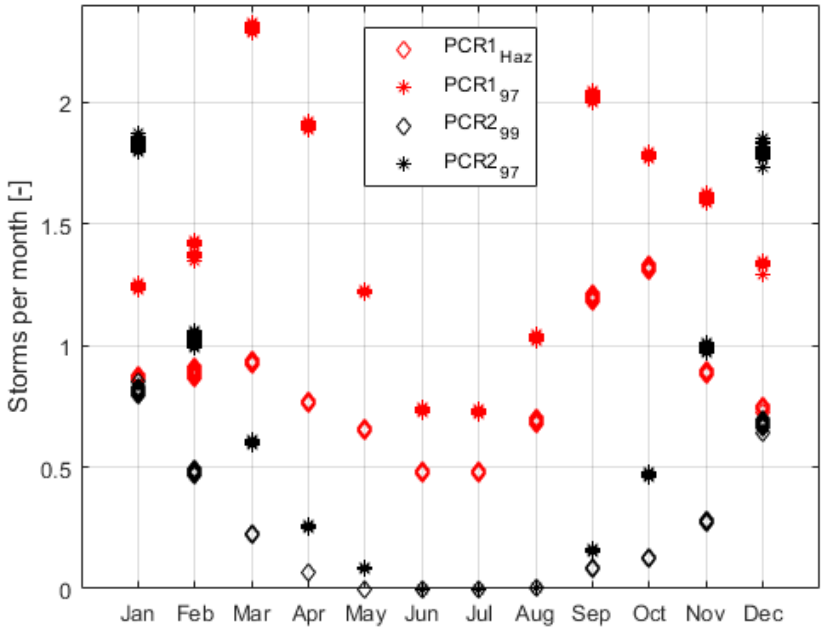

Figure 6-4. Number of storms per month generated by the PCR models for sites 1 and 2. Per month and per PCR model 83 data points are present, representing the 83 years of the simulation period.

6.2 Comparison of the Bruun rule with the PCR

The Bruun rule estimates were compared with R_{max} per year from the PCR models. The comparison was done by deriving per Bruun rule estimate what the exceedance probability was according to the ECDFs of the R_{max} as produced by the associated PCR models. The ECDFs of R_{max} were used that had the year, RCP scenario and site in common with the particular Bruun rule estimate. Bruun rule estimates for site 2 for RCP2.6 in 2030 were thus compared with ECDFs of R_{max} for RCP2.6 from $PCR2_{97}$ and $PCR2_{99}$ in 2030. The methodology of the comparison is explained in section 1.4.5.

The Bruun rule estimates and their comparisons with the ECDFs of R_{max} are shown per location. Considerable differences were observed when Bruun rule estimates were compared to the PCR results. These differences were seen between the different PCR model setups for the same beaches, and between the different sites. The Bruun rule estimates were reproduced according to the work of Udo and Takeda (2017) (see section 2.2). Their recession estimates were not used in this research, because their estimates were made for large coastal sections rather than for the comparatively smaller study areas in this research. Beach profiles, sediment sizes and slopes were generalised over the coastal in their research, while these characteristics are known per site in this research. Observed berm heights were used in Equation 1 rather than berm heights calculated with Equation 5. This meant that only Equations 1 and 2 were used from the equations shown in section 2.2. The submerged section of the profiles had to be extrapolated to determine the DoC and subsequently the slope of the beach. This was necessary for using Equation 1. A relation described by Equation 2 was fitted to the submerged sections based on best fit or sediment size. The fits are shown in Appendix II. It was observed for all sites that the curves made with annual Bruun rule estimates (Figure 6-5, Figure 6-7 and Figure 6-9) resembled the SLR curves in Figure 2-1. Per site, 332 recession estimates (for 83 years times 4 SLR scenarios) were calculated with the Bruun rule.

6.2.1 Site 1 – Near Onahama port

In Figure 6-5, the Bruun rule estimates are shown for site 1. In Figure 6-6, the exceedance probabilities are shown of the Bruun rule estimates according to the ECDFs for R_{max}. For both PCR1 models, the exceedance probabilities corresponding to the Bruun rule estimates became more conservative.

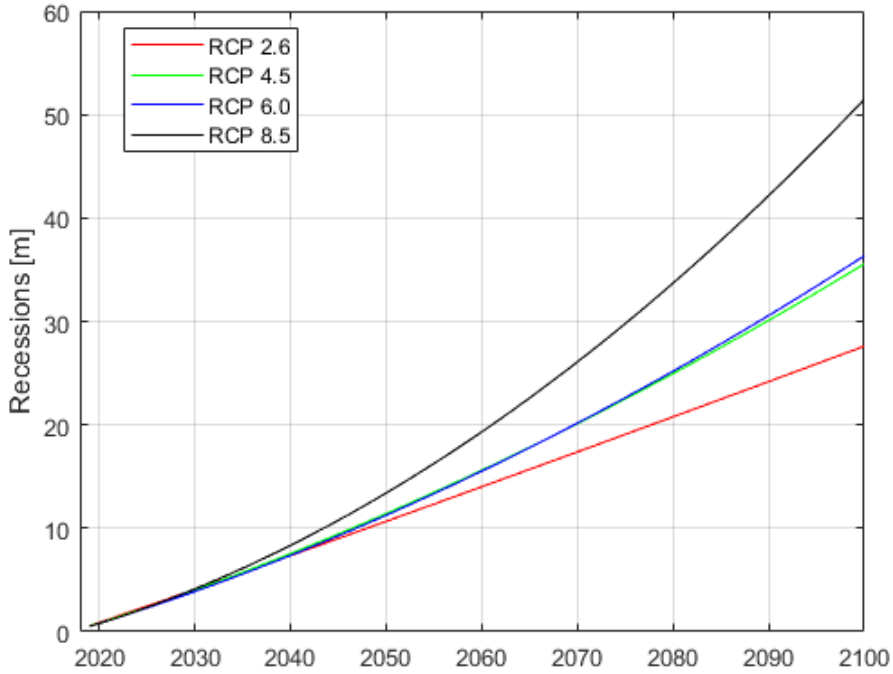

Figure 6-5. Yearly Bruun rule recession estimates for site 1.

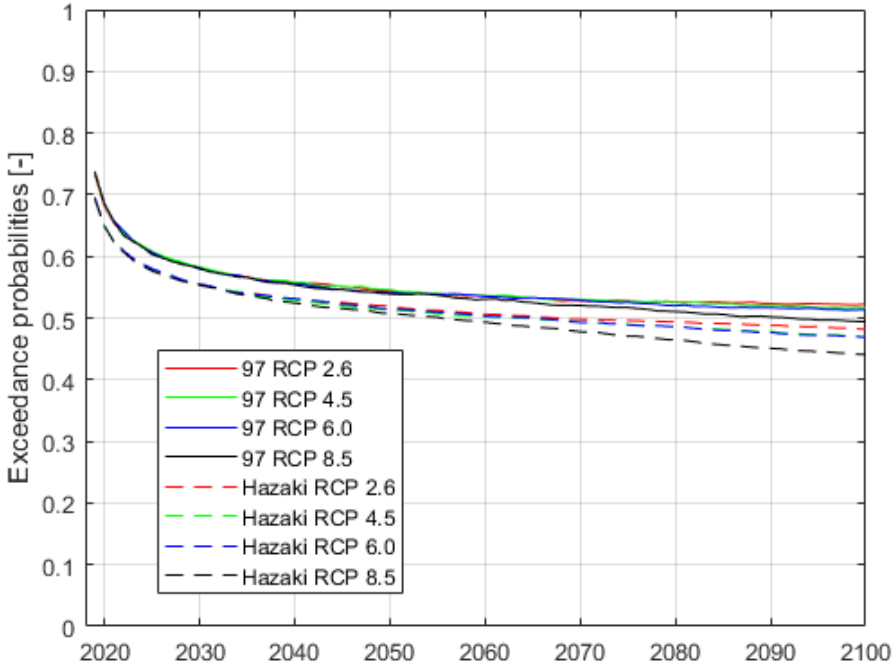

Figure 6-6. Yearly Bruun rule exceedance probabilities for site 1, based on the ECDFs for the annual R_{max} produced with the $PCR1_{97}$ and $PCR1_{Haz}$ models. Probabilities were determined by comparing Bruun rule estimates to yearly ECDFs for R_{max}.

6.2.2 Site 2 – Tottori sand dunes

In Figure 6-7, the Bruun rule estimates are shown for site 2. In Figure 6-8, the exceedance probabilities are shown of the Bruun rule estimates according to the ECDFs for R_{max}. For $PCR2_{99}$, it was observed that the derived exceedance probabilities of the Bruun rule estimates became more conservative at a faster rate than for site 1 (Figure 6-6). For $PCR2_{97}$, the derived exceedance probabilities of the Bruun rule estimates became less conservative over time.

Both observations could be explained with the ECDFs for site 2. The ECDFs for sites 1 and 3 (Figure 6-1 and Figure 6-3) all intersected with each other near the null recession mark with the exceedance probability of 60%. The angle of intersection decreased over the years. The consequence was that over the years the exceedance probability of the same recession distance grew larger. Bruun rule estimates became relatively more conservative, because the estimated recessions increased over the years 'faster' than the ECDFs shifted. For $PCR2_{99}$, it was seen that the ECDF for each year was positioned slightly above those of previous years. The curves did not intersect at null recession distance. The shift of the curves occurred at a faster pace than the Bruun rule estimates increased. This resulted in the observation that Bruun rule estimates became less conservative over the years according to the PCR results.

For $PCR2_{97}$, the exceedance probabilities of the Bruun rule estimates according to the ECDFs were more in line with the findings at site 1. Exceedance probabilities decreased over the years. This occurred at a higher rate than for site 1. The annual ECDFs for this setup intersected over the years at recession distances up to 100 m. This meant that recession distances up to 100 m had increasingly smaller instead of larger exceedance probabilities. Bruun rule estimates also increased over the years, thus the exceedance probabilities for the Bruun rule estimates according to the ECDFs grew increasingly more conservative than was the case for site 1.

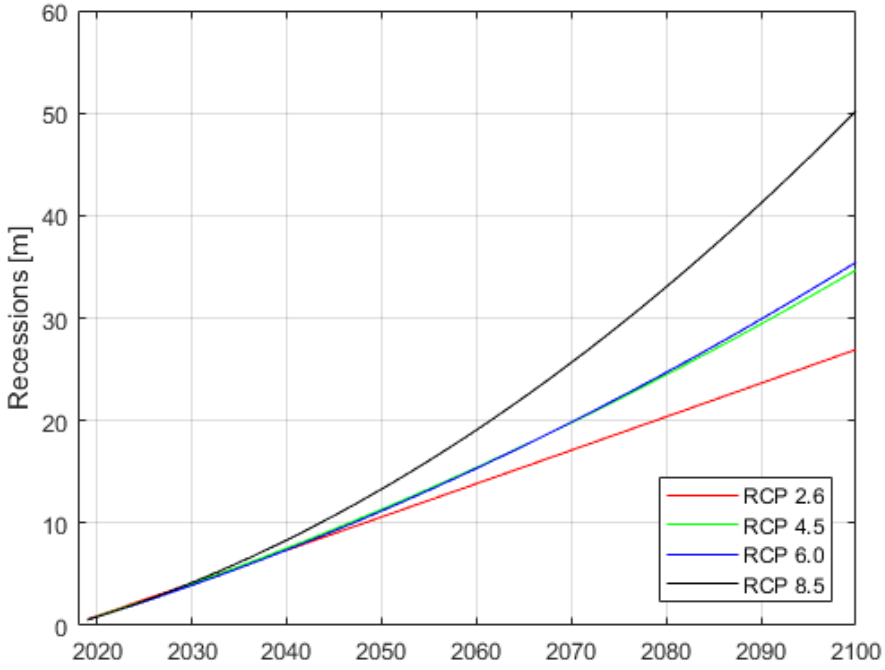

Figure 6-7. Yearly Bruun rule recession estimates for site 2.

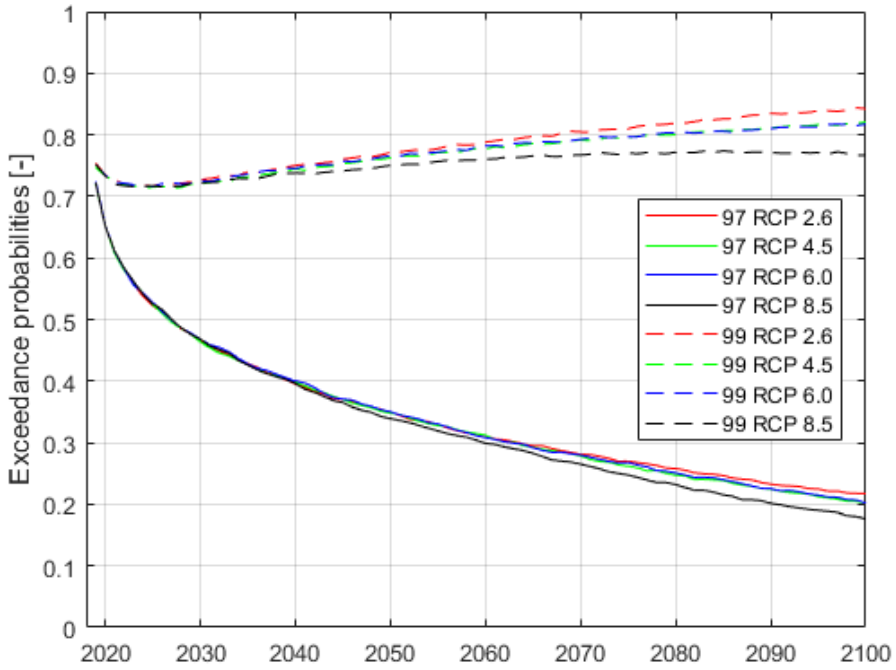

Figure 6-8. Yearly Bruun rule probabilities for site 2, based on the ECDFs for the annual R_{max} produced with the $PCR2_{97}$ and $PCR2_{99}$ models. Probabilities were determined by comparing Bruun rule estimates to yearly PCR curves.

6.2.3 Site 3 – Yumigahama peninsula

In Figure 6-9, the Bruun rule estimates are shown for site 3. In Figure 6-10, the exceedance probabilities are shown of the Bruun rule estimates according to ECDFs for R_{max}. The rate at which this happened was similar to the rate for site 1 (Figure 6-5).

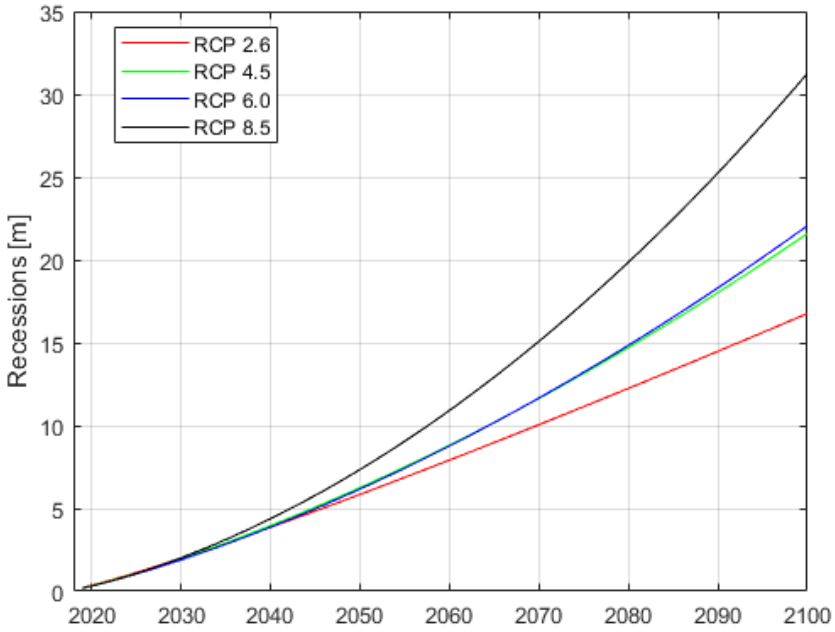

Figure 6-9. Yearly Bruun rule recession estimates for site 3.

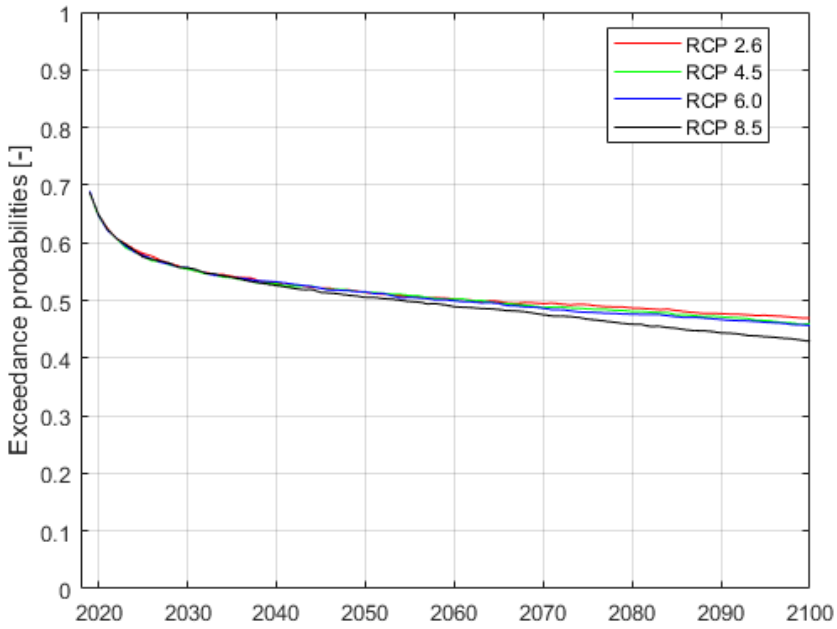

Figure 6-10. Yearly Bruun rule probabilities for site 3, based on the ECDFs for the annual R_{max} produced with the PCR3 model. Probabilities were determined by comparing Bruun rule estimations to yearly PCR curves.

6.3 Alternative PCR-Bruun Rule comparison

Exceedance probabilities of Bruun rule estimates were also derived with ECDFs of R_{trend}. Instead of focusing on R_{max} for each year, shoreline positions before and after storms were considered between 2095 and 2100. A trendline was drawn through these points. The R_{trend} was then calculated by using January 1st 2098 as input for the derived linear relation. This shoreline position could be derived for other 5-year periods, but in this study only the period 2095-2100 was considered due to lack of time. The difference between the derivations of R_{trend} and R_{max} (used in section 6.1) is illustrated in Figure 6-11. For the same period (2095-2100), five R_{max} values are evaluated and one R_{trend}.

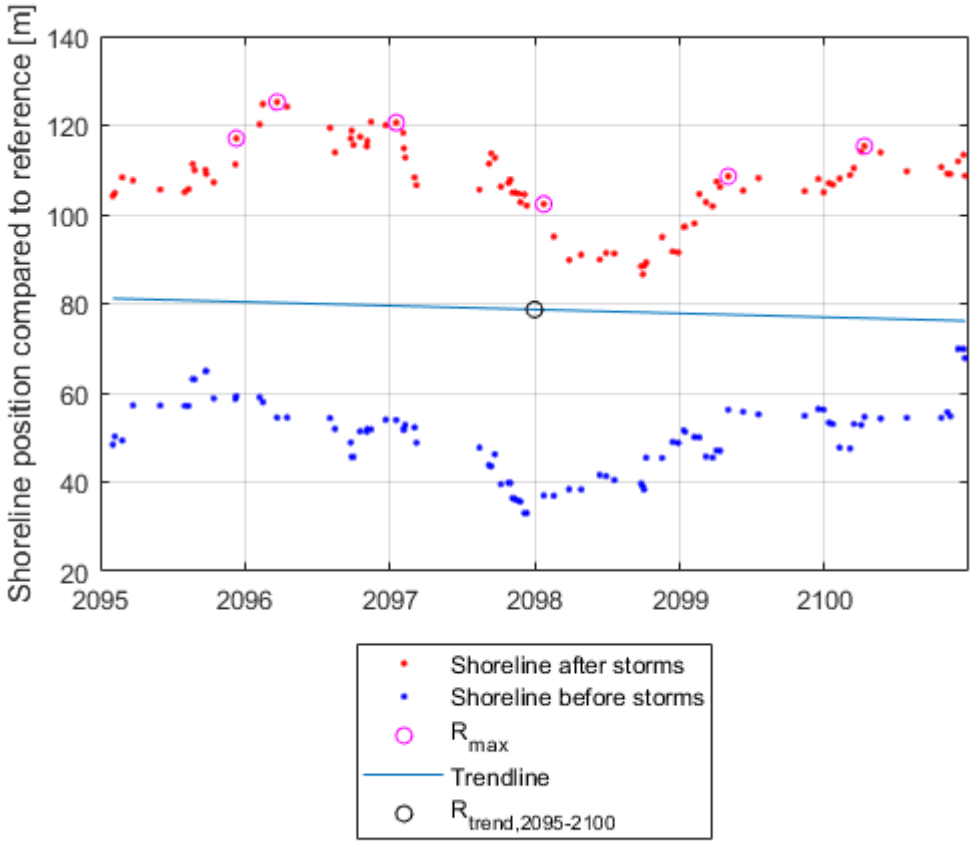

Figure 6-11. Derivation of R_{max} vs R_{trend} over 2095-2100. These shoreline positions were simulated in one of the model runs for site 3 with RCP2.6. The shoreline positions were relative to the shoreline in 2018. Negative values mean seaward positions and positive values landward positions.

In Figure 6-12, the ECDFs of R_{max} in 2100 and R_{trend} over 2095-2100 are shown as produced by $PCR1_{Haz}$. Both methods yield approximately the same null recession exceedance probabilities. The difference between predicted recessions grows larger with decreasing exceedance probabilities. At the exceedance probability of 0.1%, the ECDF with R_{trend} shows a recession of 310 m, whereas the ECDFs with R_{max} shows a recession of 400 to 410 m. The ECDFs for R_{max} showed higher exceedance probabilities for the same shoreline positions when compared with the ECDFs for R_{trend}. The increasing difference in predicted recessions between the ECDFs with R_{trend} and R_{max} with decreasing exceedance probability was observed for all the results of the PCR models. The ECDFs of the other PCR models are shown in Appendix III per site and setup. Because R_{trend} has a more averaged 'nature' than R_{max}, the extremes that R_{max} focuses on are dampened by the use of the trend line, which is used for determining R_{trend} values. This is then the reason that the exceedance probabilities for the same recession are

smaller in the ECDFs for R_{trend} then they are in the ECDFs for R_{max}. It also explains why the difference in exceedance probabilities increases towards more extreme recessions.

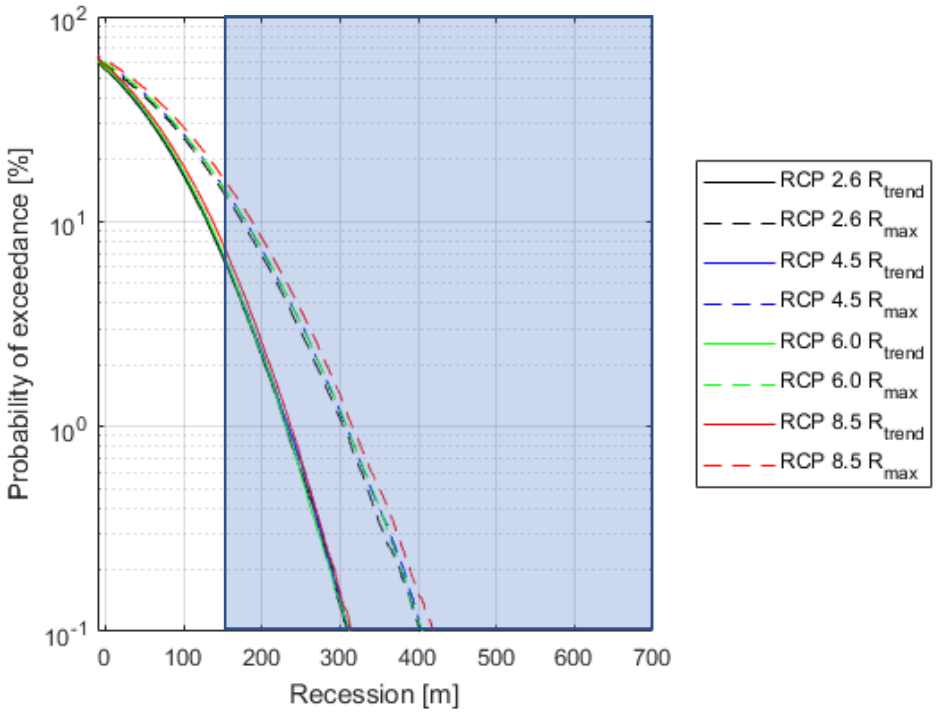

Figure 6-12. ECDFs for R_{max} in 2100 and R_{trend} over 2095-2100 for site 1. Both are derived from the results of the $PCR1_{Haz}$ model. The blue rectangle indicates impossible shoreline positions, as the beach at site 1 is only 160 metres wide.

In Table 6-1, Table 6-2 and Table 6-3, the exceedance probabilities are shown for the Bruun rule estimates per site and model setup as derived from the corresponding PCR ECDFs. It is observed that the exceedance probabilities for the Bruun rule estimates become smaller when R_{trend} ECDFs were used. The difference between the exceedance probabilities for Bruun rule estimates has not the same order of magnitude as seen between the extremes (P=0.1%) in Figure 6-12, because the Bruun rule estimated shoreline recessions are relatively small when compared to the extremes as simulated by the PCR models.

Table 6-1. Bruun rule estimates for site 1 with their exceedance probabilities according to the PCR1 models. The exceedance probabilities were derived with ECDFs made with R_{trend} over 2095-2100 and R_{max} in 2100.

Bruun rule estimates		PCR1$_{97}$ exceedance probabilities [%]		PCR1$_{Haz}$ exceedance probabilities [%]	
RCP	Recession [m]	R_{trend}	R_{max}	R_{trend}	R_{max}
2.6	27.6	0.47	0.52	0.43	0.48
4.5	35.6	0.46	0.52	0.40	0.47
6.0	36.3	0.46	0.51	0.40	0.47
8.5	51.5	0.43	0.49	0.36	0.44

Table 6-2. Bruun rule estimates for site 2 with their exceedance probabilities according to the PCR2 models. The exceedance probabilities were derived with ECDFs made with R_{trend} over 2095-2100 and R_{max} in 2100.

Bruun rule estimates		PCR2$_{97}$ exceedance probabilities [%]		PCR2$_{99}$ exceedance probabilities [%]	
RCP	Recession [m]	R_{trend}	R_{max}	R_{trend}	R_{max}
2.6	26.9	0.19	0.22	0.77	0.84
4.5	34.7	0.18	0.20	0.73	0.82
6.0	35.4	0.18	0.20	0.73	0.82
8.5	50.2	0.15	0.18	0.64	0.77

Table 6-3. Bruun rule estimates for site 3 with their exceedance probabilities according to the PCR3 model. The exceedance probabilities were derived with ECDFs made with R_{trend} over 2095-2100 and R_{max} in 2100.

Bruun rule estimates		PCR3 exceedance probabilities [%]	
RCP	Recession [m]	R_{trend}	R_{max}
2.6	16.8	0.43	0.47
4.5	21.6	0.41	0.46
6.0	22.1	0.40	0.46
8.5	31.3	0.37	0.43

7 Discussion

This chapter discusses the answers to the research sub-questions as presented in section 1.3. Besides the answers, assumptions and issues are discussed that were associated with the questions. A summary of the discussed issues is given in section 7.5.

7.1 Inclusion of water levels in the wave height-eroded volume relation

No significant relation could be found between wave heights and eroded volumes when combining the data for water levels and wave heights. Furthermore, the correlation coefficient improved by altering the eroded volumes by changing the section over which they had been measured.

Including the surge level was thought to yield a strong correlation between water surface heights and erosion. This was not the result, which had implications for this research. This study was built on the assumed relation between wave heights (with or without water levels) and eroded volumes. Da Cruz (2018) found that these variables had a weak correlation when using the data of Hazaki. However, it must be considered that this relation is a direct one. The setup of the Mendoza-Jiménez erosion model (Mendoza & Jiménez, 2006) is such that a significant correlation has to be found between eroded volumes and predictor values. It is a more indirect relation between wave heights (with or without storm surge) and eroded volumes, because other storm characteristics are also included in the predictor. Da Cruz (2018) found a significant correlation for the eroded volumes and the P predictor (Mendoza & Jiménez, 2006). This relation was used in this study. The issue with the weak relation between wave heights and erosion was thought to be resolved.

Excluding the water levels is not in line with previous research. Li et al. (2014) and Callaghan et al. (2008) included water levels as variables in their PCR models. The erosion models they used required water levels. Dastgheib et al. (2017) did not include water levels, because they found that water levels changed insignificantly during storms at the east coast of Sri Lanka. In this research, only a small analysis was performed to justify the exclusion of water levels. Perhaps a larger reanalysis of the erosion model with the inclusion of water levels would have resulted in the conclusion that water levels had to be included. On the other hand, this may not be needed, as Mendoza and Jiménez (2006) only used water levels as a variable to categorise storms with.

7.2 Similarities between the HORS and the study areas

The beach profiles and the wave climates of the HORS and site 1 were assumed to be similar. The beach profiles were similar, because both sites had approximately the same sediment size and because the submerged profiles and swash zones were similar. The latter conclusion was important as the effects of SLR were determined with the inclination of the swash zone. The wave climates were assumed similar in the sense that storms occurred at the same dates, and not in the sense that the wave climates were the same. The beach profiles and wave climates of the HORS and sites 2 and 3 shared no similarities.

The beach profile comparison brings a major issue. For the HORS, a long time series existed with daily beach profile measurements. Measurements were taken annually at best (site 3) for the study areas. An average profile could be made for the Hazaki beach, which could not be done for the other beaches. Instead, the few beach profiles from literature had to be used as equivalent for the average beach profile. This meant that these profiles may not have represented the actual 'standard' beach profile. Other problems were that:

- for sites 1 and 2 the profiles were dated (>20 years);
- the beach at site 2 was assumed to be stable because of an ongoing beach nourishment program;

- the beach at site 3 was 'tilting' with the southern end eroding while the northern end was accreting;
- at site 1 a large erosion event had happened after the beach profile measurements.

These issues combined make the use of the profiles questionable. Furthermore, data for verifying the profiles could not be obtained, since beach profile measurements performed during the site visits failed. Beach profiles could only be verified by visual observation or with satellite imagery. Especially with the visual observation, considerable human error was involved. Since the beaches were only successfully verified with visual observation, it would have been desirable to also visit Hazaki beach. Visual observations of Hazaki beach and the study areas could have been compared. However, the visit did not occur.

Another issue with the beach comparison was that only the beach profiles were compared. Features such as river mouths or long/cross-shore currents were not taken into account. It was too difficult to find information on these features and especially on their impacts, due to the ignorance of the author about the Japanese language. It was also beyond the scope of this study, because the model did not incorporate these features.

Regarding the wave climate comparison, the wave climates at the HORS and site 1 were comparable. Wave heights at both sites followed the same pattern of extremes, but the wave directions were dissimilar. Wave direction and height, however, had no correlation. Thus, the wave climates were assumed to be similar regarding wave height patterns. This meant that the waves acted similarly on the same dates. The similarity did not mean that the same waves occurred at both sites at the same dates. Since the sites 2 and 3 were located on the western site of Japan, it was assumed that no similarities could exist with the HORS.

No major issues were had during the wave climate comparison, as the data was well-provided. The exact locations of the measurement stations were known. Checking whether wave characteristics measured by these stations represented the wave characteristics for the sites was done easily.

A considerable issue in this study was defining the exact requirement for similarity of wave climate and beach structure. Requirements were conceived *a posteriori*, instead of formulating them *a priori*. As a consequence, the model setup for site 1 with the Hazaki storm dates might have been fallible.

7.3 PCR model application

The Hazaki modelling methodology (Da Cruz, 2018) was used in this study to make five PCR models that were run each with four different SLR scenarios. The Hazaki modelling methodology was based on the PCR framework as explained by Ranasinghe et al. (2012). Differences between the Hazaki model and the PCR models of the study areas were primarily due to the different input variable values (different beach structure and wave characteristics). More substantial differences (e.g. using different erosion models) were not made. This fact raises several points of discussion. A major issue was the question whether the erosion and recession models of the Hazaki model should be used for other beaches, since these were calibrated and validated with HORS data only. This study was, however, an interesting exercise to see if PCR models could be generalised. Recalibration of the Mendoza-Jiménez model could not be done in this research, because no beach profile time series or erosion data were available for the study areas. Synthetic beach evolution data could have been generated with XBEACH (Roelvink et al., 2009) and could have been used for calibrating the erosion model. This was what Dastgheib et al. (2017) did. It was outside the scope of this research to recalibrate the Mendoza-Jiménez erosion model or to apply other erosion or recession models. If other erosion models would have been applied and no (generated) erosion data was available, the convolution method (Kriebel &

Dean, 1993) would be recommended, because no calibration would be needed for this erosion model. Validation would be an issue as the erosion data would still not be available.

An additional issue is the use of the recession model of Hazaki beach at sites 2 and 3. Initially, the Mendoza-Jiménez recession model (Mendoza & Jiménez, 2006) was used to calculate shoreline movement from eroded volumes for sites 2 and 3 (Equation 11 in section 2.3.2). Sites 2 and 3 did not share any similarities in beach profile and wave climate with Hazaki beach. These findings did not support the application of the recession model of Hazaki beach to sites 2 and 3. However, the extreme recessions generated with the Mendoza-Jiménez recession model were observed to be an order of magnitude larger than the extreme recessions generated at site 1 with the Hazaki recession model, even though the eroded volumes were in the same order of magnitude. The decision was made to use the Hazaki recession model for sites 2 and 3, even when it was concluded that they were not similar to Hazaki beach.

A last issue regarding the erosion and recession models is that the models did not allow profile changes. It was assumed in the PCR models of this study that the beach profile would always be the same profile before a storm. Physically speaking, if a storm happened only a few days after a previous storm, the beach profile would probably not have recovered. In the model, the beach profile regained the equilibrium profile at the shoreline to which the beach had recovered before the next storm. In this scenario, the equilibrium profile is attacked by 'normal' waves rather than by waves which lost their energy on the accreted submerged profile.

The choice for a storm detection method proves to be an issue, because different methods produced considerably different ECDFs for the same sites. Detected storm events should be events at which erosion happened. This certainty of storm erosion was not available for the study areas due to the lack of beach volume time series. Events causing erosion at the HORS were assumed to be also erosion events for site 1. In other PCR model setups, this assumption for storm detection could not be used. Wave thresholding was used instead. Thresholds were based on findings in literature (99^{th} wave thresholding for site 2) or were arbitrarily chosen (97^{th} wave thresholding). For wave height thresholding, multiple choices for a threshold were viable. Different wave height thresholds led to different model setups and results for site 2 (although that may be also due to storm gap modelling). Hazaki storm dates ($PCR1_{Haz}$) and 97^{th} percentile wave height thresholding ($PCR1_{97}$) were used for storm detection at site 1, which also resulted in different results. However, differences due to different storm detection for site 2 were not the same as the differences seen between the two model setups for site 1. For site 2, the ECDFs curved differently and the extremes (P=0.1%) were 20 m apart from each other in 2100. For site 1, the ECDFs were similar and the extremes (P=0.1%) were 300 m apart from each other.

Another issue is the method for modelling the time periods in between storms. A non-homogeneous Poisson distribution was used for this. A rate parameter was assigned to every month, because the number of storm events changed throughout the year (seasonality). This was done for sites 1 and 3. Some months were excluded for site 2 due to the absence of storm events during those months. This was probably the cause of the difference in ECDF curving between Figure 6-2 (site 2) on the one hand, and Figure 6-1 and Figure 6-3 (sites 1 and 3) on the other hand. The approach Dastgheib et al. (2017) used would have been better for including stormless months at site 2. Instead of continuing the generation of storms over the whole time period, they generated storms per storm season. This method could not be included in the model, because the issue was noticed too late.

A last remark on the setup of the PCR models is that important insight was had in this research regarding the generalisation of a PCR model with reusing the Hazaki modelling methodology. The methodology used for Hazaki worked quite well for site 1 and 3. For site 2, it was thought to be less successful due to the issues with the stormless months. Nothing could be said about the predictive success of the PCR models due to the lack of data for validation.

7.4 Comparison between Bruun rule estimates and PCR results

The five PCR models were run each with four different SLR scenarios and produced in total twenty data sets with shoreline positions between 2018 and 2100. From these data sets, ECDFs were produced with annual R_{max} and R_{trend} over 2095-2100. Per Bruun rule estimate, an exceedance probability was derived with an ECDF for R_{max} that matched the year, site and SLR scenario. For the Bruun rule estimates predicting recessions in 2100, an additional exceedance probability was derived with the ECDFs for R_{trend} over 2095-2100. The exceedance probabilities of Bruun rule estimates for site 1 and 3 ranged respectively between 44% (RCP8.5) and 52% (RCP2.6) and between 43% (RCP8.5) and 47% (RCP2.6) in 2100 when using R_{max} ECDFs. For site 2, the exceedance probabilities of Bruun rule estimates ranged between 18% and 84%. This large range was due to the different storm detection methods and due to the storm gap generation with stormless months. For all five PCR models, the Bruun rule estimates had lower exceedance probabilities when derived with the R_{trend} ECDFs than when they were derived with the R_{max} ECDFs. Exceedance probabilities of Bruun rule estimates derived with both kinds of ECDF were not as conservative as were indicated by Ranasinghe et al. (2012).

The exceedance probabilities of Bruun rule estimates changed over time. This was due to two factors, namely 1) the temporal increase of the SLR and Bruun rule recession projections and 2) the increase of exceedance probabilities of the same shoreline position according to the PCR results. The synergy of these factors determined at what rate the exceedance probabilities of the estimates changed over time. If the Bruun rule estimates grew larger at a faster rate than the probabilities increased for the same shoreline positions in the PCR ECDFs, Bruun rule estimate exceedance probabilities grew more conservative. If vice versa, the Bruun rule estimate exceedance probabilities would grow less conservative over time. This is illustrated in Figure 7-1. If both factors increased at the same rate, the Bruun rule estimates would continue to have the same exceedance probabilities. For most sites, exceedance probabilities of the Bruun rule estimates derived with the R_{max} ECDFs decreased, or became more conservative, over time. It was also observed that the synergy could result in Bruun estimates actually becoming less conservative over time ($PCR2_{99}$).

Using the results of the comparison between Bruun rule estimates and PCR ECDFs for coastal hazard risk management has implications, because the results from this comparison are very sensitive to choices for the Bruun rule and PCR model setups. Firstly, the translation of SLR to Bruun rule estimates varied heavily according to the choice of the DoC. Ranasinghe and Stive (2009) reported that estimates could vary over 500% for Narrabeen beach, Australia, by using different methods for estimating the DoC. The exceedance probability of the Bruun rule estimates could then also vary significantly. In this study, the scope was to only use the Bruun rule estimates as Udo and Takeda (2017) calculated them. Secondly, choices in the setup of the PCR model attribute to significant changes in the ECDFs of shoreline position. By changing the PCR model setup, the same Bruun rule estimate has a different derived exceedance probability.

The direct results of the PCR model, the ECDFs, caused another issue for the use the Bruun rule estimate exceedance probabilities. The ECDFs for sites 1 and 3 all intersected near the point where the null shoreline movement had an exceedance probability of 60%. This indicated that the beach would remain stable over the years. This was regarded as unlikely, because SLR would cause instability of the beach. It was unknown which exact part of the model caused the prediction of stable beaches. However, the recovery model or the recession model was thought to be the cause. In the model, the recovery rate was the daily rate of horizontal seaward shoreline movement in between storms. The recession model also allowed for recovery. The copula took into account that for the same eroded volumes both landward and seaward movement of the shoreline could be observed (Da Cruz, 2018).

The Mendoza-Jiménez recession model did not accommodate recovery, as eroded volumes only translated to landward shoreline movement.

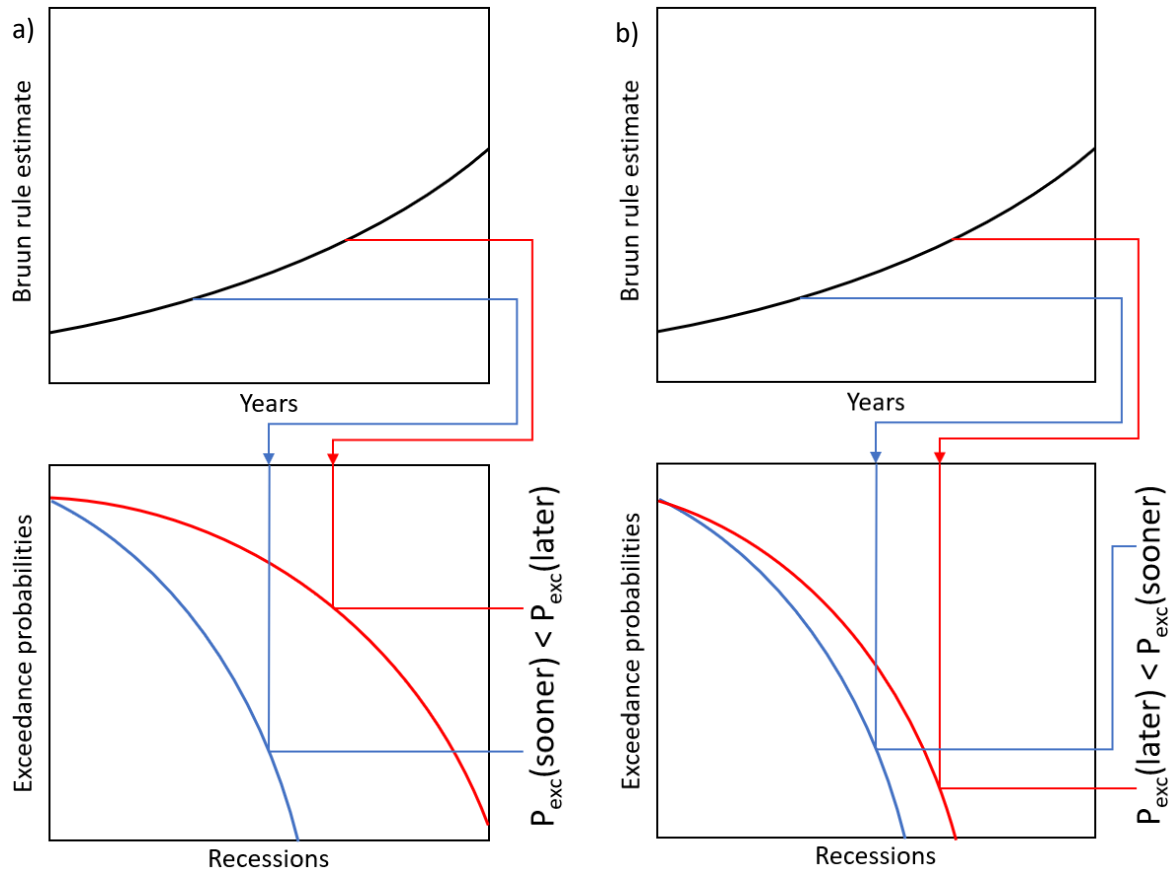

Figure 7-1. Explanation of the synergy between the rate of change of Bruun rule estimates and the shift of PCR ECDFs over time, and the influence on the derived Bruun rule estimate exceedance probability. a) shows a higher exceedance probability for a Bruun rule estimate when the rate of increase of the Bruun rule estimate is smaller than the shift of the PCR ECDF. b) shows a lower exceedance probability for a Bruun rule estimate when the rate of increase of the Bruun rule estimate is larger than the shift of the PCR ECDF. The presented graphs are hypothetical and not based on any site, PCR model setup, or RCP scenario.

The PCR model results were, on the other hand, relatively insensitive to different SLR scenarios. In ECDFs that only differed by RCP scenario, small differences were seen between the four SLR scenarios. The 8.5 RCP scenario caused some R_{max} to be more seaward for the same year and exceedance probability than R_{max} produced with other RCP scenarios. Considerable larger differences between ECDFs are present when they were produced with the same RCP scenario and PCR model, but for a different year. It is concluded that choosing the year for which an ECDF is evaluated has more effect than choosing the RCP scenario.

A final discussion point regarding the comparison between PCR ECDFs and Bruun rule estimated recessions, is the choice of which PCR simulated shoreline positions are used in the comparison. In this study, extensive attention was given to using R_{max} as was done by Ranasinghe et al. (2012), Li et al. (2014), Dastgheib et al. (2017) and Da Cruz (2018). As mentioned in section 1.4.5, R_{max} are the recessions most threatening to assets on the coast. ECDFs made with R_{max} provide the exceedance probabilities needed for coastal hazard risk management when considering buildings and infrastructure in sandy coastal strips. It is then questionable how ECDFs with R_{trend} should be used, other than as PCR results that are more comparable to Bruun rule estimates, because R_{trend} values have a more averaged 'nature'. The R_{trend} ECDFs are useful when average beach widths need to be evaluated

besides worst-case scenario beach width projections. For beach tourism, maximum landward positions are interesting for understanding the long term 'survivability' of a beach, but average beach widths are also important to know. Predictions on income from tourism could be made based on beach widths projections (Klein & Osleeb, 2010). Besides, the ecological value of beaches could also be evaluated with average beach widths. Beach animals, like beach birds, are dependent on the existence of a beach, which could be evaluated using R_{max}, but knowledge of the average size of their habitat needs to be evaluated from R_{trend}. Considering the worst-case scenario might result in too conservative projections. Coastal hazard risk management regarding tourism and ecology based on R_{max} ECDFs might lead to too exaggerated mitigation strategies that could disrupt beach tourism (Klein & Osleeb, 2010) and beach ecology.

7.5 Summary of issues

All research questions were answered in this study. Per answer also issues related to the answer were discussed. A summary of the major issues is given below:

1. Use of the Hazaki model – There was no justification for using the Hazaki erosion and recession models for sites 2 and 3. It was dubious whether this generalisation of a PCR model could be done for these sites. Besides, the erosion model of the Hazaki model was used in the PCR models of the study areas, while it was assumed that a direct relation existed between wave heights and erosion. Da Cruz (2018) did not find such a relation, nor was this relation found in this study after redoing her analysis with inclusion of water levels. A last implication is that the erosion and recession models did not allow beach profile change.
2. Different storm detection methods, different results – Using different methods for storm detection resulted in considerable differences between PCR results and subsequently Bruun rule estimate exceedance probabilities derived from PCR ECDFs.
3. Absence of SLR effects – ECDFs made with R_{max} showed that the beaches at site 1 and 3 remained stable even with SLR, whereas this was not the case for site 2. This was not due to differences in SLR and it could probably be explained by issues related to the modelling of storm gaps. Marginal differences are present between the shoreline positions when only the difference in SLR scenario is considered.
4. Interpretation of the PCR results – Interpreting the results from the PCR models in different ways results in different exceedance probabilities for the Bruun rule estimates. Bruun rule estimates were less conservative when they were compared with ECDFs based on R_{max} than when they were compared with ECDFs made with R_{trend}.
5. Applicability of the PCR model to the beaches – In order to apply the PCR framework sufficient knowledge is needed to describe the sites. The requirement for PCR model application is that beaches are stable. If they are not stable, then information is needed on the beach profile evolution. In this study, ample wave data was available for all sites. Beach cross-sections were not available, except for some observations that were annual at best. Most of them were also dated (>20 years for site 1 and 2). This meant that no information was available on the average profile and that considerable changes in between or after the observations were not recorded. Information on the 'stability' of beaches at site 2 and 3 was found in literature. Site 2 was stable with an ongoing beach nourishment programme. The beach at site 3 was tilting as one end was eroding while the other end was accreting. Concluding, the application quality of the PCR model in this study is only as high as the quality of the used beach profiles.

8 Conclusion

The goal of this research was to quantify uncertainty related to sea level rise and storm definition in the Bruun rule-derived future shoreline positions in Japan. This was done by determining the exceedance probabilities of Bruun rule estimates with the results of probabilistic coastal recession (PCR) models (Ranasinghe et al., 2012). The shoreline positions were simulated between 2018 and 2100 for three sites in Japan, being the beach near Onahama port (site 1), the Tottori sand dunes (site 2), and the Yumigahama peninsula (site 3). Instead of building a new PCR model, the Hazaki beach (Japan) modelling methodology was implemented (Da Cruz, 2018) for the study areas. For sites 1 and 2, two different PCR model setups were made based on two storm definitions. For site 3, one storm definition was used. The five model setups were run with four different sea level rise (SLR) scenarios. Twenty PCR data sets were made in total in this research. For each set of PCR modelling results, two exceedance probability empirical cumulative distribution functions (ECDFs) were made with the annual maximum landward shoreline positions (R_{max}) and shoreline positions derived from 5-year trend lines (R_{trend}). Per model setup, 332 ECDFs (for 83 years times 4 SLR scenarios) were made with R_{max}, and 4 ECDFs (for 1 period times 4 SLR scenarios) were made with R_{trend}. Per site, 332 recession estimates (for 83 years times 4 SLR scenarios) were calculated with the Bruun rule. At sites 1 and 2, two probabilities were derived for one Bruun rule estimate. For 2100 and the most severe SLR scenario, the exceedance probabilities were 49% and 44% for the two different model setups for site 1, 18% and 77% for the two different model setups for site 2, 43% for the single model setup for site 3.

Considering that other uncertainties remained constant (e.g. choice for Depth of Closure (DoC)), the uncertainty due to SLR and storm definition could be quantified with the use of PCR produced shoreline ECDFs. The models were significantly more sensitive to the choice of storm detection method than to the choice of SLR scenario. However, no general quantified relation could be evaluated between Bruun rule estimates and their exceedance probabilities derived with the PCR model results. The shape of the curve that describes the temporal change of these exceedance probabilities is closest to an observable general relation. Besides these main conclusions, also other findings are reported:

- Temporal change of Bruun rule estimate probabilities – In this study, the PCR exceedance probabilities for Bruun rule estimates grow primarily more conservative over time. This is in line with the findings of Da Cruz (2018). The rate of change of PCR exceedance probabilities for Bruun rule estimates differs per site and per used storm definition. This iss explained by the different rates of increase of 1) the Bruun rule estimates and 2) the exceedance probabilities of the same shoreline positions in the ECDFs.
- Generalisation of PCR models – Sites 1, 2 and 3 lacked beach evolution time series. Instead of generating these time series and calibrating erosion and recession models with this data (Dastgheib et al., 2017), the erosion and recession models of the Hazaki model were used. Also other parts of the Hazaki modelling methodology were used in the PCR models of the study areas. This saved time, but the predictive successfulness of the models is unknown as the generated eroded volumes and shoreline positions could not be validated due to lack of data on beach evolution of the study areas.
- Reusability of storm dates – For the study areas, no data was available that linked wave characteristics and erosion. Subsequently, no erosion-causing storm wave characteristics were known for storm event detection in the wave time series, which in turn would have supplied storm variable values as validated input for the storm generator in the PCR models. For site 1, this problem was circumvented in this study by assuming that the wave climates at site 1 and the HORS were similar. No storms had to be detected; storm variable values only had to be determined at site 1 for the dates when erosion occurred at the HORS. The predictive

successfulness of this PCR model setup for site 1 is unknown, because the generated erosions and shoreline positions could not be validated.

Despite these conclusions, using the results of this study for coastal hazard risk management should be done with care. The following reasons are given:

- Questionable use of the erosion and recession models of the Hazaki model at sites 2 and 3, because these study areas are dissimilar from Hazaki beach. Also, the model does not allow beach profile change;
- Different storm detection methods influence the results of the PCR model significantly;
- Null shoreline movement at site 1 and 3 is predicted to have an exceedance probability of approximately 60% in all annual ECDFs from 2018 to 2100 in all SLR scenarios. This continuity is doubted;
- Shoreline positions simulated with the PCR model could be used to make ECDFs for R_{max} or R_{trend}, depending on what interpretation is needed;
- Beaches at the study areas were assumed to be stable. In literature or data no evidence was found that these beaches were stable, or it was found that beaches remained stable due to human interference.

9 Recommendations

Several recommendations were made for future research to resolve some of the issues that were mentioned in chapter 8.

The major issue in this study was the applicability of the Hazaki erosion and recession models to other sites. This was done due to the lack of beach volume change time series. It would be recommended, if new PCR models were made for the sites in this study, to use the Mendoza-Jiménez model (Mendoza & Jiménez, 2006) that is calibrated with generated erosion data (like Dastgheib et al. (2017) did in their research), or use another erosion model that relies less on beach change data (e.g. the Convolution method (Kriebel & Dean, 1993)). Other erosion models could be considered if beach volume change time series would be generated. Examples are SBEACH (Larson & Kraus, 1989) and XBEACH (Roelvink et al., 2009). Computation time would increase significantly though (Callaghan, Ranasinghe, & Roelvink, 2013).

Wave thresholding seemed to be the only viable storm detection method when no erosion time series or information on storm characteristics was available. Choosing an appropriate threshold is challenging. The 97^{th} and 99^{th} percentiles for wave heights were chosen as thresholds for site 2 and subsequently major differences in results were observed. The sensitivity of the model to the choice for storm detection method would be an interesting subject for future research.

If other PCR models would be applied to sites 1 and 2, it is advised to retake the cross-sections with appropriate instruments. For site 3, this would not be necessary, because recent beach cross-sections could be acquired from the Tottori prefecture administration. Evidence for this was found in the paper of Shibutani et al. (2016), but this data could not be acquired in this research due to the lack of knowledge of the Japanese language. Knowledge of the Japanese language is recommended anyway if one would desire to apply PCR models to sites in Japan, due to the information that Japanese journal papers and institutions have.

10 References

Abe, M., Fukuyama, T., Sato, S., Isobe, M., & Kumagai, T. (2002). Field observation on the deformation of the Samegawa estuary sandbar and the geomorphological process of the Nakoso coast (in Japanese). *Coastal Engineering*, (49), 531–535. Retrieved from http://library.jsce.or.jp/jsce/open/00008/2002/49-0531.pdf

Bruun, P. (1962). Sea-Level Rise as a Cause of Shore Erosion. *Journal of the Waterways and Harbors Division*, *88*(1), 117–132.

Callaghan, D. P., Nielsen, P., Short, A., & Ranasinghe, R. (2008). Statistical simulation of wave climate and extreme beach erosion. *Coastal Engineering*, *55*(5), 375–390. https://doi.org/10.1016/j.coastaleng.2007.12.003

Callaghan, D. P., Ranasinghe, R., & Roelvink, D. (2013). Probabilistic estimation of storm erosion using analytical, semi-empirical, and process based storm erosion models. *Coastal Engineering*, *82*, 64–75. https://doi.org/10.1016/j.coastaleng.2013.08.007

Church, J. A., Clark, P. U., Cazenave, A., Gregory, J. M., Jevrejeva, S., Levermann, A., … Unnikrishnan, A. S. (2013). Sea level change. In T. F. Stocker, D. Qin, G. K. Plattner, M. Tignor, S. K. Allen, J. Boschung, … P. M. Midgley (Eds.), *Climate Change 2013: The Physical Science Basis. Contribution of Working Group I to the Fifth Assessment Report of the Intergovernmental Panel on Climate Change* (pp. 1137–1216). Cambridge, United Kingdom and New York, NY, USA: Cambridge University Press. https://doi.org/10.1017/CB09781107415315.026

Cooper, J. A. G., & Pilkey, O. H. (2004). Sea-level rise and shoreline retreat: Time to abandon the Bruun Rule. *Global and Planetary Change*. https://doi.org/10.1016/j.gloplacha.2004.07.001

Creel, L. (2003). Ripple effects: Population and coastal regions. Retrieved September 14, 2018, from https://www.prb.org/rippleeffectspopulationandcoastalregions/

Da Cruz, C. M. (2018). *Stochastic Projections of Coastline Variations - Application to Hasaki Beach, Japan*. IHE, Delft, The Netherlands.

Dastgheib, A., Jongejan, R., Mehvar, A., & Ranasinghe, R. (2017). *Coastal Risk Assessment along the East Coast of Sri Lanka*. Delft.

Dean, R. G., Walton, T. L., & Kriebel, D. L. (1994). *Cross-shore sediment transport*.

Fan, Y., Held, I. M., Lin, S.-J., & Wang, X. L. (2013). Ocean Warming Effect on Surface Gravity Wave Climate Change for the End of the Twenty-First Century. *Journal of Climate*, *26*(16), 6046–6066. https://doi.org/10.1175/JCLI-D-12-00410.1

Hemer, M. A., Fan, Y., Mori, N., Semedo, A., & Wang, X. L. (2013). Projected changes in wave climate from a multi-model ensemble. *Nature Climate Change*, *3*(5), 471–476. https://doi.org/10.1038/nclimate1791

Hemer, M. A., Katzfey, J., & Trenham, C. E. (2013). Global dynamical projections of surface ocean wave climate for a future high greenhouse gas emission scenario. *Ocean Modelling*, *70*, 221–245. https://doi.org/10.1016/j.ocemod.2012.09.008

Hinrichsen, D. (1998). The Coastal Population Explosion. In B. Cicin-Sain, R. W. Knecht, & N. Foster (Eds.), *The Next 25 Years: Global Issues* (pp. 27–29). Washington, D. C.: NOAA. Retrieved from https://www.google.com/url?sa=t&rct=j&q=&esrc=s&source=web&cd=4&ved=0ahUKEwikj4yL_4DSAhXrylQKHQ47BKoQFggwMAM&url=https%3A%2F%2Fpdfs.semanticscholar.org%2F1775%2F6d46a6a9ede105538d385566f9e853b9caba.pdf&usg=AFQjCNE75aVqANcr8zs5y5U4B7PWaPOoFQ&sig2=Bf6bH0_DJ

IPCC. (2013). *"Climate change 2013: The physical science basis," Contribution of Wokring Group I to the Fifth Assessment Report of the Intergovernmental Panel on Climate Change*. (T. F. Stocker, D. Qin, G. K. Plattner, M. Tignor, S. K. Allen, J. Boschung, … P. M. Midgley, Eds.). Cambridge, United Kingdom and New York, NY, USA: Campbridge University Press.

Jiménez, J. A., Sánchez-Arcilla, A., & Stive, M. J. F. (1993). "Discussion on prediction of storm/normal beach profiles." *Journal of Waterway, Port, Coastal, and Ocean Engineering*, *119*(4), 466–468. https://doi.org/10.1061/(ASCE)0733-950X(1993)119:4(466)

Jiménez, J. A., Sánchez-Arcilla, A., & Valdemoro, H. I. (1997). Predicción de los cambios en el perfil de

playa utilizando parámetros adimensionales sencillos. *Recista de Obras Publicas*, (3362), 29–39.
Kakani, N. R., & Sadakata, N. (2006). Coastal zone management along the Yumigahama peninsula , Japan - an appraisal. *Annals of the Yamaguchi Geographical Association*, *35*, 21–29.
Klein, Y. L., & Osleeb, J. (2010). Determinants of Coastal Tourism: A Case Study of Florida Beach Counties. *Journal of Coastal Research*, *26*(April), 1149–1156. https://doi.org/10.2112/JCOASTRES-D-09-00152.1
Kraus, N. C., Larson, M., & Kriebel, D. L. (1991). Evaluation of beach erosion and accretion predictors. In *Coastal sediments* (pp. 527–587).
Kriebel, D. L., & Dean, R. G. (1993). Convolution Method for Time-Dependent Beach-Profile Response. *Journal of Waterway, Port, Coastal, and Ocean Engineering*, *119*(2), 204–226. https://doi.org/10.1061/(ASCE)0733-950X(1993)119:2(204)
Kuroiwa, M., Matsubara, Y., Fujimoto, H., & Ichimura, Y. (2013). Characteristics of beach cross-section of Shishi Coast (in Japanese). In *Public Works Association Chinese Branch Research Presentation Outline Summary (土木学会中国支部研究発表会発表概要集)* (Vol. 65, p. II-20). Retrieved from http://library.jsce.or.jp/jsce/open/00549/2013/65-02-0020.pdf
Larson, M., & Kraus, N. C. (1989). *SBEACH. Numerical Model for Simulating Storm-induced Erosion; Report 1. Empirical Foundation and Model Development*.
Lee, H. S. (2013). Abnormal storm waves in the East Sea (Japan Sea) in April 2012. *Journal of Coastal Research*, *65*(April), 748–753. https://doi.org/10.2112/SI65-127.1
Lee, H. S., Kim, K. O., Yamashita, T., Komaguchi, T., & Mishima, T. (2010). Abnormal storm waves in the winter East/Japan Sea: Generation process and hindcasting using an atmosphere-wind wave modelling system. *Natural Hazards and Earth System Science*, *10*(4), 773–792. https://doi.org/10.5194/nhess-10-773-2010
Li, F., Gelder, P. H. A. J. M. van, Vrijling, J. K., Callaghan, D. P., Jongejan, R. B., & Ranasinghe, R. (2014). Probabilistic estimation of coastal dune erosion and recession by statistical simulation of storm events. *Applied Ocean Research*, *47*, 53–62. https://doi.org/10.1016/j.apor.2014.01.002
Mamoru, M., Takami, U., Kaoka, K., Oishi, H., & Yamamoto, K. (1991). Beach deformation and sediment balance at Suruga coast (in Japanese). *Coastal Engineering Journal*, *38*, 281–285. Retrieved from http://library.jsce.or.jp/jsce/open/00008/1991/38-0281.pdf
Mehta, A., Khare, Y., & Andrew, M. (2016). Sediment deposition and erosion processes. Retrieved September 19, 2018, from http://www.theseusproject.eu/wiki/Sediment_deposition_and_erosion_processes
Mendoza, E. T., & Jiménez, J. A. (2006). Storm-Induced Beach Erosion Potential on the Catalonian Coast. *Journal of Coastal Research*, (48), 81–88.
MLIT. (2018). NOWPAHS - The Nationwide Ocean Wave information network for Ports and HArbourS data. Retrieved from https://nowphas.mlit.go.jp/prg/pastdata/?lng=eng
Mori, N., Yasuda, T., Mase, H., Tom, T., & Oku, Y. (2010). Projection of Extreme Wave Climate Change under Global Warming. *Hydrological Research Letters*, *4*, 15–19. https://doi.org/10.3178/hrl.4.15
Nicholls, R. J., Birkemeier, W. A., & Hallermeier, R. J. (1997). Application of the Depth of Closure Concept. In *Coastal Engineering 1996* (pp. 3874–3887). New York, NY: American Society of Civil Engineers. https://doi.org/10.1061/9780784402429.299
Nicholls, R. J., Hanson, S. E., Lowe, J. A., Warrick, R. A., Lu, X., Long, A. J., & Carter, T. R. (2011). Constructing sea-level scenarios for impact and adaptation assessment of coastal areas: A guidance document. *Supporting Material, Intergovernmental Panel on Climate Change Task Group on Data and Scenario Support for Impact and Climate Analysis (TGICA)*, *47*.
Ranasinghe, R., Callaghan, D. P., & Stive, M. J. F. (2012). Estimating coastal recession due to sea level rise: Beyond the Bruun rule. *Climatic Change*. https://doi.org/10.1007/s10584-011-0107-8
Ranasinghe, R., & Stive, M. J. F. (2009). Rising seas and retreating coastlines. *Climatic Change*, *97*, 465–468. https://doi.org/10.1007/s10584-009-9593-3
Ranasinghe, R., Watson, P., Lord, D., Hanslow, D., & Cowell, P. J. (2007). Sea level rise, coastal

recession and the Bruun Rule. In *Proceedings of Coasts and Ports* (p. 8). Engineers Australia.
Roelvink, D., Reniers, A., van Dongeren, A., van Thiel de Vries, J., McCall, R., & Lescinski, J. (2009). Modelling storm impacts on beaches, dunes and barrier islands. *Coastal Engineering*, *56*(11–12), 1133–1152. https://doi.org/10.1016/j.coastaleng.2009.08.006
Saito, A., & Kosuge, S. (1988). Waves and Littoral Drift at Suruga Bay (in Japanese). *Journal of Oceanography*, *26*(1), 1–10.
Semedo, A., Weisse, R., Behrens, A., Sterl, A., Bengtsson, L., & Günther, H. (2013). Projection of Global Wave Climate Change toward the End of the Twenty-First Century. *Journal of Climate*, *26*(21), 8269–8288. https://doi.org/10.1175/JCLI-D-12-00658.1
Shibutani, Y., Kuroiwa, M., & Matsubara, Y. (2016). Effect of the Coastal Protection using the Beach Nourishment at Tottori Sand Dune Coast, JAPAN. *Journal of Coastal Research*, *75*(sp1), 695–699. https://doi.org/10.2112/SI75-139.1
Sunamura, T. (1983). coastal and beach changes by waves. *Transactions, Japanese Geomorphological Union*, *4*, 179–188.
Takeda, I., & Sunamura, T. (1983). Formation and spacing of beach cusps. *Proceedings Oastal Engineering*, *26*, 121–135.
Toimil, A., Losada, I. J., Camus, P., & Díaz-Simal, P. (2017). Managing coastal erosion under climate change at the regional scale. *Coastal Engineering*, *128*, 106–122. https://doi.org/10.1016/j.coastaleng.2017.08.004
Toshima, Y. (1970). *Investigation report on the coast and ocean floor in the Tottori prefecture (in Japanese)*.
Udo, K., & Takeda, Y. (2014). Uncertainty in Estimation of Future Beach Erosion in Japan due to Sea Level Rise. *Journal of Japan Society of Civil Engineers, Ser. G (Environmental Research)*, *70*(5), I_101-I_110. https://doi.org/10.2208/jscejer.70.I_101
Udo, K., & Takeda, Y. (2017). Projections of Future Beach Loss in Japan Due to Sea-Level Rise and Uncertainties in Projected Beach Loss. *Coastal Engineering Journal*. https://doi.org/10.1142/S057856341740006X
Wang, X. L., & Swail, V. R. (2006). Climate change signal and uncertainty in projections of ocean wave heights. *Climate Dynamics*, *26*(2–3), 109–126. https://doi.org/10.1007/s00382-005-0080-x
Watson, J. M. (2018). Coastal Change. Retrieved September 14, 2018, from https://pubs.usgs.gov/circ/c1075/change.html
Yasumoto, Y., Uda, T., Matsubara, Y., & Hirano, G. (2007). Beach Erosion along Tottori Coast and Comprehensive Sediment Management. *Journal of Coastal Research*, (September 2015), 82–87.
Zhang, K., Douglas, B. C., & Leatherman, S. P. (2004). Global Warming and Coastal Erosion. *Climatic Change*, *64*(1–2), 41–58. https://doi.org/10.1023/B:CLIM.0000024690.32682.48

Appendix I: PCR model inputs

Model setup titles include the location, storm detection method and model name.

I.1 Site 1 – Near Onahama port, Hazaki storm dates ($PCR1_{Haz}$)

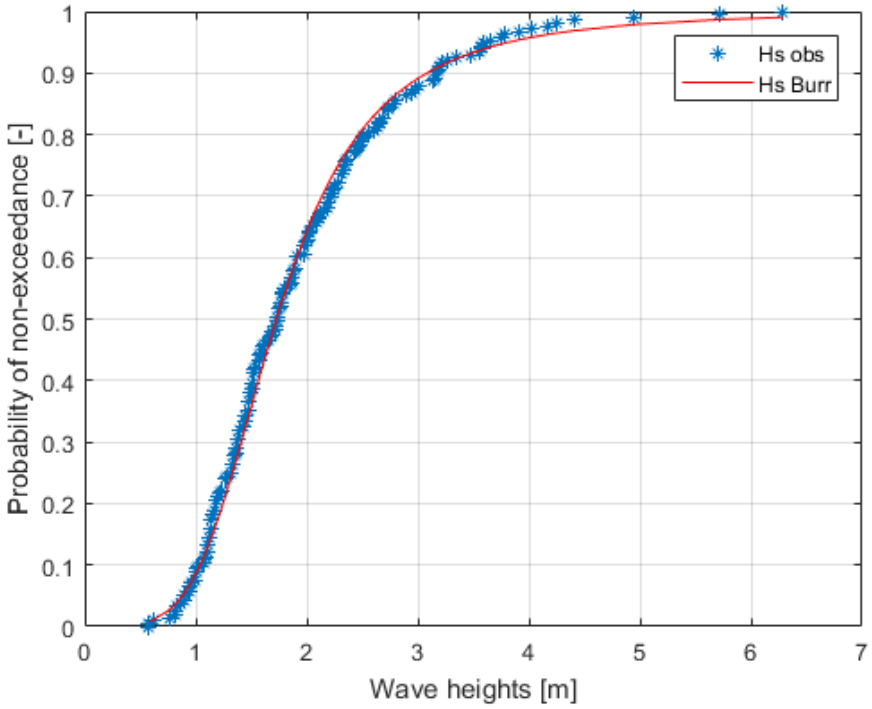

Figure I-1. Storm wave heights at site 1 fitted to a Burr distribution. The storm wave heights were selected based on the comparison between the date of occurrence and the date of erosion at the HORS (Hazaki storm dates). Data acquired from the Onahama measuring station (MLIT, 2018).

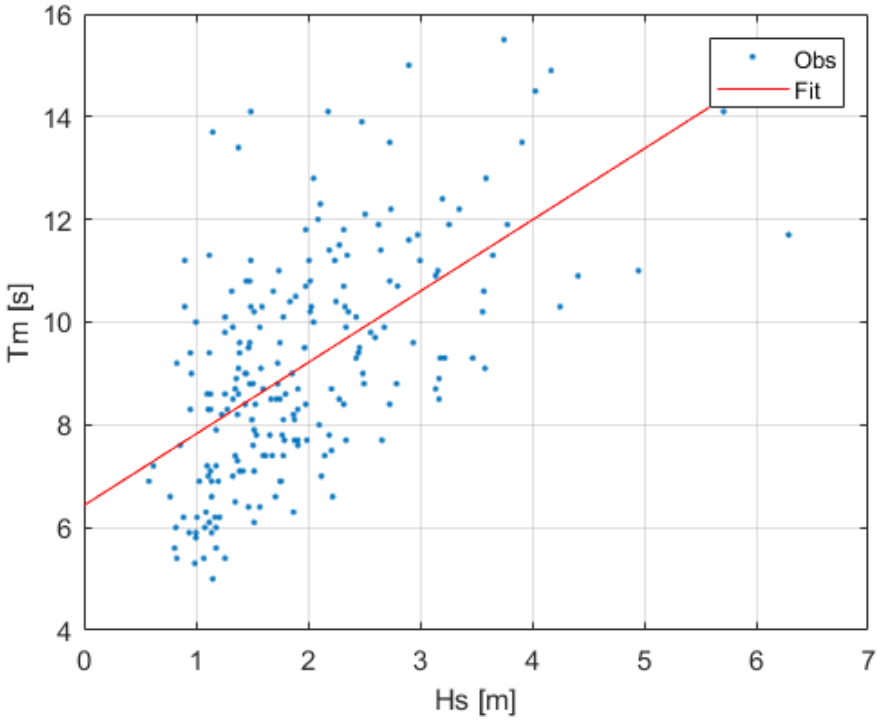

Figure I-2. Linear relation between storm wave heights and their wave periods for site 1. The storm wave heights were selected based on the comparison between the date of occurrence and the date of erosion at the HORS (Hazaki storm dates). Data acquired from the Onahama measuring station (MLIT, 2018).

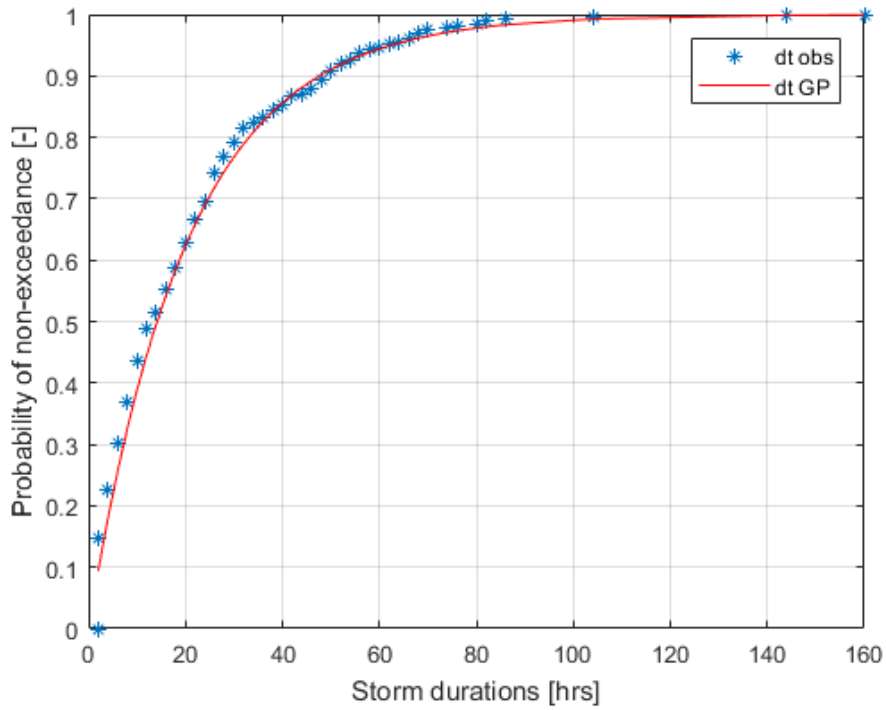

Figure I-3. Storm durations fitted to Generalised Pareto distribution for site 1. Storm durations were determined from storm heights based on two requirements: 1) exceedance of the 97th wave height threshold and 2) period of at least 24 hours between exceedances. Data acquired from the Onahama measuring station (MLIT, 2018).

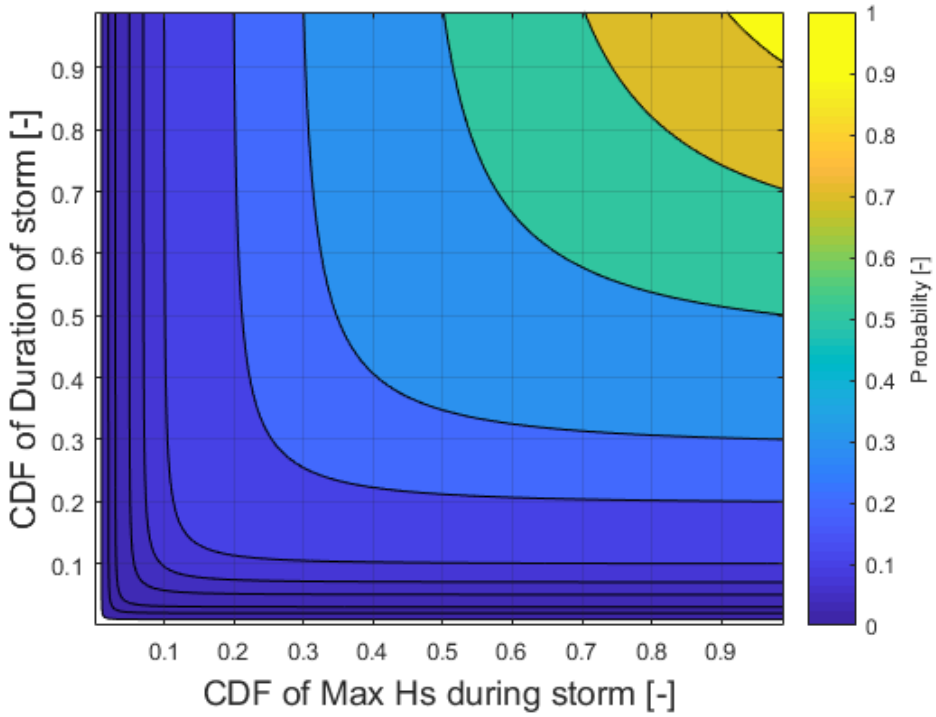

Figure I-4. Copula joining the cumulative distribution functions of wave heights and storm durations for site 1. The storm wave heights were selected based on the comparison between the date of occurrence and the date of erosion at the HORS (Hazaki storm dates).

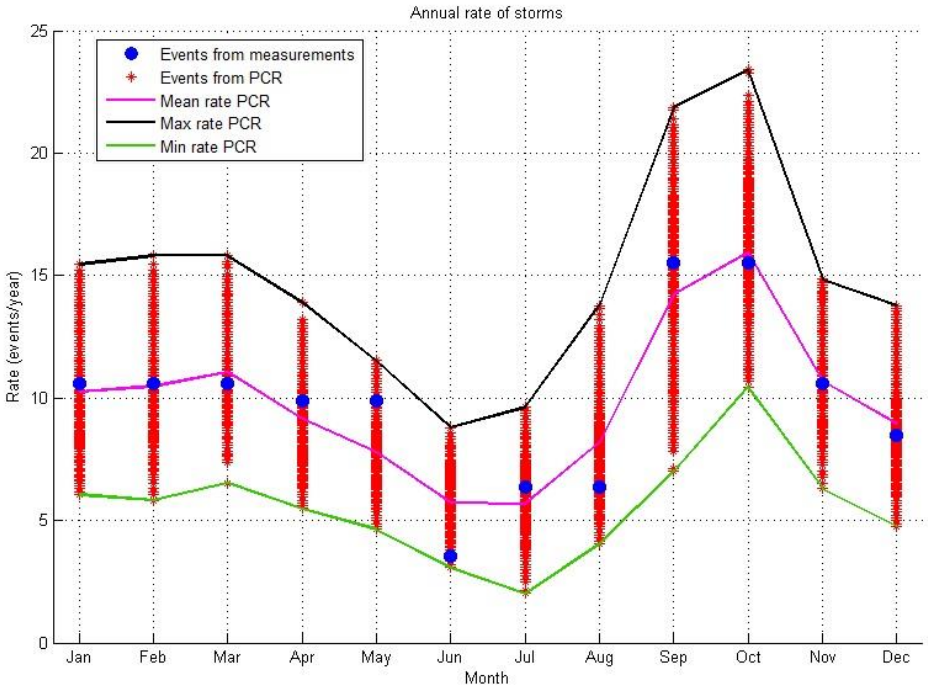

Figure I-5. Observed and generated events per month for site 1. Since storm detection was based on the Hazaki storm dates, the same occurrence of storms was used for site 1. Adopted from Da Cruz (2018). N.B.: event rates are given in events per year, not per month as in other similar figures.

I.2 Site 1 – Near Onahama port, 97th wave thresholding (PCR1$_{97}$)

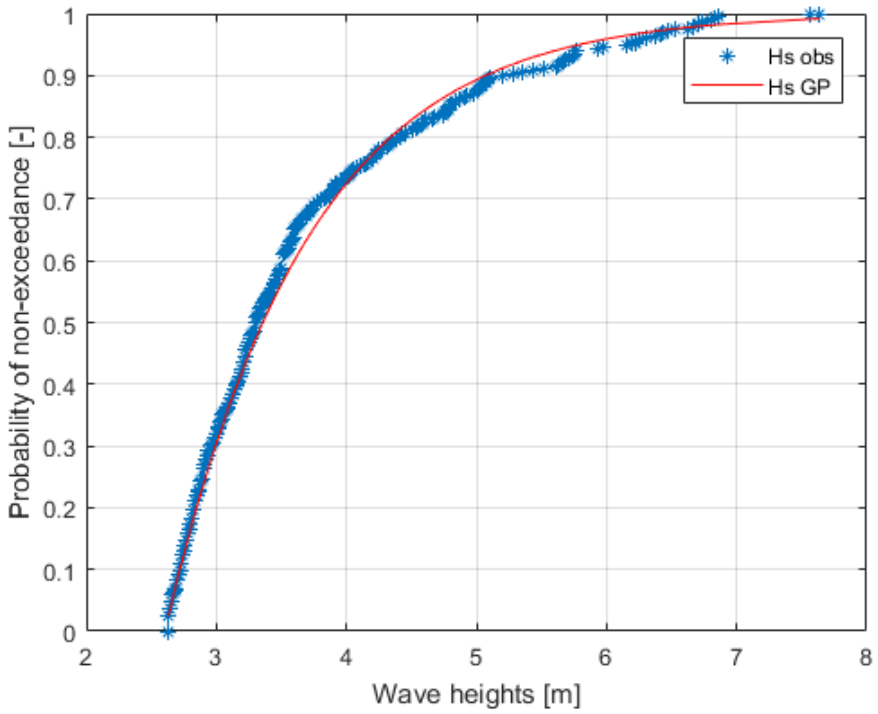

Figure I-6. Storm wave heights at site 1 fitted to a Generalised Pareto distribution. The storm wave heights were selected based on 97th percentile wave height thresholding. Data acquired from the Onahama measuring station (MLIT, 2018).

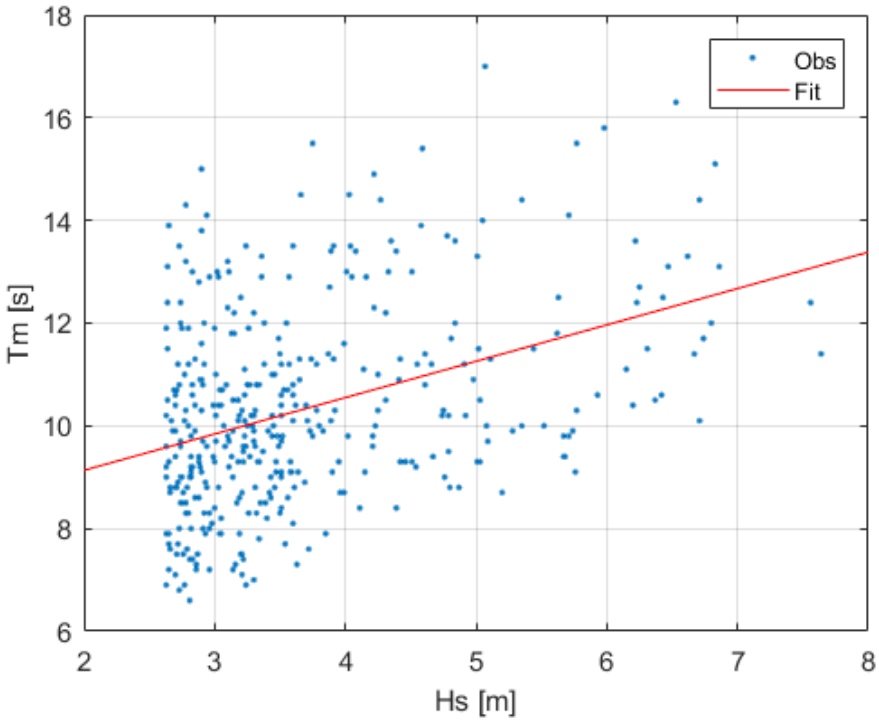

Figure I-7. Linear relation between storm wave heights and their wave periods for site 1. The storm wave heights were selected based on 97th percentile wave height thresholding. Data acquired from the Onahama measuring station (MLIT, 2018).

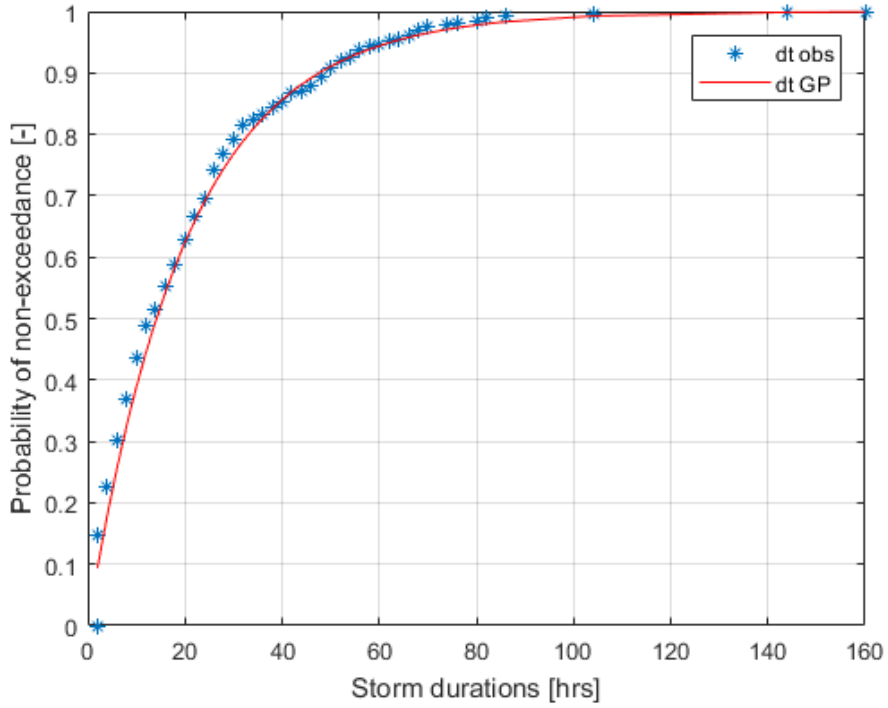

Figure I-8. Storm durations fitted to Generalised Pareto distribution for site 1. Storm durations were determined from storm heights based on two requirements: 1) exceedance of the 97th wave height threshold and 2) period of at least 24 hours between exceedances. Data acquired from the Onahama measuring station (MLIT, 2018).

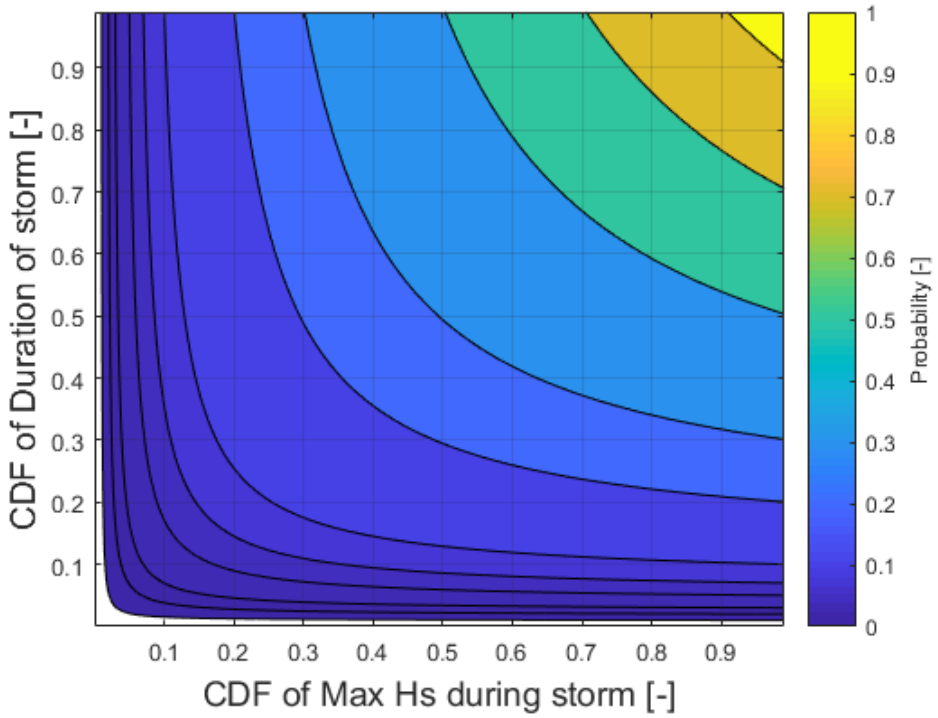

Figure I-9. Copula joining the cumulative distribution functions of wave heights and storm durations for site 1. The storm wave heights were selected based on 97th percentile wave height thresholding.

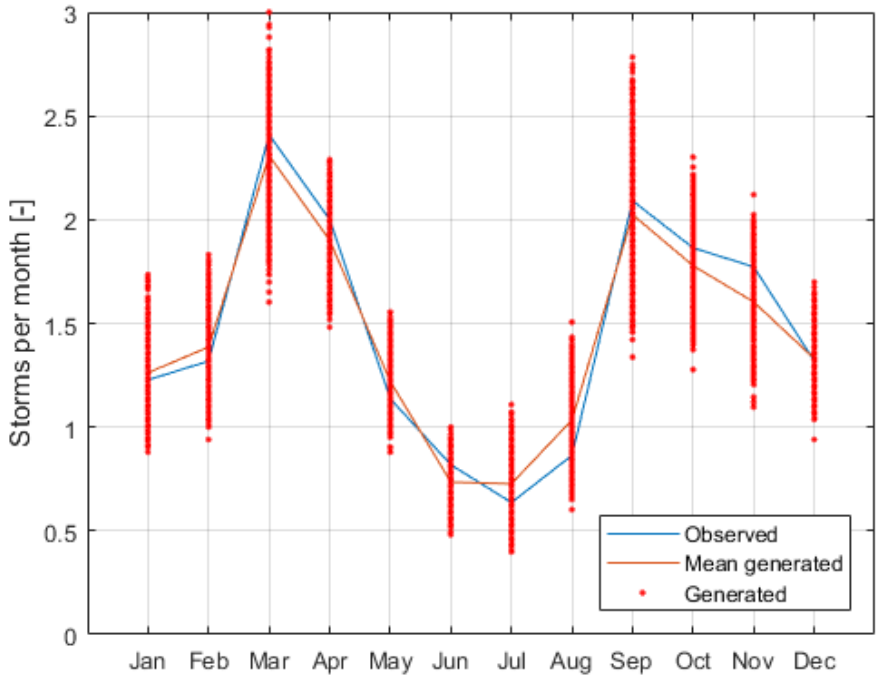

Figure I-10. Observed and generated events per month for site 1. Storm detection was done based on two requirements: 1) exceedance of the 97th wave height threshold and 2) period of at least 24 hours between exceedances. Data acquired from the Onahama measuring station (MLIT, 2018).

I.3 Site 2 – Tottori sand dunes, 99th wave thresholding (PCR2$_{99}$)

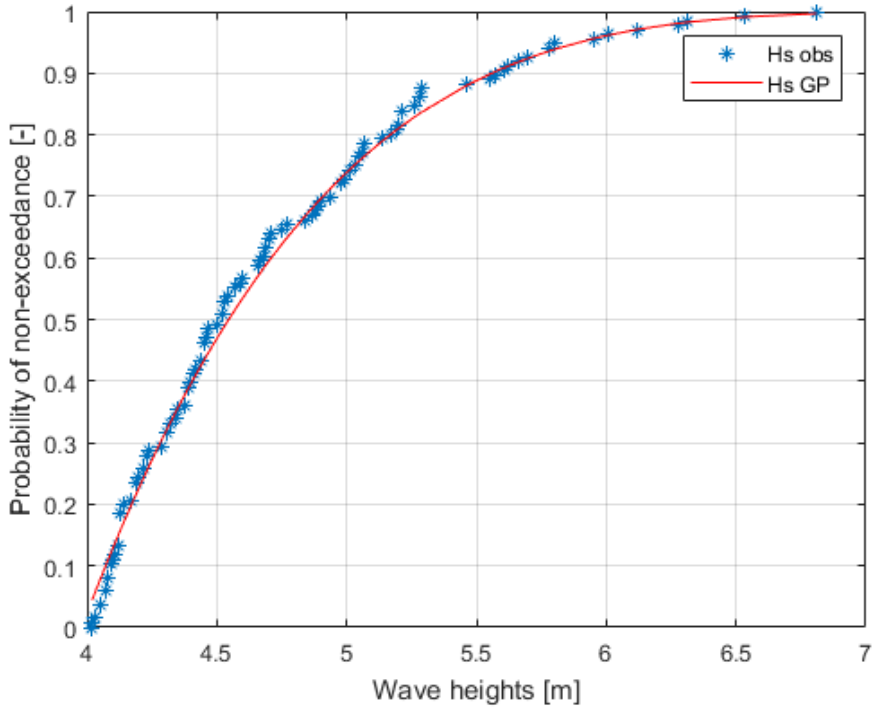

Figure I-11. Storm wave heights at site 2 fitted to a Generalised Pareto distribution. The storm wave heights were selected based on 99th percentile wave height thresholding. Data acquired from the Tottori measuring station (MLIT, 2018).

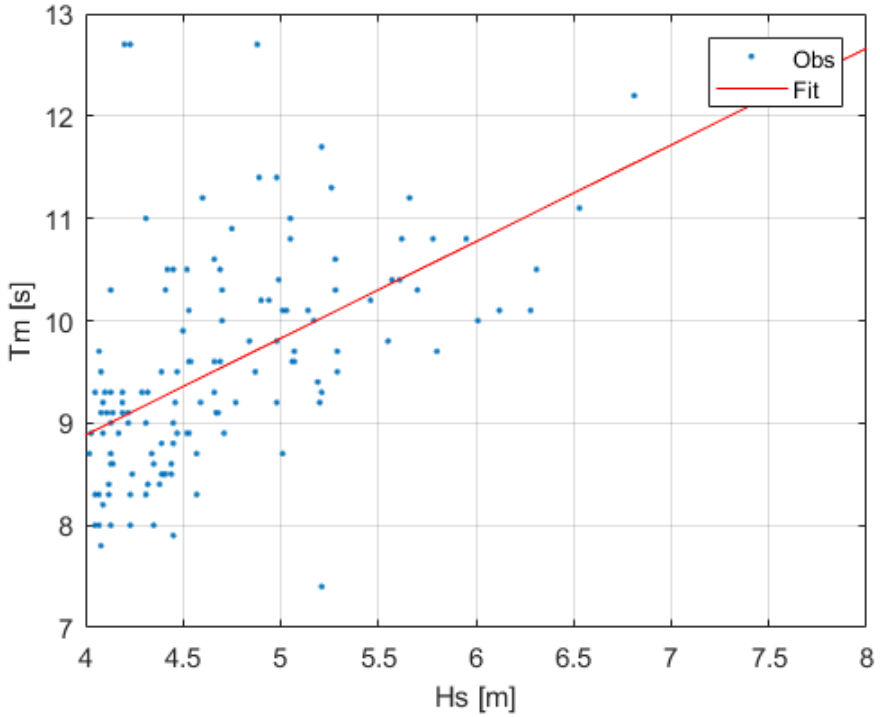

Figure I-12. Linear relation between storm wave heights and their wave periods for site 2. The storm wave heights were selected based on 99th percentile wave height thresholding. Data acquired from the Tottori measuring station (MLIT, 2018).

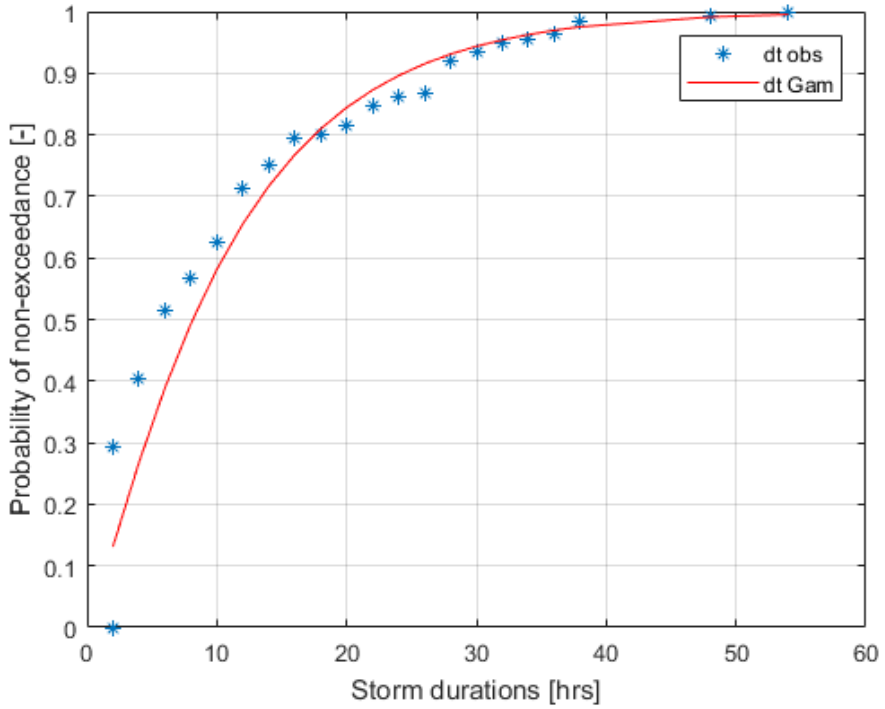

Figure I-13. Storm durations fitted to Generalised Pareto distribution for site 2. Storm durations were determined from storm heights based on two requirements: 1) exceedance of the 99th wave height threshold and 2) period of at least 24 hours between exceedances. Data acquired from the Tottori measuring station (MLIT, 2018).

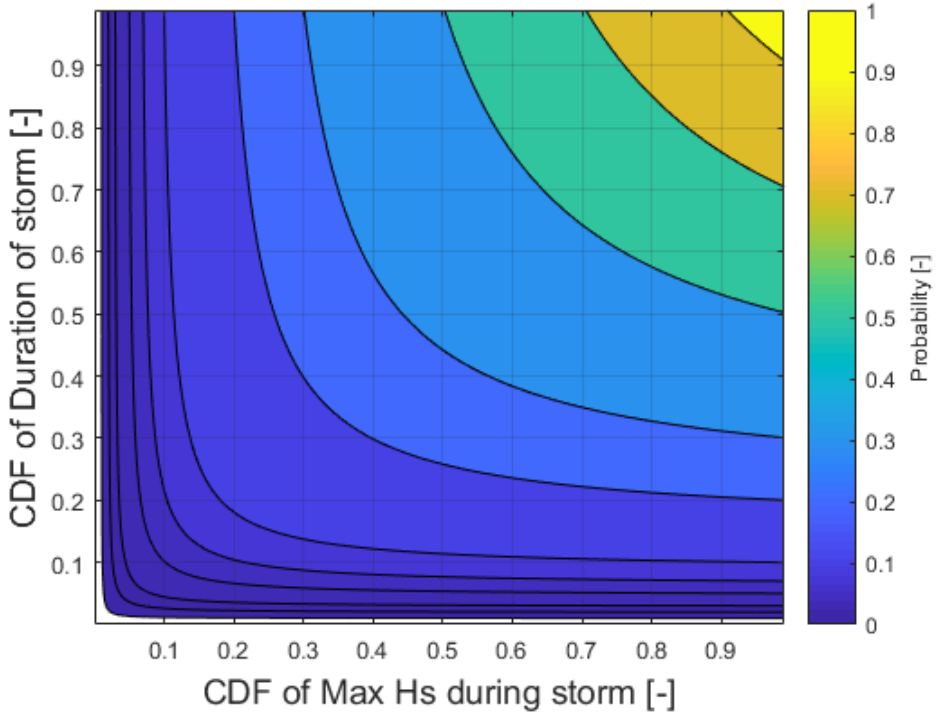

Figure I-14. Copula joining the cumulative distribution functions of wave heights and storm durations for site 2. The storm wave heights were selected based on 99th percentile wave height thresholding.

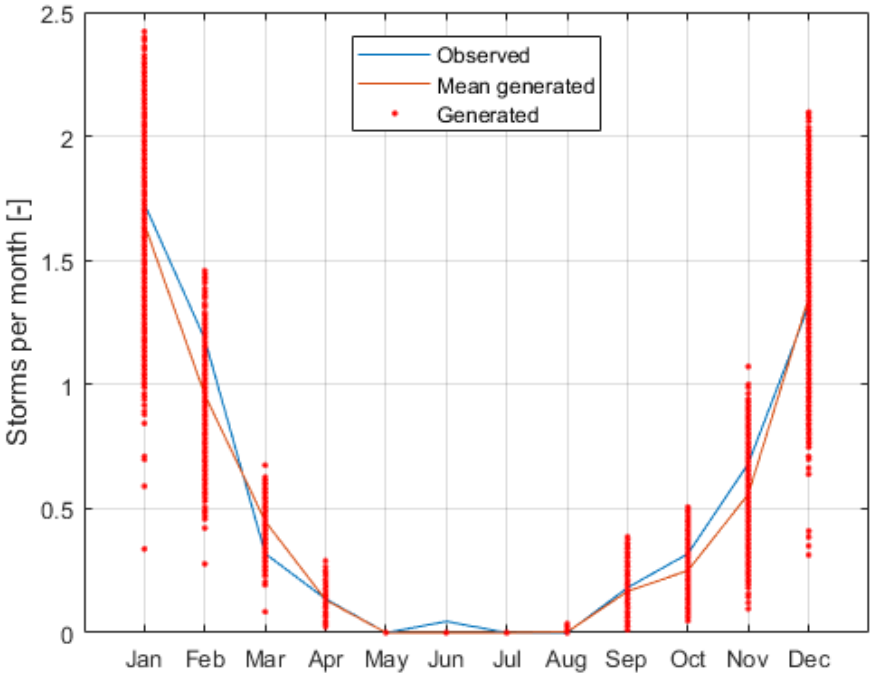

Figure I-15. Observed and generated events per month for site 2. Storm detection was done based on two requirements: 1) exceedance of the 99th wave height threshold and 2) period of at least 24 hours between exceedances. Data acquired from the Onahama measuring station (MLIT, 2018).

I.4 Site 2 – Tottori sand dunes, 97th wave thresholding (PCR2$_{97}$)

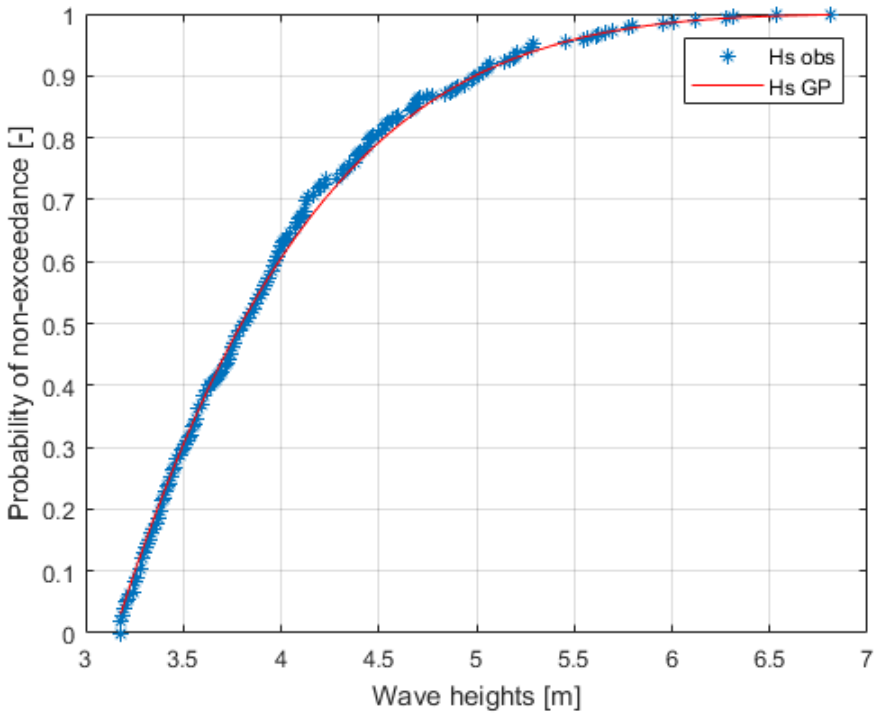

Figure I-16. Storm wave heights at site 2 fitted to a Generalised Pareto distribution. The storm wave heights were selected based on 97th percentile wave height thresholding. Data acquired from the Tottori measuring station (MLIT, 2018).

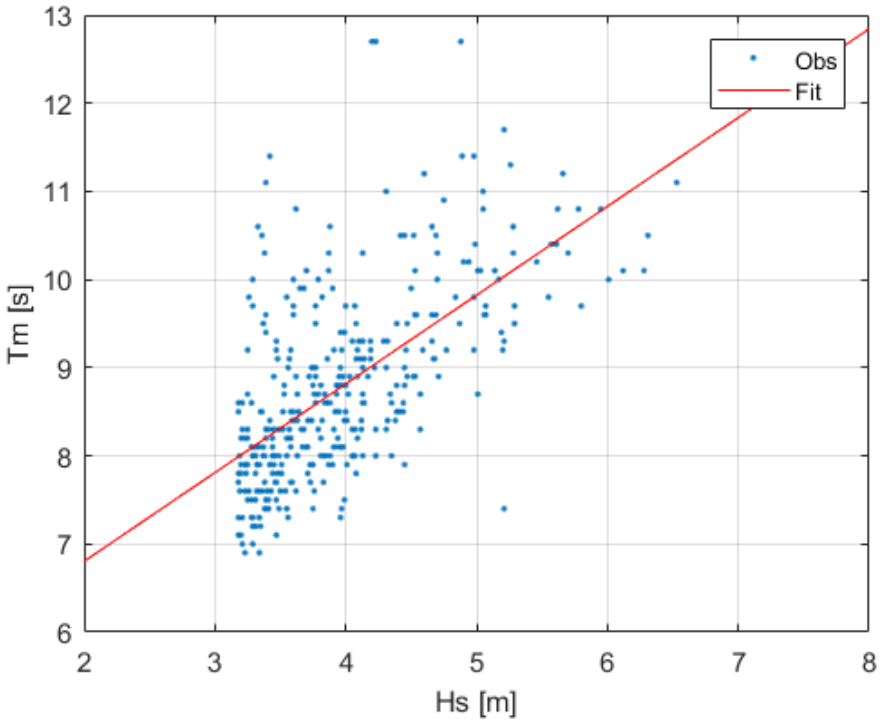

Figure I-17. Linear relation between storm wave heights and their wave periods for site 2. The storm wave heights were selected based on 97th percentile wave height thresholding. Data acquired from the Tottori measuring station (MLIT, 2018)

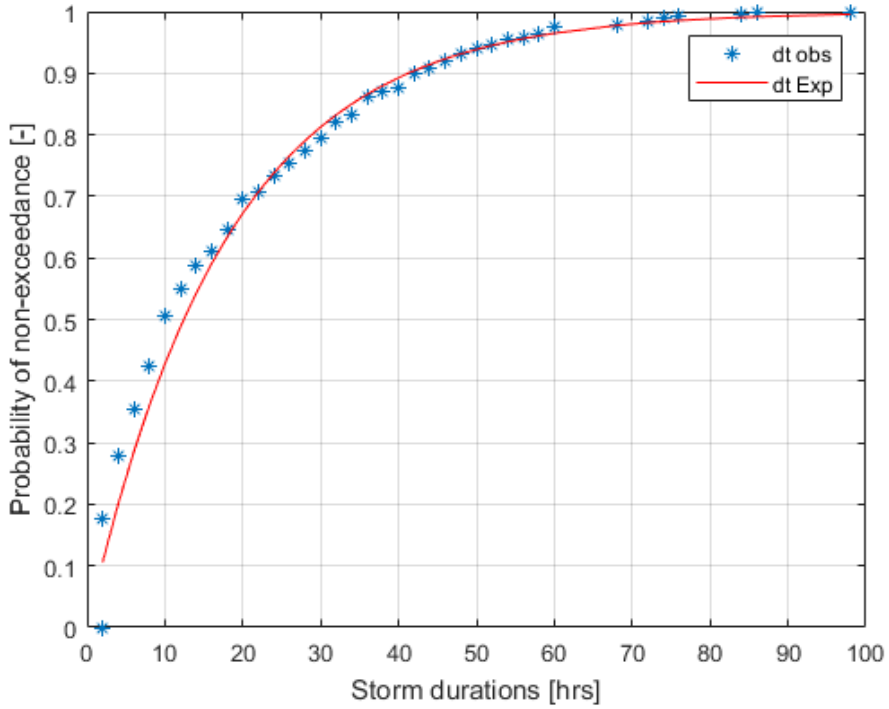

Figure I-18. Storm durations fitted to Generalised Pareto distribution for site 2. Storm durations were determined from storm heights based on two requirements: 1) exceedance of the 97th wave height threshold and 2) period of at least 24 hours between exceedances. Data acquired from the Tottori measuring station (MLIT, 2018).

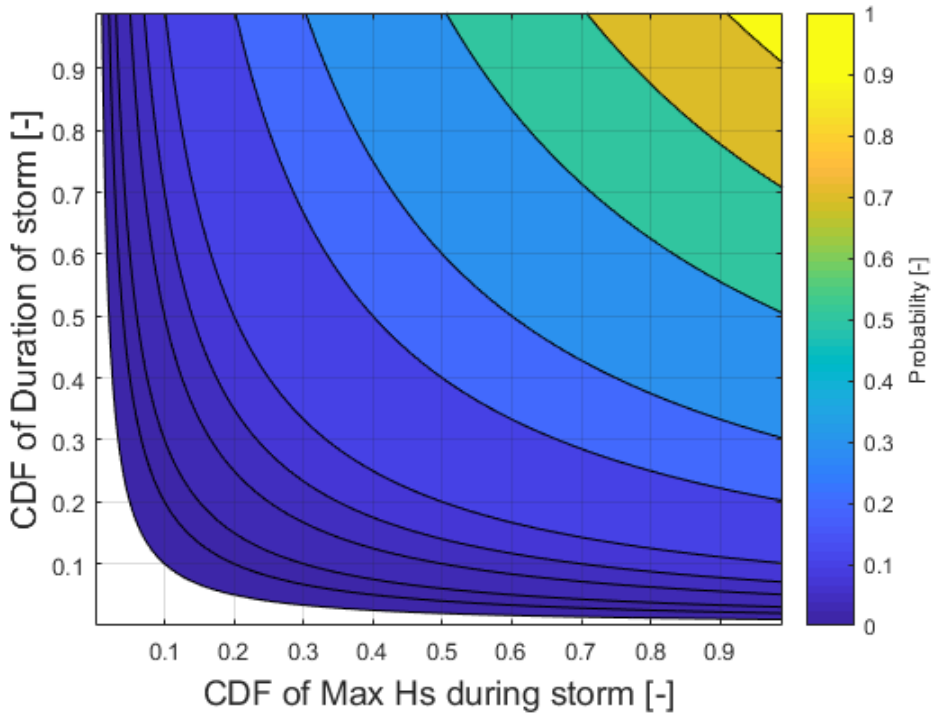

Figure I-19. Copula joining the cumulative distribution functions of wave heights and storm durations for site 2. The storm wave heights were selected based on 97th percentile wave height thresholding.

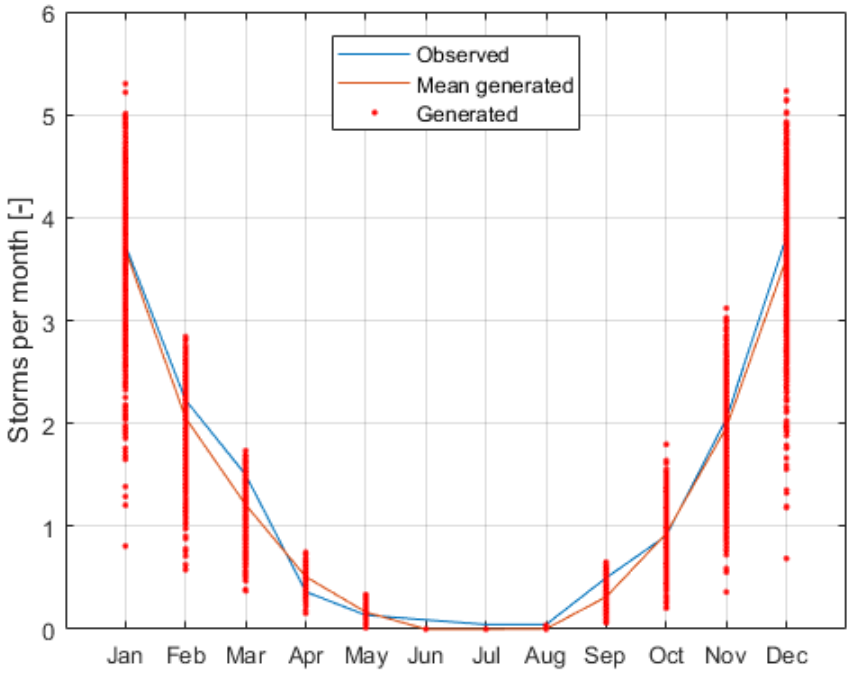

Figure I-20. Observed and generated events per month for site 2. Storm detection was done based on two requirements: 1) exceedance of the 97th wave height threshold and 2) period of at least 24 hours between exceedances. Data acquired from the Onahama measuring station (MLIT, 2018).

I.5 Site 3 – Yumigahama peninsula, 97th wave thresholding (PCR3)

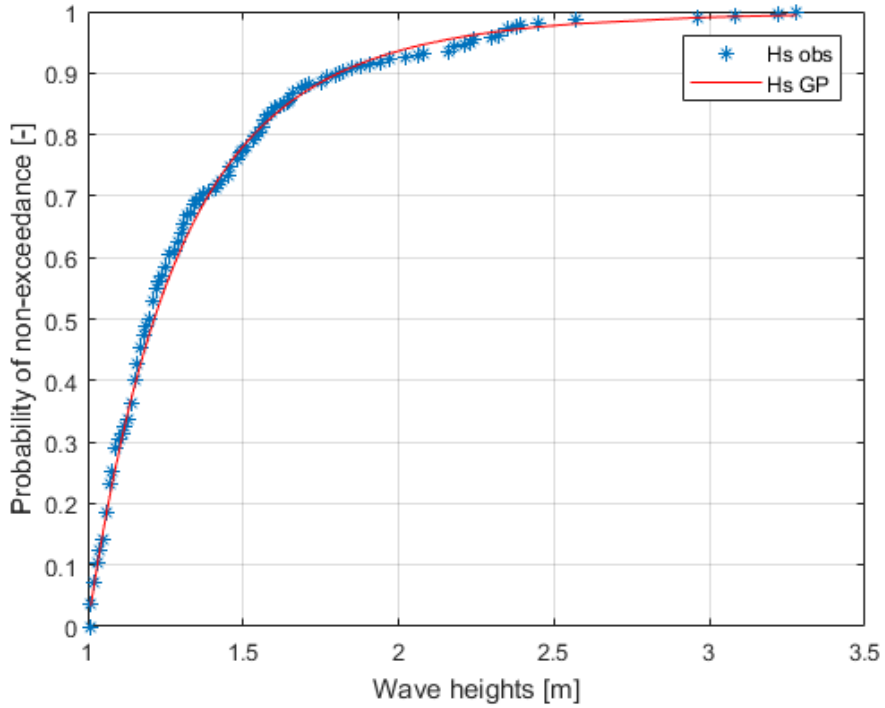

Figure I-21. Storm wave heights at site 3 fitted to a Generalised Pareto distribution. The storm wave heights were selected based on 97th percentile wave height thresholding. Data acquired from the Sakai measuring station (MLIT, 2018).

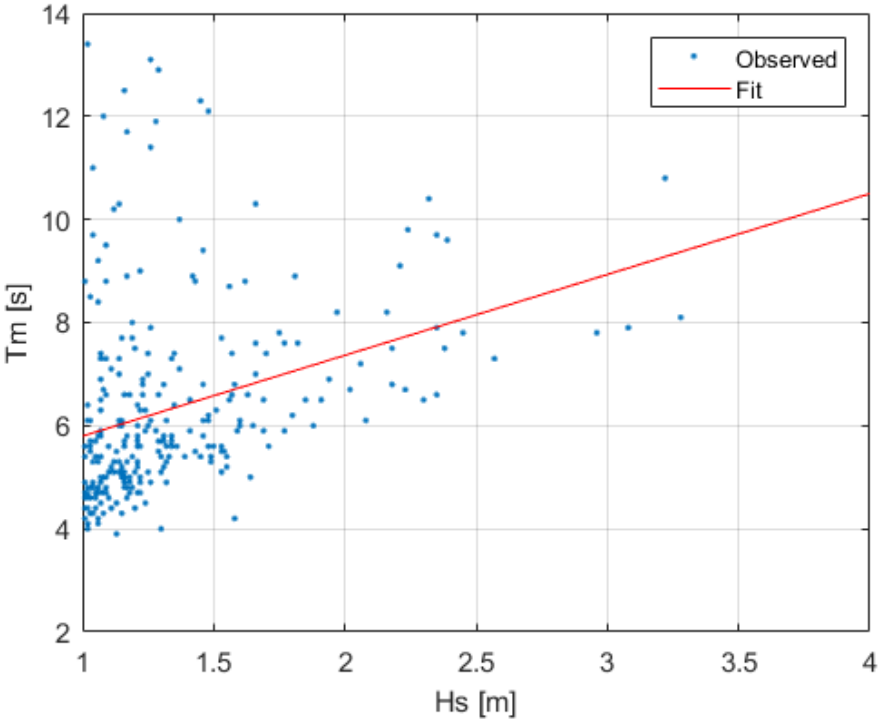

Figure I-22. Linear relation between storm wave heights and their wave periods for site 3. The storm wave heights were selected based on 97th percentile wave height thresholding. Data acquired from the Sakai measuring station (MLIT, 2018).

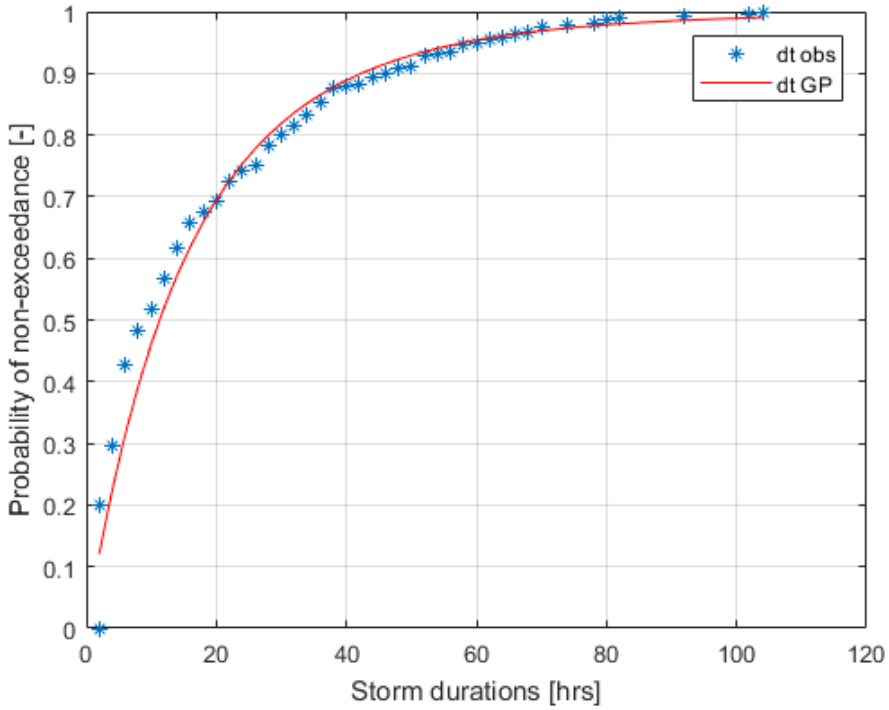

Figure I-23. Storm durations fitted to Generalised Pareto distribution for site 3. Storm durations were determined from storm heights based on two requirements: 1) exceedance of the 97th wave height threshold and 2) period of at least 24 hours between exceedances. Data acquired from the Tottori measuring station (MLIT, 2018).

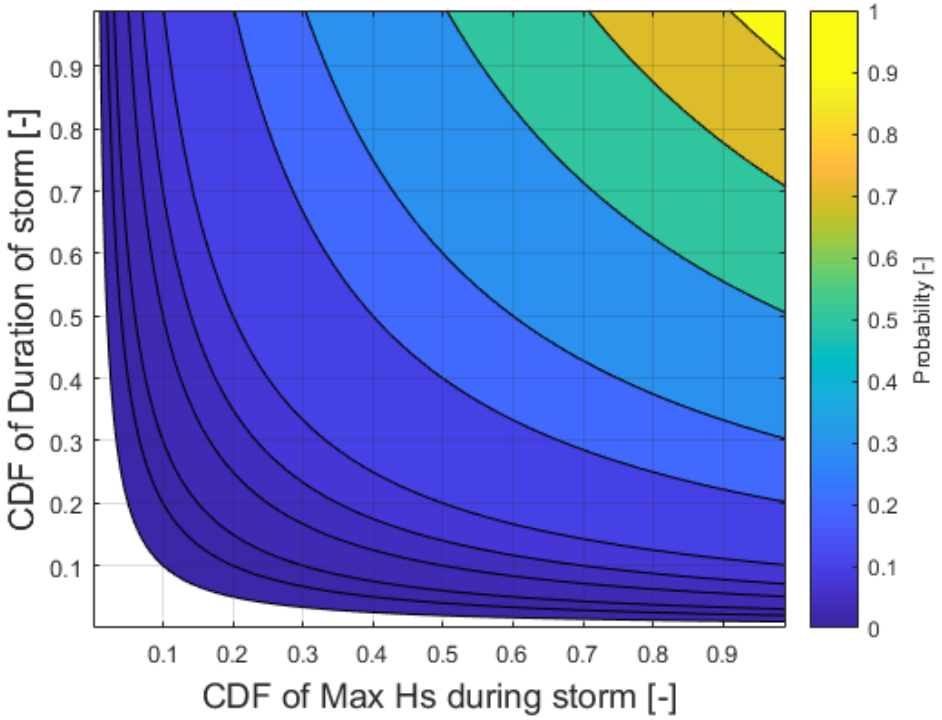

Figure I-24. Copula joining the cumulative distribution functions of wave heights and storm durations for site 3. The storm wave heights were selected based on 97th percentile wave height thresholding.

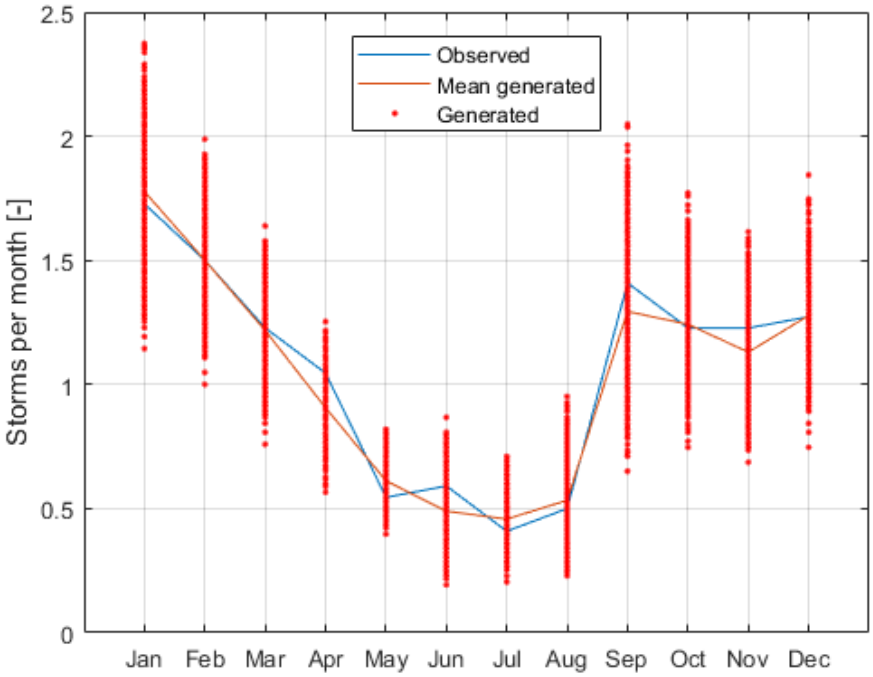

Figure I-25. Observed and generated events per month for site 3. Storm detection was done based on two requirements: 1) exceedance of the 97th wave height threshold and 2) period of at least 24 hours between exceedances. Data acquired from the Onahama measuring station (MLIT, 2018).

Appendix II: Equilibrium profile fitting

To the submerged section of the beach profiles was the following equation fitted:

$$y = Ax^{\frac{2}{3}} \tag{14}$$

Coefficient *A* was then found with a best fit-algorithm or calculated with:

$$A = 0.067 w_s^{0.44} \tag{15}$$

Fall velocity w_s was derived from the D50 at the site.

II.1 Site 1 – Near Onahama port

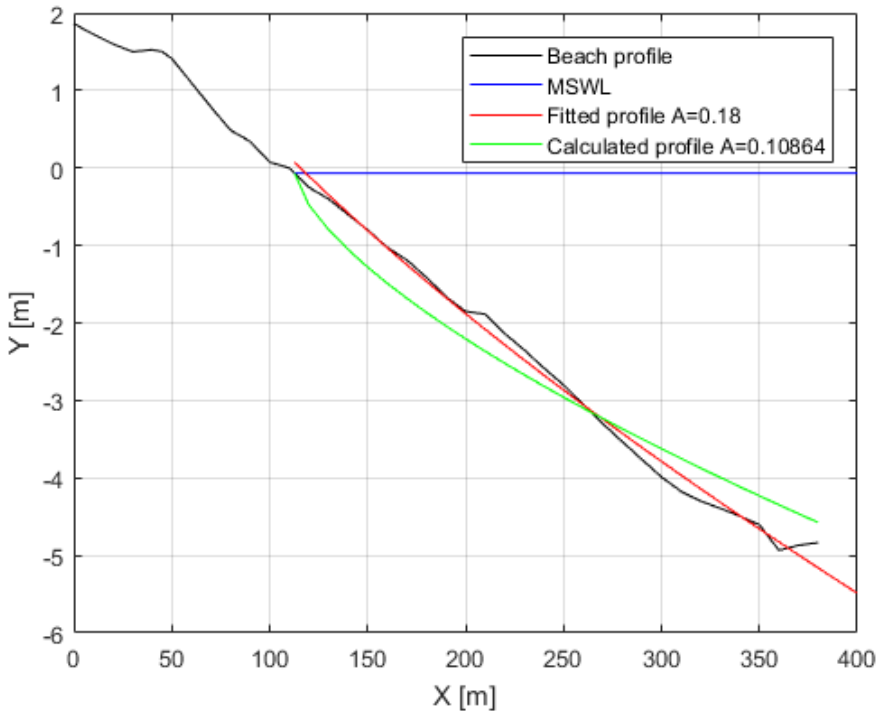

Figure II-1. Submerged profiles fitted to the beach profile. The submerged profiles were made with a fitting algorithm (red) or calculated from the D50 (green). The red profile was used.

II.2 Site 2 – Tottori sand dunes

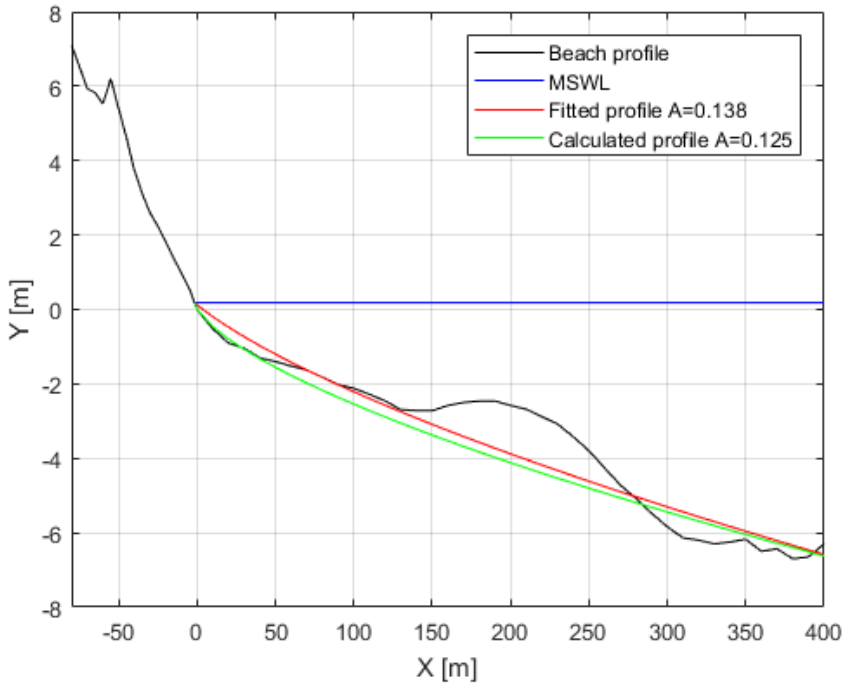

Figure II-2. Submerged profiles fitted to the beach profile. The submerged profiles were made with a fitting algorithm (red) or calculated from the D50 (green). The red profile was used

II.3 Site 3 – Yumigahama peninsula

Kuroiwa et al. (2013) already calculated recessions of the beach along the Yumigahama peninsula with the Bruun rule method. They used another approach, but they also had to approximate the submerged section of the beach profile with Equation 13. The value for *A* they found was 0.182. It was decided to use this value as a satisfactory fit was made.

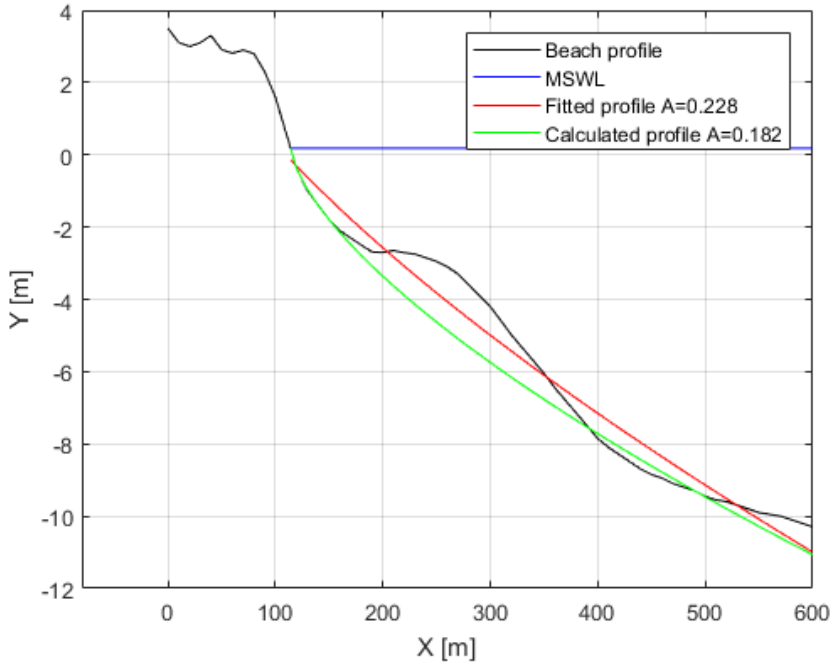

Figure II-3. Submerged profiles fitted to the beach profile. The submerged profiles were made with a fitting algorithm (red) or calculated from the D50 (green). The green profile was used.

Appendix III: ECDFs with averaged shoreline positions

Model setup titles include the location, storm detection method and model name.

III.1 Site 1 – Near Onahama port, Hazaki storm dates ($PCR1_{Haz}$)

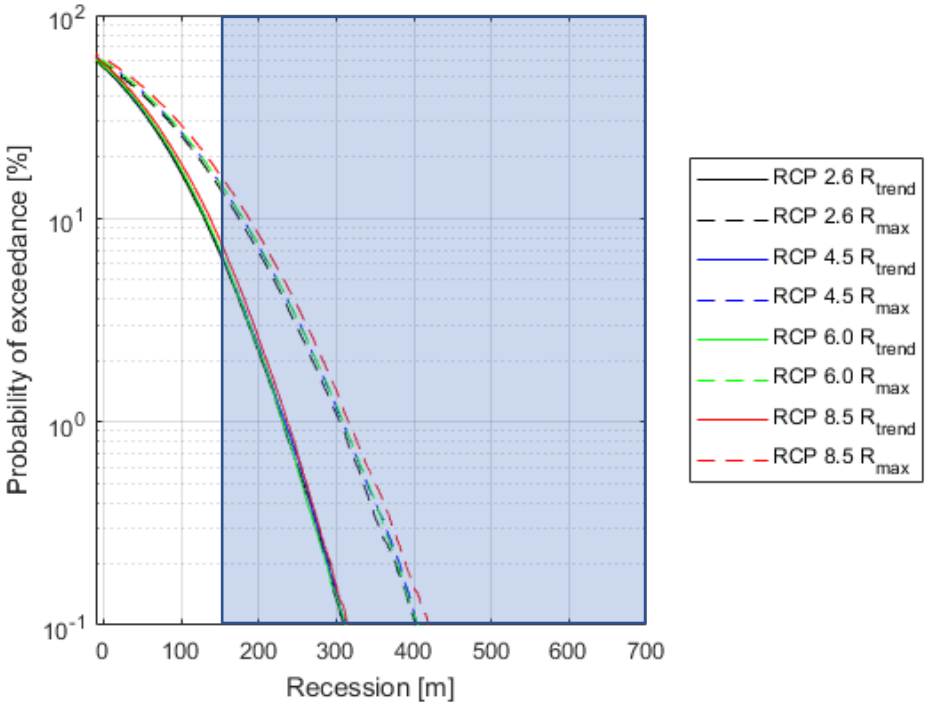

Figure III-1. ECDFs for R_{max} in 2100 and R_{trend} over 2095-2100 for site 1. Both are derived from the results of the $PCR1_{Haz}$ model. The blue rectangle indicates impossible shoreline positions, as the beach at site 1 is only 160 metres wide.

III.2 Site 1 – Near Onahama port, 97th wave thresholding ($PCR1_{97}$)

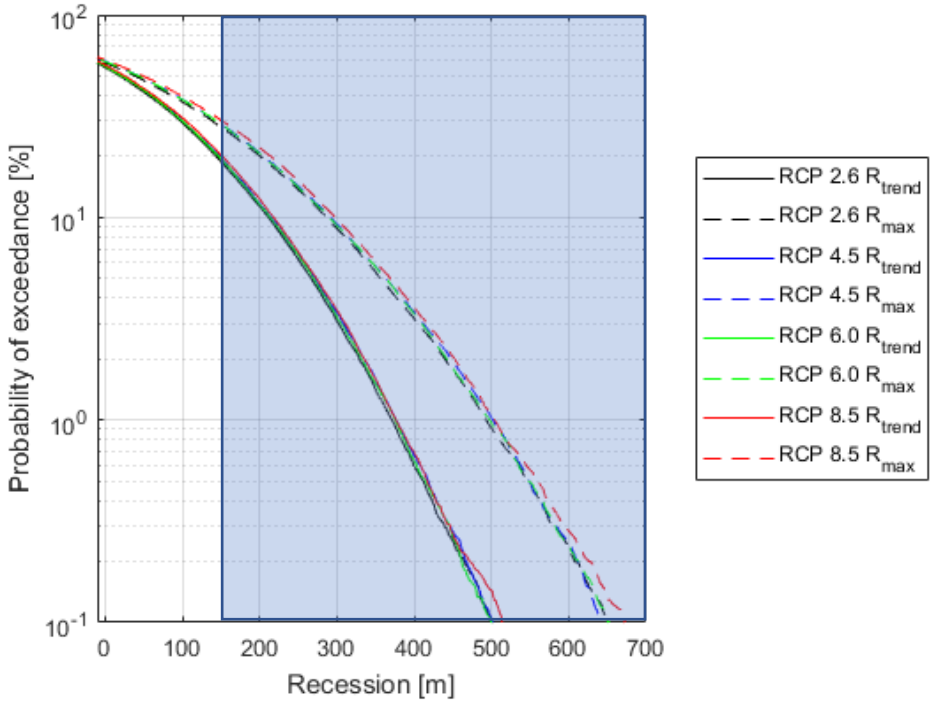

Figure III-2. ECDFs for R_{max} in 2100 and R_{trend} over 2095-2100 for site 1. Both are derived from the results of the $PCR1_{97}$ model. The blue rectangle indicates impossible shoreline positions, as the beach at site 1 is only 160 metres wide.

III.3 Site 2 – Tottori sand dunes, 99th wave thresholding ($PCR2_{99}$)

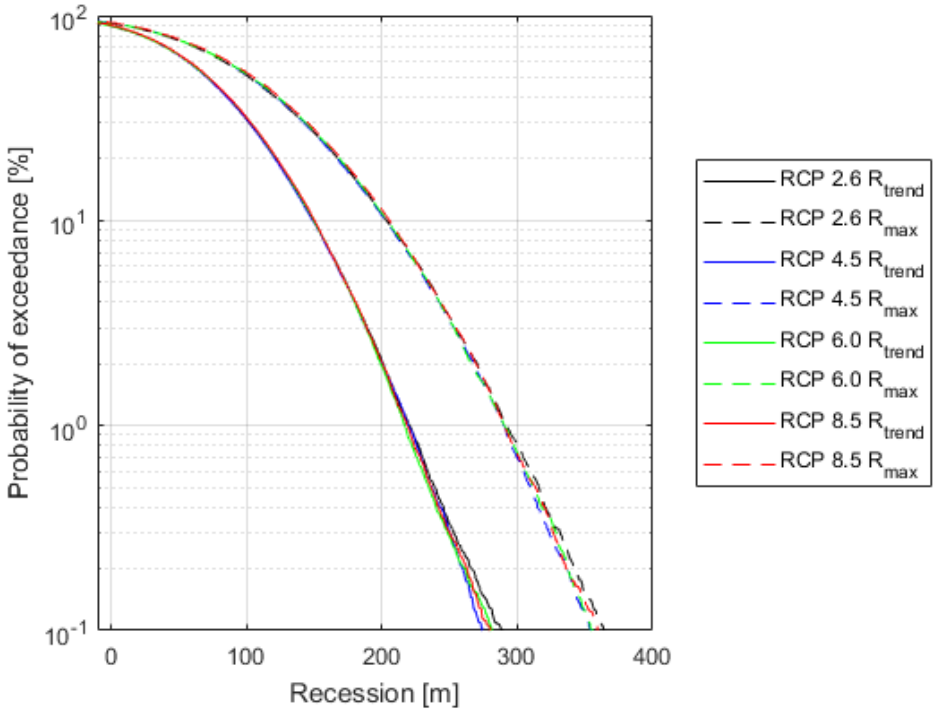

Figure III-3. ECDFs for R_{max} in 2100 and R_{trend} over 2095-2100 for site 2. Both are derived from the results of the $PCR2_{99}$ model.

III.4 Site 2 – Tottori sand dunes, 97th wave thresholding ($PCR2_{97}$)

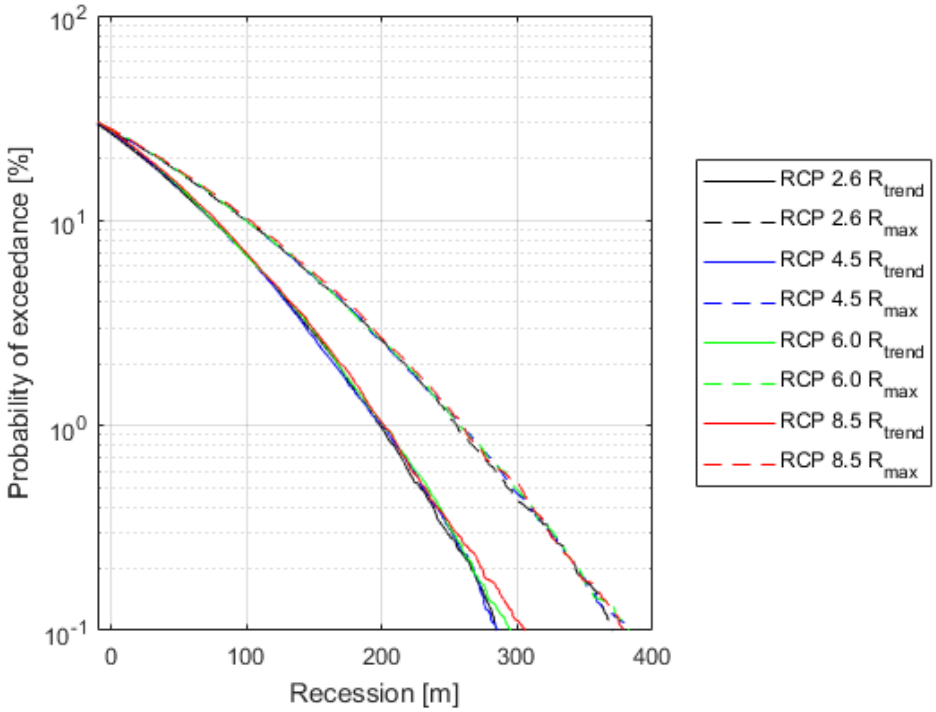

Figure III-4. ECDFs for R_{max} in 2100 and R_{trend} over 2095-2100 for site 2. Both are derived from the results of the $PCR2_{97}$ model.

III.5 Site 3 – Yumigahama peninsula, 97th wave thresholding (PCR3)

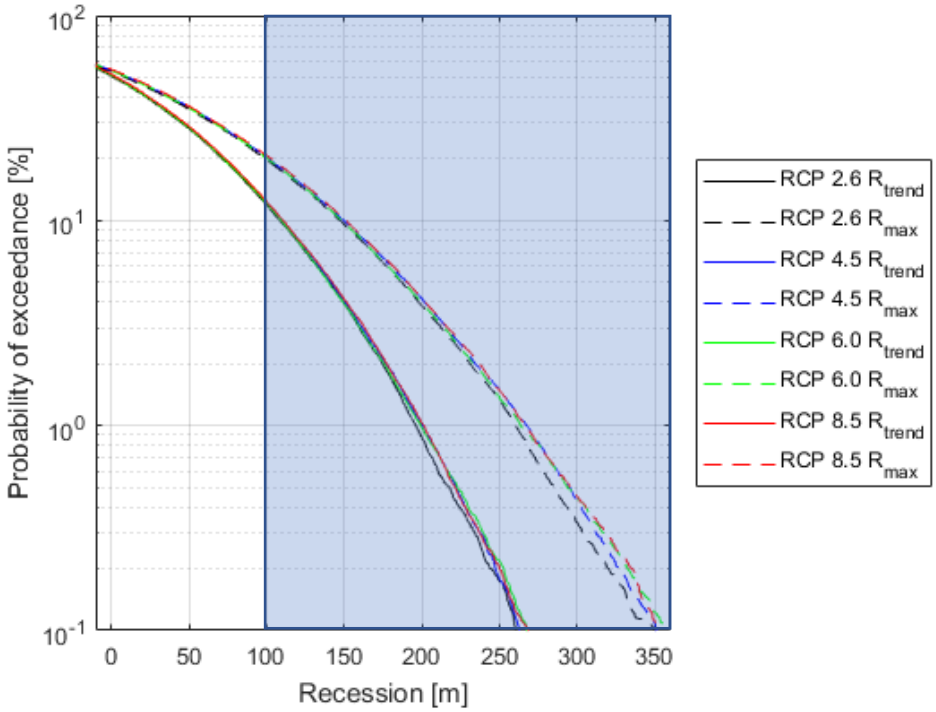

Figure III-5. ECDFs for R_{max} in 2100 and R_{trend} over 2095-2100 for site 3. Both are derived from the results of the PCR3 model. The blue rectangle indicates impossible shoreline positions, as the beach at site 3 is only 100 metres wide.